Abstract

MOENING, TARA NICOLE. Assessment of a New Hybrid Technique, Matrix Enhanced Nanostructured Initiator Mass Spectrometry (ME-NIMS), for the Analysis and Mass Spectrometry Imaging (MSI) of Drug Compounds. (Under the direction of Lin He).

In the ever changing medical field, there have been great strides made to understand diseases, drugs and how they affect the body. Such techniques as magnetic resonance spectroscopy imaging (MRI), positron emission tomography (PET), autoradiography and immunolabeling are used to try to image and map out molecules throughout the body but come with limitations. These techniques typically require the molecules of interest to be tagged; only allowing one molecule at a time to be imaged and studied. Mass spectrometry imaging (MSI), a label free technique, is a powerful tool that provides the identity and spatial localization of molecules within a sample. This allows for the simultaneous detection of multiple molecules within samples such as biological tissue. As a soft ionization technique, matrix-assisted laser desorption ionization (MALDI) is often times coupled with MSI for biological samples. Due to matrix interference in the low molecular weight range for MALDI, there has been much effort put for to circumvent that issue. One of the more successful alternatives is to utilize porous silicon (pSi) for surface-assisted laser desorption ionization (SALDI) which uses the pSi surface to transfer energy to enhance desorption/ionization and it does not require matrix. Other pSi techniques such as nanostructured initiator mass spectrometry (NIMS) have also shown advantageous results.

The focus of this dissertation is to explore the potential of multiple different pSi surface techniques for MSI. There are three main goals that are addressed in this work: 1) pSi technique optimization and comparison, 2) spatial resolution for MSI applications, and 3) drug analysis

utilizing the pSi techniques. Several pSi wafer techniques including matrix-enhance SALDI (ME-SALDI), NIMS and a new hybrid technique, matrix-enhanced NIMS (ME-NIMS), were evaluated in order to determine their sensitivity, reproducibility, and stability. The spatial resolutions for MSI of MALDI, NIMS and ME-NIMS was performed to determine the lowest achievable spatial resolution for each technique. Tandem mass spectrometry (MS/MS) and the determination of limit of detection (LOD) were completed on pentamidine (PTA), a drug compound used in the treatment of human African trypanosomiasis (HAT).

Assessment of a New Hybrid Technique, Matrix Enhanced Nanostructured Initiator Mass Spectrometry (ME-NIMS), for the Analysis and Mass Spectrometry Imaging (MSI) of Drug Compounds

by
Tara Nicole Moening

A dissertation submitted to the Graduate Faculty of
North Carolina State University
in partial fulfillment of the
requirements of the Degree of
Doctor of Philosophy

Chemistry

Raleigh, North Carolina

2017

APPROVED BY:

_____	_____
Dr. David Muddiman	Dr. Michael Goshe
_____	_____
Dr. Lin He Committee Co-Chair	Dr. Edmond Bowden Committee Co-Chair

DEDICATION

To my parents, siblings, nieces and nephews, and grandparents. I want to thank you for all the support and encouragement you have provided for the last few years. I also dedicate this to my friends, especially Jessica; all of your love and support have helped me to reach my goals.

BIOGRAPHY

Born: November 16, 1988

Parents: Michael and Jane Moening

Siblings: Chad (Beth) Moening, Gina (Dwight) Wiltheiss, and Kari (Cody) Niese

Nieces and Nephews: Caitlyn, Mitchell, Lee, Makenzie, and Emmitt Moening, Marla and Nolan Wiltheiss, and Madison Niese

High School: Ottawa-Glandorf High School (graduated in 2007)

Undergraduate: University of Cincinnati

B.S. Chemistry, graduated in 2012

Minor in Material Engineering

ACKNOWLEDGMENTS

I would like to thank my advisor, Dr. Lin He, for all her support, guidance, and advice throughout my graduate research. With her help, I have been able to grow as a scientist, researcher, writer and individual. I would also like to thank current and past group members for all of their support and friendship; Kangshu Zhan, Dr. Thomas Chase, Victoria Brown, Antoine Levy and Nathalia Ortiz.

I am very grateful to Dr. Muddiman Lab group, especially Mark Bokhart for his assistance with the use of the cryostat. Thank you to the NCSU Mass Spectrometry Facility for allowing me to use and work in their facility and also for their assistance with instrument repairs and troubleshooting. I want to acknowledge the Analytical Instrument Facility for their help with SEM characterization.

Also I would like to thank my committee members, Dr. David Muddiman, Dr. Edmond Bowden, and Dr. Michael Goshe. They have given me valuable guidance during my graduate career. I would like to acknowledge my undergraduate advisor, Dr. Apryll Stalcup, for her guidance and support during my undergraduate studies. Also thank you to my friend, Dr. Paula Powell, for pushing me to continue my education and to pursue a career in analytical chemistry.

Lastly, I would like to thank my family and friends for their encouragement. I am forever grateful for their support and love. I have set my goals high and they have inspired me to achieve my personal and professional dreams. Thank you so much for everything.

TABLE OF CONTENTS

LIST OF TABLES

LIST OF FIGURES

LIST OF ABBREVIATIONS

ANOVA	analysis of variance
BisF17	bis(heptadecafluoro-1,1,2,2-tetrahydrodecyl)tetramethyldisiloxane
DHB	dihydroxybenzoic acid
DIOS	desorption ionization on silicon
HAT	human African trypanosomiasis
LOD	limit of detection
MALDI	matrix-assisted laser desorption ionization
ME-NIMS	matrix-enhanced nanostructured initiator mass spectrometry
ME-SALDI	matrix-enhanced surface-assisted laser desorption ionization
MS	mass spectrometry
MSI	mass spectrometry imaging
MS/MS	tandem mass spectrometry
NIMS	nanostructured initiator mass spectrometry
PDMS	polydimethylsiloxane
pSi	porous silicon
PTA	pentamidine
RT	room temperature
SALDI	surface-assisted laser desorption ionization
SEM	scanning electron microscopy
S/N	signal-to-noise
TEM	transmission electron microscopy

CHAPTER 1: INTRODUCTION AND SIGNIFICANCE

1.1 Matrix-assisted Laser Desorption Ionization (MALDI)

Mass spectrometry got its start approximately 100 years ago with Sir J.J. Thomson constructing the first mass spectrometer in order to investigate the mass-to-charge ratio of ions released through electrical discharge.[1, 2] This became an important invention to explore such ions that Thomson studied to biological samples such as tissue specimens. There have been many different mass spectrometry ionization methods used for analysis. There are hard ionization techniques, such as fast atom bombardment, that highly fragment the analyte being studied and there are also softer ionization techniques, such as matrix-assisted laser desorption ionization (MALDI) and electrospray ionization (ESI), that rarely fragment the analyte of interest. The soft ionization techniques allow the study of the intact compounds.

MALDI was first introduced in the late 1980s by Hillenkamp and Karas.[3] MALDI uses an organic matrix that helps in the ionization and desorption process. An important factor when performing MALDI is that the matrix and the analyte must co-crystallize.[4, 5] This is vital to the ionization of the analytes of interest. If the matrix and analyte don't co-crystallize well, the ionization efficiency is greatly affected. There have been different methods of matrix application studied to help with the issues of the matrix-analyte co-crystallization. Some methods that are currently used are the dried droplet method, automated deposition, and sublimation.[6-14] Each of these techniques has their own advantages. For example, automated deposition of matrix should theoretically have the most homogenous layer of matrix with the analyte of interest; whereas sublimation allows for the smallest crystal size allowing for a much higher spatial resolution compared to other matrix deposition methods. The dried droplet

method is a widely used sample preparation method. This method consists of mixing the matrix and analyte in an organic-aqueous solution. For this method, typically the matrix is thousands of times higher in concentration than the analyte. This is needed so that the matrix can effectively absorb the energy from the laser without fragmenting the analyte. This matrix-analyte solution is then spotted on the sample plate for analysis and they will co-crystallize together. One downfall to this method is that it is not very controllable in the uniformness of the crystals. If the crystals aren't uniform on the MALDI plate, this can cause a variance in the signal that is obtained at different spots of the sample leading to "sweet spots".[9, 15]

Since the introduction of MALDI, different matrices have been investigated in looking at small metabolites up to large proteins. Depending on what type of analyte is being studied, a different matrix should be used. Some common matrices that are used are ultra-fine metal powder in glycerol, carbon nanotubes, 2,5-dihydroxybenzoic acid (DHB), and α-cyano-4-hydroxycinnanic acid (CHCA); just to name a few.[9, 13, 16-26] It has been shown that some of these matrices work better for certain classes of molecules. DHB is known to be a universal matrix and is used when analyzing small molecules, small peptides, nucleotides, oligonucleotides and oligosaccharides. CHCA is a slightly larger organic matrix and is used in the study of peptides, lipids and nucleotides. It should be noted though that choosing a suitable matrix for the analyte of interest is still an empirical and time consuming process.

By using a matrix, the ionization process is dramatically softened since the matrix absorbs most of the energy from the laser instead of the molecule of interest having to absorb all the energy and fragmenting. Although the exact process of desorption and ionization is not fully understood, it is seen that when the laser irradiates the sample surface, a plume of analyte and matrix desorb into the gas phase.[27-29] The most common form of ionization is for the

analyte of interest to be protonated from the acidic nature of the matrix but it could also form a radical ion.[28] Typically the radical ion is not seen due to the high abundance of protonated species.

The exact mechanism of MALDI is still under debate in the mass spectrometry community. It is thought that the matrix serves a couple purposes; as a photon trap and a proton donor to the analyte of interest.[30] There are many factors that the desorption process for MALDI depends on such as laser intensity, matrix-analyte crystal structure and the matrix being used. There have been several models suggested to help explain the MALDI process.[12, 30-35] The two most popular models are photochemical ionization and cluster ionization mechanisms. Photochemical ionization was proposed by Ering et al. is known to be the primary model for analyte ionization in the gas phase.[34, 36] This model proposes that positive or negative analyte ions are formed by protonation or deprotonation due to colliding with a matrix ion. This process is typically described as a two-step ionization process. The first step is to produce matrix ions followed immediately by the production of analyte ions from the interaction of analyte molecules with matrix ions.[34, 37, 38] Although this process is generally accepted to explain the MALDI process, it does not fully explain such issues as matrix suppression, "sweet spots" and other experimental observations.[34] Another proposed MALDI model is the cluster ionization mechanism. This modal assumes that analyte polymers exist in the matrix environment and desorb upon laser irradiation.[27, 34, 39, 40] Once in the gas phase, analyte ions are formed by desolvation of neutral matix molecules; this is thought to be a similar process compared to ESI. Although the cluster ionization model agrees with observations seen after the MALDI process, it doesn't answer such questions as why this method produces mono-charged analytes when ESI forms multi-charged analytes.[34, 39]

Although a single model cannot be agreed upon, it is generally agreed that matrix molecules surround analyte molecules in which the matrix and analyte will co-crystallize together. When the laser irradiates the co-crystals, the matrix absorbs the energy from the laser and will convert it to thermal energy. The matrix then transfers this energy to the analyte so that they desorb from the surface. The matrix protects the analyte from being excessively heated and highly fragmented, thus making MALDI a soft ionization technique.

There are some draw-backs to the MALDI technique. There is typically strong background noise in the low molecular weight region in the mass spectrum due to the high concentration of matrix that is being used. There has been much effort put forward to try to minimize this effect. A few of the methods to decrease the background noise are matrix suppressing and using binary matrices.[41] One way to suppress the matrix noise is to adjust the ratio of matrix-to-analyte. This has been studied and shown that the smaller the analyte the smaller the matrix:analyte ratio can be and vice versa.[10] Additives to the matrix such as ammonium salts are also a common approach to suppressing matrix signal.[23, 42, 43] Binary matrices have been successfully used by mixing two matrices which suppressed the formation of matrix clusters and fragments.[44, 45] Even with these novel ways to try to reduce the matrix background noise, the success of studying small molecules is still limited. There are other approaches that can lead to more successful analysis of those small molecules.

1.2 Surface-assisted Laser Desorption Ionization (SALDI)

There has been much effort made to try to minimize the amount of background noise in the lower molecular weight range of the mass spectrum. One plausible approach is to remove the matrix from the mixture during MS analysis. Surface-assisted laser desorption/ionization

(SALDI) is a matrix-free approach that has been developed in parallel with MALDI. The first example of SALDI was done by suspending cobalt nanoparticles in glycerol to act as a matrix to detect proteins up to m/z 100,000 daltons.[16] Other materials have also been explored such as carbon nanotubes, Si, TiO_2, Au and Ag nanoparticles.[46-48] The most successful SALDI approach was reported by the Siuzdak group where they used porous silicon. This technique was coined desorption/ionization on silicon (DIOS).[49-52] This technique is matrix-free which allows for the analysis of small metabolites without the overlap and noise of matrix signal seen in conventional MALDI. Just like MALDI, SALDI is a soft ionization technique. The desorption/ionization process is still debated upon but research has supplied information on the process. One proposed model depends heavily on the high surface area of the pSi surface while another model solely focuses on the thermal mechanism.[52-56] For both models, the laser irradiates the surface allowing the thermal energy from the laser to heat the pSi surface causing it to restructure, driving the desorption process. In general, the electronic and physical properties of porous Si (pSi) has been thought to lead to desorption and ionization of the analyte of interest, specifically the low thermal conductivity, high surface area and the ability of Si to absorb UV energy.[57] When the porous surface is hit by the laser, there is rapid heating of the pores which was thought to be one of the main causes of desorption for SALDI. The laser pulse heats the pore walls causing the energy to be transferred from the pSi substrate to the analyte causing the analyte to desorb from the surface. The desorption of the analyte of interest can happen through a one of two processes. One process happens through direct desorption form the pSi surface and the other happens through a plume caused my trapped solvent molecules.[49, 58] The ionization process is thought to happen through either residual charge from the surface or from solvent-analyte interactions in the plume where the solvent acts similar to a matrix.

Other factors that play a role in ionization are pore depth, surface roughness, and the analyte's proton affinity.[49, 58, 59]

Just like most techniques, there are advantages and disadvantages to DIOS. DIOS has a significantly better sensitivity than MALDI for certain molecules. It has been seen that with DIOS, a sensitivity in the fmol range is achievable where MALDI has a sensitivity in the pmol range.[60] This increase in the sensitivity is beneficial when studying pharmaceutical compounds since typically these compounds are used in biological samples at lower concentrations in order to eliminate the risk of an overdose. A downfall to DIOS is its stability and reproducibility. DIOS is electrochemically etched using HF in ethanol. When the etching process is completed the surface of the pSi is hydride terminated. When the surface is completely hydride terminated, DIOS achieves its best detection. Although this type of surface is desired, it is easily oxidized causing the detection signal to decrease. Between different pSi wafers, the oxidation can happen at different rates causing the surface of the DIOS wafer hard to reproduce repeatedly. One way to help to reduce the oxidation step is to store the pSi wafers in ethanol until ready to analyze but as soon as the wafer is exposed to air, it will begin to oxidize.

In an attempt to further improve the ionization efficiency of SALDI, a hybrid technique was introduced called matrix enhanced surface-assisted laser desorption ionization (ME-SALDI).[61] This technique takes the advantages of both MALDI and SALDI to combine them into one technique. For ME-SALDI, a thin layer of MALDI matrix is sublimed onto the pSi surface. The matrix acts just as it would for conventional MALDI in that the matrix absorbs the laser energy then subsequently transfers that energy to the analyte allowing the analyte of interest to desorb from the pSi surface as well as provides a proton rich environment to aid in the ionization of analytes of interest. Since SALDI uses a lower laser intensity than

conventional MALDI, fewer matrix molecules desorb from the surface and the background noise is minimal which allows for the analysis of low-mass molecules. ME-SALDI has been shown to have improved MS performance over both conventional MALDI and SALDI with reduced matrix interference, little analyte fragmentation, a larger mass range than SALDI and improved analyte ionization efficiency for low-mass species.

1.3 Nanostructured Initiator Mass Spectrometry (NIMS)

Nanostructured initiator mass spectrometry (NIMS), one of the most successful SALDI techniques, was introduced in 2007 by the Siuzdak group.[62] NIMS is an extension of DIOS where the flat silicon surface is modified by electrochemically etching nano-sized pores by using dilute hydrofluoric acid (HF).[59, 60, 62-66] Because the etching conditions are different, the pores formed are smaller and deeper than those on a DIOS substrate. More importantly, a layer of "initiator" is applied after etching. The NIMS pores, approximately 10-20 nm in diameter, trap initiator molecules inside.[62, 67] Just as it is important to choose an appropriate matrix for conventional MALDI, it is just as important to choose the correct initiator for NIMS. The Siuzdak group composed a preliminary table with possible initiators that can be used for MS analysis which primarily consists of polysiloxanes, siloxanes, and silanes.[62, 67] The most used initiator thus far seems to be bis(heptadecafluoro-1,1,2,2-tetrahydrodecyl) tetramethyldisiloxane (BisF17). This highly fluorinated initiator, along with many of the other initiators on the table, are hydrophobic in nature allowing for hydrophilic analytes to adsorb onto the surface in a smaller, more concentrated area. The ionization process for NIMS isn't completely understood but it has been hypothesized that it is closely related to the acidic conditions used in the HF electrochemical etching process.[68] Meanwhile, similar to the

behavior of residual solvents in DIOS, upon heating of the surface by a laser, the initiator rapidly expands, vaporizes, and desorbs the analyte that was adsorbed onto the NIMS surface. By concentrating the analytes of interest in a small area, the ion abundance is greatly increased thus decreasing the limit of detection NIMS can obtain. NIMS has been shown to achieve detection as low as the yoctomole range.[67]

NIMS is a good technique to use when investigating low molecular weight species, such as metabolites, peptides and drugs. This is mainly due to the properties of the initiator which allows minimal background noise in the low molecular weight region. The rule of thumb for choosing an initiator for NIMS is that it should not ionize, should be transparent to the laser that is being used and should not co-crystallize with the analyte being investigated.[67, 68] This is very different from MALDI matrices in that the matrix must have strong absorption in the UV region and must co-crystallize with the analyte in an optimal fashion. Also MALDI matrices will ionize and show up in the low mass-to-charge region of the spectra; possibly overlapping the matrix with analytes of interest. With NIMS since the initiator doesn't ionize extensively, there is a very small probability of this overlap happening allowing for more extensive studies on small metabolites. Another advantage of using NIMS over conventional MALDI is the spatial resolution that can be achieved. For MALDI, the spatial resolution is dependent on the size of the matrix crystal that must co-crystalize with the analyte of interest, the homogeneity of the matrix with the sample and laser spot size.[19] There have been many methods in trying to reduce the impact of these factors so that the resolution of MALDI can be increased. Some of these methods include sublimation of the matrix onto the analyte surface, electrospray deposition, washing protocols to remove any contaminants, and development of optical lenses in order to focus the laser to smaller dimensions.[7, 19, 69] These methods have been shown to

work to a certain degree but they do require time to work out the correct parameters which in turn increases sample preparation time before analysis. For NIMS, the spatial resolution is really only dependent on the size of the laser being used for analysis which corresponds to a reduction in sample preparation time.

1.4 Mass Spectrometry Imaging (MSI)

There has always been a need and desire to study the biological make up of plants, animals, etc. By studying these biological make ups, much can be learned about the cellular structure, function and distribution of peptides and proteins. There has been much effort recently in studying tissue samples to look at peptide, lipid, and protein distribution as well as drug and small molecule distribution within tissue samples. In the past, such techniques as magnetic resonance spectroscopy imaging (MRI), positron emission tomography (PET), autoradiography and immunolabeling were used to try to map out molecules throughout the body.[70-73] These techniques typically require the molecule of interest that is being imaged to be tagged so that it can be seen using the method of choice. This tagging can lead to problems when the drug is administered into the target. The drug could behave differently since it is tagged. Also, it is hard to study the parent compound along with its metabolites when it begins to break down since the metabolite would need to have the tag attached to it in order to image the metabolite molecule. A novel and new way to study these functions is with mass spectrometry imaging (MSI). MSI started with the inception of MS but really took off when the Caprioli group first introduced the combination of MALDI and MSI in 1997.[74] After this introduction, the development and methodologies of MSI greatly expanded. It is noted that although MSI is a destructive method, the unprecedented capabilities of MSI in rapid and un-

discriminatively profiling biological species have allowed this technique to become widely used within industrial research and academia.

MSI is a label free technique that can map out numerous molecules and compounds simultaneously.[70, 71, 75-77] Since this is a label free technique, the parent molecule as well as any fragments and metabolites are able to be investigated as well. This allows a lot more information to be obtained and analyzed. MALDI-MSI has been focused primarily on protein and peptide distribution in tissue samples and has expanded to the study of lipids, sugars, etc. With this focus on mapping out tissue samples, MALDI-MSI has shown great advantages in biomarker discovery and with pharmaceutical compounds. Although pharmaceutical compounds are typically small molecules, great efforts have been put forth to improve their analysis. With the choice of appropriate matrix, these compounds have been profiled and imaged in order to study the drug effectiveness and metabolite activity.[78, 79]

One aspect of MSI that is still being worked on is the resolution. With MALDI-MSI, resolution is dependent on crystal size of the matrix as well as the size of the laser being used. One way to help with this is to use SALDI and NIMS to perform imaging on the samples. This removes the issue of crystal size of the matrix and allows the resolution to be effected by mainly the laser size. Spatial resolution is an important aspect to considering when performing MSI. Different ionization techniques as well as sample preparation requirements will yield different spatial resolutions. MALDI has reported an achievable spatial resolution between 20-125µm.[80-82] SIMS has a similar spatial resolution range at 1-100µm.[81, 82] Initial spatial resolution for SALDI using DIOS was 20-30µm but NIMS actually achieves a slightly higher resolution at 10-20µm.[82, 83] Desorption electrospray ionization (DESI) is an ambient ionization technique which has minimal sample preparation allowing for a fast through put and the spatial

resolution has recently been improved from 180-200μm down to 35μm.[82, 84] It should be noted that the lower the achievable spatial resolution wanted, the experimental time required will be much longer. Depending on what is most important for that specific experiment, a decision will have to be made either for lower spatial resolution or shorter experimental time.

Another limitation to MSI is the destructive and invasive nature of this technique. Since a laser is irradiating a tissue sample and heating is occurring in order to desorb/ionize analytes, the sample is being destroyed. Also the collection of the tissue samples is typically very invasive; they require biopsies or post-mortem collection. Other limitations that exist with MSI are variation between samples, sample preparation, and user experience. These limitations can cause the quality and reproducibility of the results obtained to differ significantly.

MSI uses an accumulation of mass spectra to help recreate an image of the area being analyzed. This happens by a laser rastering over the surface in the x-y coordinate, typically moving from left to right. Each time the laser irradiates the sample, a spectrum is accumulated at that point. All the spectra are then processed and combined in order to construct a 2D or 3D image. When constructing the images, the user is able to choose any m/z value from the spectra to see how it is distributed throughout the sample. This is a great improvement from other imaging techniques in which you can typically only look at one molecule per imaging experiment. A vital aspect to MSI is sample collection, sample handling and preparation. In order to obtain reliable MSI results, the preservation of the sample's molecular integrity is mandatory. If the sample is not handled properly, migration or redistribution of analytes in the sample can occur, causing inconsistent/unreliable mapping of the sample being analyzed. This migration of analytes can also happen when applying solvent based matrix onto the sample.

Homogenous solvent free application through sublimation has been proven to work and has subsided any concern of redistribution of analytes within the sample.

1.5 Significance in MSI of Pentamidine and its analogs for treatment of Human African Trypanosomiasis (HAT)

Human African trypanosomiasis (HAT) is a disease that effects millions of people in Africa. In the 1930s, administrations from sub-Saharan Africa came together to establish disease control programs.[85] The advent of these programs helped reduce that amount of HAT cases dramatically by screening and treating millions of people throughout Africa. As some nations began gaining their independence, the priority of maintaining those disease control programs diminished and the HAT epidemic began again. HAT is known as the sleeping sickness because it affects the central nervous system of people affected causing changes in their sleep/wake patterns.[85-89] There are two forms of this disease; *Trypanosoma brucei gambiense* is found in west and central Africa and *Trypanosoma brucei rhodesiense* is found in eastern and southern Africa.[85] *T.b. gambiense* accounts for 90% of the cases that are reported for HAT. There are also two stages to HAT. The first stage involves the parasite to invade the blood and lymphs but is typically treatable with current medication. The second stage of HAT is much harder to treat than the first stage. In the second stage, the parasite begins effecting the central nervous system by passing through the blood-brain barrier (BBB) which makes it much more difficult to treat. Currently there are four drugs that are used to treat patients with HAT. Pentamidine, suramin, eflornithine, and melarsoprol are used to treat both forms of HAT; two for the first stage and two for the second stage of HAT.[86, 88] Pentamidine has been used for over 60 years to treat the first stage of *T.b gambiense*. It is not fully known how this drug kills

the parasite but it is known that diamidines bind to DNA and causes mitochondrial dysfunction.[86] Pentamidine is typically well tolerated and has minimal adverse drug reactions. Suramin was first introduced in 1922 to treat the first stage of *T.b rhodesiense*. This drug compound has a higher activity than pentamidine which puts patients at risk for severe allergic reactions as well as other adverse drug reactions but since the treatments are short, these reactions are tolerable.[86, 88] Melarsoprol is an organoarsenic compound that is used to treat the second stage of both forms of HAT. This drug is one of the most harmful drugs that is legally administered to humans.[86] Due to the harmful nature, melarsoprol induces harsh reactions which includes a high rate of fatality. There have also been suggestions as of late of the emergence of resistance of this drug.[86, 88] Eflornithine is the only new drug to treat HAT that has been introduced in the last 50 years. It is used to treat the second stage of *T.b gambiense* and has shown a large reduction in mortality rate compared to melarsoprol.[88] There are some adverse drug reactions with eflornithine but they are much less severe than with melarsoprol.

Currently there are harsh treatments for this disease which often times leads to fatal drug reactions.[87] One requirement for drugs that can treat the second stage of HAT is that they must be able to permeate through the BBB. Although there is a reduction in the amount of HAT cases reported, there is still much effort going into synthesizing new drug compounds that will both penetrate the BBB as well as effectively treat HAT. The biggest challenge for new drug discovery is to make a safe drug with few adverse reactions that will treat both forms of HAT as well as both stages.[85] With new drugs being discovered, there is a need to analyze the drugs to make sure they are going to regions of tissue where they are expected to be in order to treat this disease. One way to analyze the drug distribution is by using MSI. MSI is a beneficial technique in that the drug will not be tagged and it will show the parent drug

compound as well as drug metabolites, proteins and lipids that the drug is being dispersed to. This will help in the discovery and trials of new drug compounds to help treat HAT.

1.6 Tandem Mass Spectrometry

With the advent of mass spectrometry and the advances in biological research, the understanding of the structural make-up of biologically relevant molecules needed to be explored. A technique that has emerged is tandem mass spectrometry (MS/MS) which elucidates structural analysis of peptides, proteins, etc. as well as pharmaceutical drugs;.[90-94] MS/MS involves the activation of a parent ion and analysis of the fragmentation ions which is used to determine structural elucidation. There are many MS/MS ion activation techniques that are used – collision-induced dissociation (CID), post-source decay (PSD), surface-induced dissociation (SID), electron capture dissociation (ECD), infrared multiphoton dissociation (IRMPD) and blackbody infrared radiative dissociation (BIRD); just to name a few.

One of the most commonly used ion activation methods is CID. This activation process involves a neutral gas molecule colliding with the parent ion of interest. Energy from this collision is transferred from the neutral gas to the parent ion; once the internal energy of the parent ion reaches its threshold, it begins fragmenting.[91, 95-97] The CID process is very dependent on the mass of both the parent ion as well as the neutral gas molecule used. Typically for CID the neutral gas that is used is either nitrogen or helium.[90] With energy transfer from one of these gases proteins/peptides mainly form b- (N-terminus) and y-type (C-terminus) fragments as well as d-type (side chain cleavages) fragments. CID can also by separated into two categories; low and high energy collisions.[90, 91, 96] Low-energy collisions are characterized as a collisional energy range from 1-100 eV and are commonly used in quadrupoles and ion

trap instruments. High-energy collisions are used in sector and TOF/TOF instruments which consist of an energy range in the kiloelectonvolts.[91]

Another widely used ion activation technique is post-source decay (PSD) which is mainly utilized with MALDI.[92-94, 98, 99] PSD has two main mechanistic pathways that lead to the fragmentation of the parent ions. The first source of activation energy happens when collisions between analytes of interest and matrix molecules occur right after the initial plume from the surface. Other collisions can also occur with residual gas molecules in the field free drift region.[92, 93] The second pathway occurs with the redistribution of internal energy which leads to fragmentation.[93] Just as with CID, PSD fragmentation does have a dependence on the size of analyte ions and matrix molecules; the larger the cross-sectional area of the ion/molecule, the higher the energy will be leading to fragments of the parent ion. Complementary to CID, b- (N-terminus) and y-type (C-terminus) fragments are seen as well as a-type (N-terminus) fragments. Due to less control over the fragmentation pattern of analytes of interest, PSD is not as practical when elucidating chemical structures of large molecules.

1.7 Motivation

The goals of this dissertation was to explore the utilization of a new hybrid pSi technique, ME-NIMS, for the detection of molecules directly from the pSi surface as well as when employing MSI. Sensitivity, reproducibility and stability data from ME-SALDI, NIMS and ME-NIMS were compared in order to determine the viability the techniques. To further improve the inter- and intra-substrate reproducibility, neat and dilute initiator studies were performed to attempt to enhance reproducibility for NIMS and ME-NIMS substrates. The spatial resolution for MALDI, NIMS and ME-NIMS was investigated for MSI. This showed

the smallest achievable spatial resolution for each technique without any instrumental modifications. This led to imaging of mouse brain samples to show lipid distribution throughout the tissue. MS/MS was utilized for identification of PTA in the absence and presence of tissue. With wanting to understand how drug compounds interact with tissue samples, MSI was employed to determine the LOD of PTA in the absence and the presence of mouse brain tissue.

1.8 References

(1) Seeley, E. H.; Caprioli, R. M. MALDI imaging mass spectrometry of human tissue: method challenges and clinical perspectives. *Trends Biotechnol* **2011,** *29* (3), 136.

(2) Falconer, I. Corpuscles, Electrons and Cathode Rays - Thomson,J.J. And the Discovery of the Electron. *Brit J Hist Sci* **1987,** *20* (66), 241.

(3) Thomson, J. J. XL. Cathode Rays. *The London, Edinburgh, and Dublin Philosophical Magazine and Journal of Science* **1897,** *44* (269), 293.

(4) Karas, M.; Bachmann, D.; Bahr, U.; Hillenkamp, F. Matrix-assisted Ultraviolet Laser Desorption of Non-volatile Compounds. *Int J Mass Spectrom Ion Processes* **1987,** (78), 53.

(5) Karas, M.; Bahr, U.; Gießmann, U. Matrix-assisted laser desorption ionization mass spectrometry. *Mass Spectrom Rev* **1991,** *10* (5), 335.

(6) Hillenkamp, F.; Karas, M.; Beavis, R. C.; Chait, B. T. Matrix-assisted laser desorption/ionization mass spectrometry of biopolymers. *Anal Chem* **1991,** *63* (24), 1193A.

(7) Baluya, D. L.; Garrett, T. J.; Yost, R. A. Automated MALDI matrix deposition method with inkjet printing for imaging mass spectrometry. *Anal Chem* **2007,** *79* (17), 6862.

(8) Hankin, J. A.; Barkley, R. M.; Murphy, R. C. Sublimation as a method of matrix application for mass spectrometric imaging. *J Am Soc Mass Spectrom* **2007,** *18* (9), 1646.

(9) Thomas, A.; Charbonneau, J. L.; Fournaise, E.; Chaurand, P. Sublimation of new matrix candidates for high spatial resolution imaging mass spectrometry of lipids: enhanced information in both positive and negative polarities after 1,5-diaminonapthalene deposition. *Anal Chem* **2012,** *84* (4), 2048.

(10) Tholey, A.; Heinzle, E. Ionic (liquid) matrices for matrix-assisted laser desorption/ionization mass spectrometry-applications and perspectives. *Anal Bioanal Chem* **2006,** *386* (1), 24.

(11) Knochenmuss, R.; Dubois, F.; Dale, M. J.; Zenobi, R. The matrix suppression effect and ionization mechanisms in matrix-assisted laser desorption/ionization. *Rapid Commun Mass Spectrom : RCM* **1996,** *10* (8), 871.

(12) Sugiura, Y.; Setou, M.; Horigome, D. Methods of Matrix Application. *Imaging Mass Spectrometry: Protocols for Mass Microscopy* **2010**, DOI:10.1007/978-4-431-09425-8_6 10.1007/978-4-431-09425-8_6, 71.

(13) Bencsura, A.; Navale, V.; Sadeghi, M.; Vertes, A. Matrix-guest energy transfer in matrix-assisted laser desorption. *Rapid Commun Mass Spectrom : RCM* **1997,** *11* (6), 679.

(14) Puolitaival, S. M.; Burnum, K. E.; Cornett, D. S.; Caprioli, R. M. Solvent-free matrix dry-coating for MALDI imaging of phospholipids. *Journal of the American Society for Mass Spectrometry* **2008,** *19* (6), 882.

(15) Trimpin, S.; Herath, T. N.; Inutan, E. D.; Wager-Miller, J.; Kowalski, P.; Claude, E.; Walker, J. M.; Mackie, K. Automated solvent-free matrix deposition for tissue imaging by mass spectrometry. *Anal Chemistry* **2010,** *82* (1), 359.

(16) Liu, Y.; Sun, X.; Guo, B. Matrix-assisted laser desorption/ionization time-of-flight analysis of low-concentration oligonucleotides and mini-sequencing products. *Rapid Commun Mass Spectrom : RCM* **2003,** *17* (20), 2354.

(17) Tanaka, K.; Waki, H.; Ido, Y.; Akita, S.; Yoshida, Y.; Yoshida, T.; Matsuo, T. Protein and polymer analyses up tom/z 100 000 by laser ionization time-of-flight mass spectrometry. *Rapid Commun Mass Spectrom : RCM* **1988,** *2* (8), 151.

(18) Ren, S. F.; Zhang, L.; Cheng, Z. H.; Guo, Y. L. Immobilized carbon nanotubes as matrix for MALDI-TOF-MS analysis: applications to neutral small carbohydrates. *J Am Soc Mass Spectrom* **2005,** *16* (3), 333.

(19) Duan, J.; Linman, M. J.; Chen, C. Y.; Cheng, Q. J. CHCA-modified Au nanoparticles for laser desorption ionization mass spectrometric analysis of peptides. *J Am Soc Mass Spectrom* **2009,** *20* (8), 1530.

(20) Altelaar, A. F. M.; Taban, I. M.; McDonnell, L. A.; Verhaert, P. D. E. M.; de Lange, R. P. J.; Adan, R. A. H.; Mooi, W. J.; Heeren, R. M. A.; Piersma, S. R. High-resolution MALDI imaging mass spectrometry allows localization of peptide distributions at cellular length scales in pituitary tissue sections. *Int J Mass Spectrom* **2007,** *260* (2-3), 203.

(21) Wu, H. P.; Yu, C. J.; Lin, C. Y.; Lin, Y. H.; Tseng, W. L. Gold nanoparticles as assisted matrices for the detection of biomolecules in a high-salt solution through laser desorption/ionization mass spectrometry. *J Am Soc Mass Spectrom* **2009,** *20* (5), 875.

(22) Shrivas, K.; Wu, H. F. Modified silver nanoparticle as a hydrophobic affinity probe for analysis of peptides and proteins in biological samples by using liquid-liquid microextraction coupled to AP-MALDI-ion trap and MALDI-TOF mass spectrometry. *Anal Chem* **2008,** *80* (7), 2583.

(23) Todd, P. J.; Schaaff, T. G.; Chaurand, P.; Caprioli, R. M. Organic ion imaging of biological tissue with secondary ion mass spectrometry and matrix-assisted laser desorption/ionization. *J Mass Spectrom : JMS* **2001,** *36* (4), 355.

(24) Kjellstrom, S.; Jensen, O. N. Phosphoric acid as a matrix additive for MALDI MS analysis of phosphopeptides and phosphoproteins. *Anal Chem* **2004,** *76* (17), 5109.

(25) McLean, J. A.; Stumpo, K. A.; Russell, D. H. Size-selected (2-10 nm) gold nanoparticles for matrix assisted laser desorption ionization of peptides. *J Am Chem Soc* **2005,** *127* (15), 5304.

(26) Lemaire, R.; Tabet, J. C.; Ducoroy, P.; Hendra, J. B.; Salzet, M.; Fournier, I. Solid ionic matrixes for direct tissue analysis and MALDI imaging. *Anal Chem* **2006,** *78* (3), 809.

(27) Moon, J. H.; Park, K. M.; Ahn, S. H.; Lee, S. H.; Kim, M. S. Investigations of Some Liquid Matrixes for Analyte Quantification by MALDI. *J Am Soc Mass Spectrom* **2015,** *26* (10), 1657.

(28) Karas, M.; Gluckmann, M.; Schafer, J. Ionization in matrix-assisted laser desorption/ionization: singly charged molecular ions are the lucky survivors. *J Mass Spectrom : JMS* **2000,** *35* (1), 1.

(29) Burton, R. D.; Watson, C. H.; Eyler, J. R.; Lang, G. L.; Powell, D. H.; Avery, M. Y. Proton affinities of eight matrices used for matrix-assisted laser desorption/ionization. *Rapid Commun Mass Spectrom: RCM* **1997,** *11* (5), 443.

(30) Knochenmuss, R. Ion formation mechanisms in UV-MALDI. *The Analyst* **2006,** *131* (9), 966.

(31) Gluckmann, M.; Pfenninger, A.; Kruger, R.; Thierolf, M.; Karas, M.; Horneffer, V.; Hillenkamp, F.; Strupat, K. Mechanisms in MALDI analysis: surface interaction or incorporation of analytes? *Int J Mass Spectrom* **2001,** *210* (1-3), 121.

(32) Johnson, R. E. Models for Matrix-Assisted Desorption by a Laser-Pulse. *Int J Mass Spectrom* **1994,** *139*, 25.

(33) Knochenmuss, R.; Zhigilei, L. V. Molecular dynamics model of ultraviolet matrix-assisted laser desorption/ionization including ionization processes. J P*hys Chem B* **2005,** *109* (48), 22947.

(34) Busch, K. L. Mechanisms of MALDI. *Spectroscopy* **1999,** *14* (10), 14.

(35) Chang, W. C.; Huang, L. C.; Wang, Y. S.; Peng, W. P.; Chang, H. C.; Hsu, N. Y.; Yang, W. B.; Chen, C. H. Matrix-assisted laser desorption/ionization (MALDI) mechanism revisited. *Anal Chim Acta* **2007,** *582* (1), 1.

(36) Bae, Y. J.; Kim, M. S. A Thermal Mechanism of Ion Formation in MALDI. *Annu Rev Anal Chem* **2015,** *8*, 41.

(37) Ehring, H.; Karas, M.; Hillenkamp, F. Role of photoionization and photochemistry in ionization processes of organic molecules and relevance for matrix-assisted laser desorption lonization mass spectrometry. *Org Mass Spectrom* **1992,** *27* (4), 472.

(38) Zenobi, R.; Knochenmuss, R. Ion formation in MALDI mass spectrometry. *Mass Spectrom Rev* **1998,** *17* (5), 337.

(39) McCarley, T. D.; McCarley, R. L.; Limbach, P. A. Electron transfer ionization in matrix assisted laser desorption/ionization mass spectrometry. *Anal Chemistry* **1998,** *70* (20), 4376.

(40) Karas, M.; Kruger, R. Ion formation in MALDI: the cluster ionization mechanism. *Chem Rev* **2003,** *103* (2), 427.

(41) Kruger, R.; Pfenninger, A.; Fournier, I.; Gluckmann, M.; Karas, M. Analyte incorporation and ionization in matrix-assisted laser desorption/ionization visualized by pH indicator molecular probes. *Anal Chem* **2001,** *73* (24), 5812.

(42) Ahn, S. H.; Bae, Y. J.; Moon, J. H.; Kim, M. S. Matrix suppression as a guideline for reliable quantification of peptides by matrix-assisted laser desorption ionization. *Anal Chem* **2013,** *85* (18), 8796.

(43) Asara, J. M.; Allison, J. Enhanced detection of oligonucleotides in UV MALDI MS using the tetraamine spermine as a matrix additive. *Anal Chem* **1999,** *71* (14), 2866.

(44) Shiau, K. J.; Hung, S. U.; Lee, H. W.; Wu, C. C. Nanodiamond-based two-step sampling of multiply and singly phosphorylated peptides for MALDI-TOF mass spectrometry analysis. *The Analyst* **2011,** *136* (9), 1922.

(45) Guo, Z.; He, L. A binary matrix for background suppression in MALDI-MS of small molecules. *Anal Bioanal Chem* **2007,** *387* (5), 1939.

(46) Feenstra, A. D.; O'Neill, K. C.; Yagnik, G. B.; Lee, Y. J. Organic–inorganic binary mixture matrix for comprehensive laser-desorption ionization mass spectrometric analysis and imaging of medium-size molecules including phospholipids, glycerolipids, and oligosaccharides. *RSC Adv.* **2016,** *6* (101), 99260.

(47) Chiang, C. K.; Chen, W. T.; Chang, H. T. Nanoparticle-based mass spectrometry for the analysis of biomolecules. *Chem Soc Rev* **2011,** *40* (3), 1269.

(48) Law, K. P.; Larkin, J. R. Recent advances in SALDI-MS techniques and their chemical and bioanalytical applications. *Anal Bioanal Chem* **2011,** *399* (8), 2597.

(49) Patti, G. J.; Woo, H. K.; Yanes, O.; Shriver, L.; Thomas, D.; Uritboonthai, W.; Apon, J. V.; Steenwyk, R.; Manchester, M.; Siuzdak, G. Detection of carbohydrates and steroids by cation-enhanced nanostructure-initiator mass spectrometry (NIMS) for biofluid analysis and tissue imaging. *Anal Chem* **2010,** *82* (1), 121.

(50) Wei, J.; Buriak, J. M.; Siuzdak, G. Desorption-ionization mass spectrometry on porous silicon. *Nature* **1999,** *399* (6733), 243.

(51) Liu, Q.; Brown, V. L.; He, L. Desorption/ionization on porous silicon (DIOS) for metabolite imaging. *Woodh Publ Ser Biom* **2014**, DOI:10.1533/9780857097156.2.270 10.1533/9780857097156.2.270(68), 270.

(52) Lewis, W. G.; Shen, Z. X.; Finn, M. G.; Siuzdak, G. Desorption/ionization on silicon (DIOS) mass spectrometry: background and applications. *Int J Mass Spectrom* **2003,** *226* (1), 107.

(53) Li, J.; Lipson, R. H. Insights into Desorption Ionization on Silicon (DIOS). *J Phys Chem C* **2013,** *117* (51), 27114.

(54) Tang, H. W.; Ng, K. M.; Lu, W.; Che, C. M. Ion desorption efficiency and internal energy transfer in carbon-based surface-assisted laser desorption/ionization mass spectrometry: desorption mechanism(s) and the design of SALDI substrates. *Anal Chem* **2009,** *81* (12), 4720.

(55) Alimpiev, S.; Nikiforov, S.; Karavanskii, V.; Minton, T.; Sunner, J. On the mechanism of laser-induced desorption-ionization of organic compounds from etched silicon and carbon surfaces. *J Chem Phys* **2001,** *115* (4), 1891.

(56) Grechnikov, A. A.; Borodkov, A. S.; Zhabin, S. N.; Alimpiev, S. S. On the mechanism of ion desorption in the process of laser desorption/ionization from silicon surfaces. *J Anal Chem* **2014,** *69* (14), 1361.

(57) Northen, T. R.; Woo, H. K.; Northen, M. T.; Nordstrom, A.; Uritboonthail, W.; Turner, K. L.; Siuzdak, G. High surface area of porous silicon drives desorption of intact molecules. *J Am Soc Mass Spectrom* **2007,** *18* (11), 1945.

(58) Arakawa, R.; Kawasaki, H. Functionalized nanoparticles and nanostructured surfaces for surface-assisted laser desorption/ionization mass spectrometry. *Analytical sciences : Int J Japan Soc Anal Chem* **2010,** *26* (12), 1229.

(59) Liu, Q.; Xiao, Y.; He, L. In *Mass Spectrometry Imaging*; Rubakhin, S. S.;Sweedler, J. V., Eds.; Humana Press, 2010; Vol. 656.

(60) Sailor, M. J. In *Porous Silicon in Practice: Preparation, Characterization and Applications* Wiley-VCH Verlag GmbH & Co. KGaA, 2011.

(61) Tuomikoski, S.; Huikko, K.; Grigoras, K.; Ostman, P.; Kostiainen, R.; Baumann, M.; Abian, J.; Kotiaho, T.; Franssila, S. Preparation of porous n-type silicon sample plates for desorption/ionization on silicon mass spectrometry (DIOS-MS). *Lab on a chip* **2002,** *2* (4), 247.

(62) Brown, V. L.; Liu, Q.; He, L. Matrix-enhanced surface-assisted laser desorption/ionization mass spectrometry (ME-SALDI-MS) for mass spectrometry imaging of small molecules. *Methods Mol Biol* **2015,** *1203*, 175.

(63) Northen, T. R.; Yanes, O.; Northen, M. T.; Marrinucci, D.; Uritboonthai, W.; Apon, J.; Golledge, S. L.; Nordstrom, A.; Siuzdak, G. Clathrate nanostructures for mass spectrometry. *Nature* **2007,** *449* (7165), 1033.

(64) Geppert, T.; Schweizer, S. L.; Gosele, U.; Wehrspohn, R. B. Deep trench etching in macroporous silicon. *Appl Phys A: Mater Sci Process* **2006,** *84* (3), 237.

(65) Lehmann, V.; Foll, H. Formation Mechanism and Properties of Electrochemically Etched Trenches in N-Type Silicon. *J Electrochem Soc* **1990,** *137* (2), 653.

(66) Smith, R. L.; Collins, S. D. Porous Silicon Formation Mechanisms. *J Appl Phys* **1992,** *71* (8), R1.

(67) Moening, T. N.; Brown, V. L.; He, L. Nanostructure-initiator mass spectrometry (NIMS) for molecular mapping of animal tissues. *Methods Mol Biol* **2015,** *1203*, 151.

(68) Woo, H. K.; Northen, T. R.; Yanes, O.; Siuzdak, G. Nanostructure-initiator mass spectrometry: a protocol for preparing and applying NIMS surfaces for high-sensitivity mass analysis. *Nature protocols* **2008,** *3* (8), 1341.

(69) Sturm, R. M.; Greer, T.; Chen, R.; Hensen, B.; Li, L. Comparison of NIMS and MALDI platforms for neuropeptide and lipid mass spectrometric imaging in C. borealis brain tissue. *Anal Methods* **2013,** *5* (6), 1623.

(70) Anderson, D. M.; Mills, D.; Spraggins, J.; Lambert, W. S.; Calkins, D. J.; Schey, K. L. High-resolution matrix-assisted laser desorption ionization-imaging mass spectrometry of lipids in rodent optic nerve tissue. *Mol Vision* **2013,** *19*, 581.

(71) Amstalden van Hove, E. R.; Smith, D. F.; Heeren, R. M. A concise review of mass spectrometry imaging. *J Chromatogr. A* **2010,** *1217* (25), 3946.

(72) Lanekoff, I.; Thomas, M.; Carson, J. P.; Smith, J. N.; Timchalk, C.; Laskin, J. Imaging nicotine in rat brain tissue by use of nanospray desorption electrospray ionization mass spectrometry. *Anal Chem* **2013,** *85* (2), 882.

(73) Cornett, D. S.; Frappier, S. L.; Caprioli, R. M. MALDI-FTICR imaging mass spectrometry of drugs and metabolites in tissue. *Anal Chem* **2008,** *80* (14), 5648.

(74) Lietz, C. B.; Gemperline, E.; Li, L. Qualitative and quantitative mass spectrometry imaging of drugs and metabolites. *Adv Drug Delivery Rev* **2013,** *65* (8), 1074.

(75) Caprioli, R. M.; Farmer, T. B.; Gile, J. Molecular imaging of biological samples: Localization of peptides and proteins using MALDI-TOF MS. *Anal Chem* **1997,** *69* (23), 4751.

(76) Chughtai, K.; Heeren, R. M. Mass spectrometric imaging for biomedical tissue analysis. *Chem Rev* **2010,** *110* (5), 3237.

(77) Eriksson, C.; Masaki, N.; Yao, I.; Hayasaka, T.; Setou, M. MALDI Imaging Mass Spectrometry-A Mini Review of Methods and Recent Developments. *Mass Spectrom (Tokyo)* **2013,** *2* (Spec Iss), S0022.

(78) Vegvari, A.; Fehniger, T. E.; Rezeli, M.; Laurell, T.; Dome, B.; Jansson, B.; Welinder, C.; Marko-Varga, G. Experimental models to study drug distributions in tissue using MALDI mass spectrometry imaging. *J Proteome Res* **2013,** *12* (12), 5626.

(79) Chandra, S.; Tjarks, W.; Lorey, D. R., 2nd; Barth, R. F. Quantitative subcellular imaging of boron compounds in individual mitotic and interphase human glioblastoma cells with imaging secondary ion mass spectrometry (SIMS). *J Microsc* **2008,** *229* (Pt 1), 92.

(80) Rubakhin, S. S.; Greenough, W. T.; Sweedler, J. V. Spatial profiling with MALDI MS: Distribution of neuropeptides within single neurons. *Anal Chem* **2003,** *75* (20), 5374.

(81) Monroe, E. B.; Annangudi, S. P.; Hatcher, N. G.; Gutstein, H. B.; Rubakhin, S. S.; Sweedler, J. V. SIMS and MALDI MS imaging of the spinal cord. *Proteomics* **2008,** *8* (18), 3746.

(82) Rubakhin, S. S.; Jurchen, J. C.; Monroe, E. B.; Sweedler, J. V. Imaging mass spectrometry: fundamentals and applications to drug discovery. *Drug Discov Today* **2005,** *10* (12), 823.

(83) Greer, T.; Sturm, R.; Li, L. Mass spectrometry imaging for drugs and metabolites. *J Proteomics* **2011,** *74* (12), 2617.

(84) Liu, Q.; Guo, Z.; He, L. Mass spectrometry imaging of small molecules using desorption/ ionization on silicon. *Anal Chem* **2007,** *79* (10), 3535.

(85) Wiseman, J. M.; Ifa, D. R.; Zhu, Y.; Kissinger, C. B.; Manicke, N. E.; Kissinger, P. T.; Cooks, R. G. Desorption electrospray ionization mass spectrometry: Imaging drugs and metabolites in tissues. *Proc Natl Acad Sci USA* **2008,** *105* (47), 18120.

(86) Simarro, P. P.; Jannin, J.; Cattand, P. Eliminating human African trypanosomiasis: where do we stand and what comes next? *PLoS Med* **2008,** *5* (2), e55.

(87) Brun, R.; Don, R.; Jacobs, R. T.; Wang, M. Z.; Barrett, M. P. Development of novel drugs for human African trypanosomiasis. *Future Microbiol* **2011,** *6* (6), 677.

(88) Sturk, L. M.; Brock, J. L.; Bagnell, C. R.; Hall, J. E.; Tidwell, R. R. Distribution and quantitation of the anti-trypanosomal diamidine 2,5-bis(4-amidinophenyl)furan (DB75) and its N-methoxy prodrug DB289 in murine brain tissue. *Acta tropica* **2004,** *91* (2), 131.

(89) Brun, R.; Blum, J.; Chappuis, F.; Burri, C. Human African trypanosomiasis. *Lancet* **2010,** *375* (9709), 148.

(90) Yang, S.; Wenzler, T.; Miller, P. N.; Wu, H.; Boykin, D. W.; Brun, R.; Wang, M. Z. Pharmacokinetic comparison to determine the mechanisms underlying the differential efficacies of cationic diamidines against first- and second-stage human African trypanosomiasis. *Antimicrob Agents Chemother* **2014,** *58* (7), 4064.

(91) Mitchell Wells, J.; McLuckey, S. A. Collision-Induced Dissociation (CID) of Peptides and Proteins. *Biol Mass Spectrom* **2005,** *402*, 148.

(92) Sleno, L.; Volmer, D. A. Ion activation methods for tandem mass spectrometry. *J Mass Spectrom : JMS* **2004,** *39* (10), 1091.

(93) Spengler, B. Post-source decay analysis in matrix-assisted laser desorption/ionization mass spectrometry of biomolecules. *J Mass Spectrom* **1997,** *32* (10), 1019.

(94) Kaufmann, R.; Kirsch, D.; Spengler, B. Sequencing of peptides in a time-of-flight mass spectrometer: evaluation of postsource decay following matrix-assisted laser desorption ionisation (MALDI). *Int J Mass Spectrom Ion Processes* **1994,** *131*, 355.

(95) Purcell, A. W.; Gorman, J. J. The use of post-source decay in matrix-assisted laser desorption/ionisation mass spectrometry to delineate T cell determinants. *J Immunol Methods* **2001,** *249* (1-2), 17.

(96) Johnson, A. R.; Carlson, E. E. Collision-Induced Dissociation Mass Spectrometry: A Powerful Tool for Natural Product Structure Elucidation. *Analy Chem* **2015,** *87* (21), 10668.

(97) Ortiz, D.; Martin-Gago, P.; Riera, A.; Song, K.; Salpin, J. Y.; Spezia, R. Gas-phase collision induced dissociation mechanisms of peptides: Theoretical and experimental study of N-formylalanylamide fragmentation. *Int J Mass Spectrom* **2013,** *335*, 33.

(98) Cooks, R. G. Collision-Induced Dissociation - Readings and Commentary. *J Mass Spectrom* **1995,** *30* (9), 1215.

(99) Spengler, B.; Kirsch, D.; Kaufmann, R. Fundamental-Aspects of Postsource Decay in Matrix-Assisted Laser Desorption Mass-Spectrometry .1. Residual-Gas Effects. *J Phys Chem-Us* **1992,** *96* (24), 9678.

(100) Al-Saad, K. A.; Siems, W. F.; Hill, H. H.; Zabrouskov, V.; Knowles, N. R. Structural analysis of phosphatidylcholines by post-source decay matrix-assisted laser desorption/ionization time-of-flight mass spectrometry. *J Am Soc Mass Spectrom* **2003,** *14* (4), 373.

CHAPTER 2: COMPARISON OF POROUS SILCON (PSI) TECHNIQUES FOR MASS SPECTROMETRY IMAGING (MSI) APPLICATIONS

2.1 Introduction

Mass spectrometry sensitivity and reproducibility relies heavily on the ionization technique used while collecting data. Matrix-assisted laser desorption/ionization (MALDI) is a reliable technique but has been challenging for the study of small metabolites due to suppression by the matrix used. A technique developed in parallel with MALDI, surface-assisted laser desorption/ionization (SALDI), has demonstrated success in investigating small molecules in a matrix-free fashion. Desorption ionization on silicon (DIOS) is one of the most successful SALDI techniques developed. DIOS uses porous silicon (pSi) substrates to aid in the desorption and ionization of analytes of interest with detections limits reported as low as zeptomole to yoctomole range but typically are seen in the high attomole to low femtomole range.[1-4] A systematic study showed the important roles played by both the substrate and local chemical environment in analyte desorption and ionization during DIOS.[4, 5] This led to the introduction of matrix-enhanced SALDI (ME-SALDI), a hybrid technique that combines the advantages of MALDI and SALDI.[5] ME-SALDI uses a thin layer of matrix on top of a pSi substrate to provide a proton rich environment increasing the ionization efficiency of the analyte of interest. Another technique was introduced by Siuzdak and co-workers coined nanostructured initiator mass spectrometry (NIMS). NIMS builds on the original SALDI method and utilizes a liquid initiator coating to facilitate local concentrating of analytes of interest. Like SALDI and ME-SALDI, NIMS relies on a porous substrate to absorb the laser energy which rapidly heats the porous surface, vaporizing “trapped” initiator molecules in the

porous structures. This rapid vaporization of the initiator molecules subsequently facilitates the desorption/ionization process for analytes under study with minimal fragmentation.[6]

ME-SALDI has become a technique that is viable for the analysis of small molecules due to the reduced noise in the low m/z region. ME-SALDI utilizes a thin layer of matrix which greatly increase the ionization efficiency of the SALDI technique by providing a proton rich environment while still utilizing the pSi to absorb photons for an effective desorption of the analytes of interest.[4, 7, 8] ME-SALDI yields clean spectra in the low mass range while still enhancing analyte signal. This technique has shown the improved signal of biomolecules.[4, 8, 9] Although ME-SALDI does have its advantages of traditional MALDI, it does still use a matrix which can suppress signal and the size of the matrix crystal plays critical role in analyte signal and reproducibilty.[4, 7, 8, 10] Mentioned earlier, NIMS is another matrix free technique that was introduced to help with the analysis of small molecular weight species. NIMS utilizes an initiator to aid in the desorption and ionization process. The initiator is typically a group of highly fluorinated, UV-transparent, and Teflon-like molecules.[3, 11-13] The utilization of this technique has been investigated by looking at biological samples.[3, 14-18] One major advantage to using NIMS is that no matrix is used with this technique allowing for the analysis of low molecular weight species[11-15, 18-20]; this is beneficial over techniques such as MALDI and ME-SALDI where the matrix overlaps and/or suppresses signal from analytes of interest. Another advantage of NIMS is that there is little to no sample preparation needed before analysis. This allows for a higher throughput of samples while still retaining information that may be lost with tissue or other biological extraction methods.[16, 18] NIMS does have a similar issue to SALDI in that the ionization efficiency is low. The application of matrix to the NIMS surface is demonstrated for the first time in this report; coined matrix-enhanced NIMS (ME-NIMS).

The advantages of both MALDI and NIMS were combined, similar to ME-SALDI, in that a thin layer of matrix was sublimed onto the NIMS surface. The pSi surface and initiator are still used to absorb photons from the laser to aid in the desorption process while the matrix provides a proton rich environment for enhanced ionization. ME-NIMS has experimentally shown an improvement in MS performance to traditional MALDI and NIMS; including increased ionization efficiency and reduced matrix interference.

With this being the first mention of ME-NIMS in literature, it is vital to compare this technique to more established techniques such as ME-SALDI and NIMS. In order to determine which technique is optimal for biological molecules of interest, a systematic comparison of ME-SALDI, NIMS, and ME-NIMS was completed for their potential analysis of different classes of analytes of interest. Parameter optimization for signal detection on n-type and p-type pSi was conducted as well as the reproducibility and stability of the substrates.

2.2 Material and Method

Materials N-type antimony (Sb)-doped <100> single crystalline silicon (Si) wafers at 0.005-0.02 Ω/cm and p-type boron (B)-doped, <100> single crystalline Si wafers at 0.005-0.02 Ω/cm resistivity were purchased from Silicon Sense, Inc. (Nashua, NH). Chloroform, hydrofluoric acid (HF, 49%), and sulfuric acid (H_2SO_4) were purchased from Fisher Scientific (Pittsburg, PA). Ethanol (95%) was purchased from Aaper Alcohol (Shelbyville, KY). Hydrogen peroxide 30% (w/w) (H_2O_2) was purchased from VWR International, LLC. (Bridgeport, NJ). Bis(heptadecafluoro-1,1,2,2-tetrahydrodecyl)tetramethyldisiloxane (BisF17) initiator was purchased from Gelest, Inc. (Morrisville, PA). Angiotensin I, angiotensin III, bradykinin, and

2,5-Dihydroxybenzoic acid (DHB) was purchased from Sigma-Aldrich (St. Louis, MO). 18 MΩ deionized (DI) H_2O (Millipore, PO) was used for all experiments.

SALDI Substrate Fabrication SALDI substrates were prepared based on a previously established protocol.[21] Briefly, unless otherwise noted, all wafers were washed thoroughly in ethanol and dried with N_2 after each step in the procedure. A 1.5-cm^2 silicon wafer was dipped in a 5% HF/ethanol solution for 1 min to remove the oxidized layer on the silicon surface (Figure 2.1).[7] After assembling the anodic etching Teflon cell the wafer was electrochemically etched in a 25% HF/ethanol solution (1:1 v/v) for 1 min at a current density of 5.5 mA/cm^2, whereby a 50 W tungsten lamp was used as the illumination source and a EG&G Princeton Potentiostat Model 273 (Princeton, NJ) was used to control the constant current. The resulting pSi substrate was then dipped in a 15% H_2O_2/ethanol (1:1 v/v) solution for 1 min to oxidize the silicon surface, followed by a 1 min dip in the 5% HF/ethanol solution to regenerate the H-terminated surface (i.e. double etch). SALDI substrates were stored in ethanol at room temperature and were used within 3 days of initial fabrication, unless otherwise specified in the text.

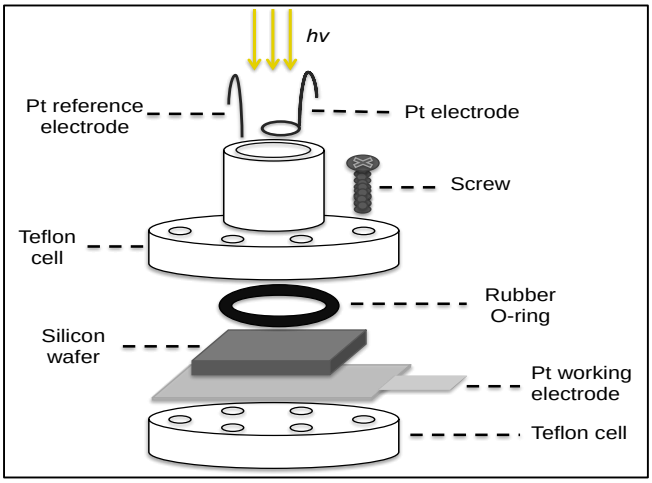

Figure 2.1: Depiction of Teflon etching cell used to make pSi substrates.

NIMS Substrate Fabrication NIMS substrates were prepared using a modified protocol reported in literature.[22] Briefly, a 1.5-cm^2 silicon wafer was cleaned in piranha solution containing a 2:1 (v/v) ratio of H_2SO_4 and H_2O_2 for 30 min, thoroughly washed in 18 MΩ DI H_2O and dried with N_2. The wafer was electrochemically etched for 30 min without additional light illumination in a 25% HF/ethanol solution with an applied current density of 32 mA/cm^2 or 48 mA/cm^2 for n-type and p-type Si, respectively. After etching, the prepared pSi substrate was washed thoroughly in ethanol, dried with a stream of N_2 and then dried in a 100˚C oven for 5 min. A neat solution of BisF17 (33 µL) was pipetted onto the pSi and allowed to soak for 30 min at room temperature (RT) to form the initiator coating. Excess initiator was removed from the pSi by applying a high-flow stream of N_2, followed by a 3-5 s drying period in a 100˚C oven; this was repeated 3 times in order to sufficiently remove excess initiator solution. NIMS substrates were stored dry in a closed petri dishes at room temperature and were used within 3 days of initial fabrication, unless otherwise specified in the text.

Matrix-Enhanced (ME)-SALDI and ME-NIMS Substrate Fabrication ME-SALDI substrates and ME-NIMS substrates were prepared using the aforementioned conditions for the respective substrate type. A thin layer of matrix was then thermally deposited on the substrate in a sublimation chamber (Figure 2.2).[7] Approximately 1 g of DHB was added and evenly spread on the bottom of the sublimation chamber. Using double-sided tape, a pSi substrate was attached upside down to the bottom of the condenser that was in direct contact with running water for cooling. An Edwards E2M8 vacuum pump with a vacuum meter was used to provide a controlled vacuum environment in the sublimation chamber. After maintaining the sublimation chamber for 2 min at approximately 50 torr, the apparatus was

submerged into a 110˚C oil bath for 1.5 min for ME-SALDI and 3 min for ME-NIMS. Under these temperature and vacuum conditions, DHB immediately vaporized and re-deposited upon contact with the pSi substrate. Once matrix deposition was completed, the sublimation apparatus was removed from the oil bath and the vacuum was slowly released. Substrates coated with matrix were removed from the apparatus and immediately loaded into the MS sample chamber for analysis.

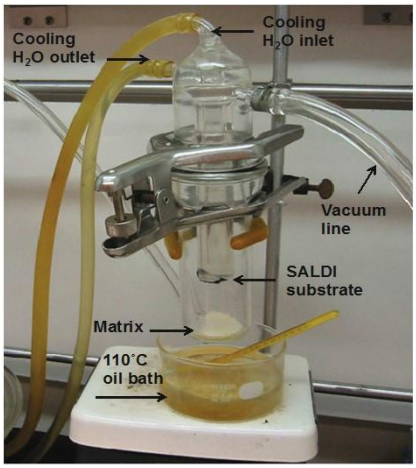

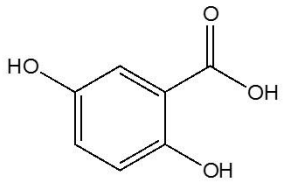

2,5-dihydroxybenzoic acid
(DHB)

Figure 2.2: Picture of matrix sublimation apparatus and the chemical structure of DHB that was used for the conventional MALDI resolution studies.

Sample Preparation for MS Measurements Stock solutions of angiotensin I, angiotensin III, and bradykinin were prepared in 50:50 acetonitrile (ACN): DI water at 12.5µM each. An aliquot of each were then mixed at a 1:1:1 (v/v) ratio to reach a final concentration of approximately 4.2µM. For ME-SALDI and ME-NIMS, the analyte solution was applied to the wafer via drop-coating and allowed to dry before sublimation occurred. After sublimation, the samples were loaded in the MS chamber. For NIMS, the peptide solution was drop-coated onto the wafer, allowed to dry, and loaded into the MS chamber. Tissue samples were cut 5µm thick using a Leica CM1950 cyrostat. The tissue section was placed on pSi surface. For NIMS, the

sample was loaded into the MS chamber; for ME-NIMS, matrix was sublimed then loaded into MS chamber.

Scanning Electron Microscopy (SEM) Measurements A JEOL JSM-6400F field-emission scanning electron microscope (FE-SEM) with an Everhart-Thornley secondary electron detector was used to examine the surface features of the pSi substrates. An accelerating voltage of 1 kV and a working distance of ~4 mm was used during the image acquisition. The magnification was varied between 500X and 500,000X to gain the best image contrast for each substrate. All substrates were attached to an aluminum block with double-sided conductive tape prior to loading into the instrument. Most substrates were imaged directly for top-down analysis; some substrates were also cleaved in half in order to attain cross-section images of the porous features. Approximately 20 pores and cross-sections from each pSi surface were chosen to measure the relative size distribution of the electrochemically-etched features.

MS Measurements An AB Sciex TOF/TOF™5800 System mass spectrometer (Framingham, MA) equipped with a 349 nm laser (Nd:YAG, 1000 Hz) was operated at an accelerating voltage of 20 kV in the reflector positive ion mode (MS-only) for all experiments. For sample spot analysis, the delay time was varied between 13.5 and 15.2 ns to achieve optimal MS performance. A mass range of 50-2000 Da (± 0.05) and a bin size of 0.5 ns was used for all experiments. The laser intensity was varied between 4300 and 5300 to achieve optimal signal acquisition for the DPPC ions. The number of shots collected per spectrum was varied between 50-500 depending upon the pSi substrate being used. The signal-to-noise (S/N) ratios and absolute ion intensities for base ions in each spectrum were calculated using the manufacturer

software. In MS imaging mode, all mass spectra were collected in an automatic MS control mode using the AB Sciex TOF/TOF Imaging software; 50-500 laser shots, as specified in the text, were averaged to yield one accumulated spectrum at each location. Mass spectra were reconstructed into 2D ion maps using the MSiReader™ software.[23]

2.3 Results and Discussion

2.3.1 pSi Substrate Fabrication

The standard and most straightforward approach to producing pSi is through galvanostatic etching.[24] To fabricate pSi, two main starting materials can be chosen: n-type or p-type silicon, which can be differentiated according to their dopant. As a Group IV element, Si possesses four electrons that have the ability to bond to four adjacent atoms; dopants are substitutional impurities that are intentionally added to replace Si atoms, ultimately affecting the electrical and conductive behavior of the bulk material. N-type Si is doped with Group V elements such as phosphorus, arsenic, or antimony. When a Group V element is substituted in for a Si atom, only four of the five electrons from the impurity atom can participate in bonding with adjacent Si atoms. Thus an extra non-bonding electron is present in the lattice, which can be considered a free or conducting electron. P-type Si is doped with Group III elements such as boron, aluminum, or gallium. Contrary to n-type dopants, Group III elements introduce electron deficiencies (holes) into the bonding lattice due to their three-electron valency. For n-type Si, illumination or high electric field can be used to generate holes and electrochemically etch pores into the surface; these conditions are not necessary for p-type Si as the material is already electron deficient. N-type and p-type Si were used in parallel due to their commercial availability at similar doping levels. The conditions, well-established in literature, were

optimized for the preparation of SALDI and NIMS substrates (Table 2.1). Although comparable ion extracting efficiencies are expected from n- and p-type substrates because of their similar resistivities, our previous studies have shown that the overall pSi performance is directly related to the substrate porosity which varies as the preparation conditions change (e.g. current density and etching time).[25] Direct inspection of the pSi substrates is therefore the first step to ensure substrate performance: for the n-type SALDI, a dark blue hue is typically indicative of porous trenches being formed on the substrate surface (Figure 2.3A). After etching the p-type SALDI under the same condition, however, the surface was bright yellow in color (Figure 2.3B). Etching of n-type NIMS yielded a dark blue surface; etching of p-type NIMS, on the other hand, yielded a light blue porous surface. Since it is known that the optical property of a pSi wafer is dictated by its surface porosity, we therefore suspect that the different substrate colors observed positively correlate to certain pore formation characteristics. SEM images of the pSi are shown in Figure 2.4.

Table 2.1: A Summary of Experiment Conditions for ME-SALDI, NIMS, and ME-NIMS substrates.

	ME-SALDI		**NIMS**		**ME-NIMS**	
	n-type	**p-type**	**n-type**	**p-type**	**n-type**	**p-type**
Piranha clean	✓	✓	✓	✓	✓	✓
5% HF wash	✓	✓	×	×	×	×
Etch time (min)	1	1	30	30	30	30
Current density (mA/cm^2)	5.5	5.5	32	48	32	48
Matrix sublimation (min)	1.5	1.5	×	×	1.5	1.5
Initiator application (min)	×	×	30	30	30	30
Storage	ethanol*		air		air	

*Prior to matrix deposition, ME-SALDI are stored in ethanol to avoid surface oxidation. After sublimation, substrates are immediately analyzed in the instrument.

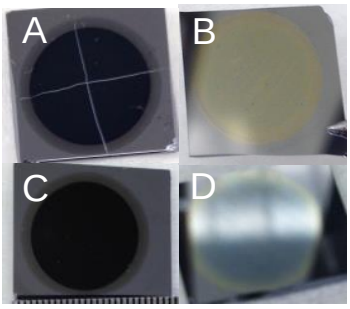

Figure 2.3: Optical images depicting the porous surface color of n-type SALDI (A), p-type SALDI (B), n-type NIMS (C) and p-type NIMS (D) substrates.

SEM was used to determine the average pore diameter and pore depth for each pSi substrate. SEM images of p-type SALDI indicated that a lack of pore formation occurred when etching conditions were applied (Figure 2.4B and Figure 2.4F); this result supports the prior suspicion that the yellow substrate color was suggestive of poor pore formation.[7] Pore formation was observed for n-type SALDI as the etching generated a surface possessing a dark blue hue. With respect to n-type SALDI (Figure 2.4A and Figure 2.4E) and n-type NIMS (Figure 2.4D and Figure 2.4H), it is clearly evident that the longer etching time leads an increase in pore depth as the NIMS substrate has a porous layer more than 15 times as thick as to the SALDI substrate. The stark differences observed for the ordering of the porous channels within each pSi substrate was also interesting. N-type SALDI resulted in randomly distributed pores with an average pore diameter of 9 ± 2 nm. It has been well documented in literature that in electrochemical dissolution of Si, random distributions of pores, as with n-type SALDI, are typically observed at lower applied current densities due to their location in the pore formation regime in current-voltage plots.[26] Since illumination-assisted etching generates holes at a much faster rate than etching in the dark, the process is difficult to control and leads to the generation of random surface features.[27] In contrast, n-type NIMS had an average pore diameter of 17 ± 6 nm and exhibited extremely narrow and highly ordered porous channels (Figure 2.4H).

Furthermore, the ordered porous channels in n-type NIMS were branched and had a "feather-like" appearance, which was found to be unique to only these types of substrates. These features should be kept in mind as they may play an important role in substrate performance in MS studies. P-type NIMS displayed larger pore depths in comparison to n-type NIMS. Since p-type silicon readily etches in the absence of light, this did not come as a surprise. P-type NIMS also had ordered pore channels, however, they were not as tightly packed as its n-type counterpart (Figure 2.4G). Additionally, features within the pore channels were more jagged in appearance which likely attributed to the lighter surface color and drop in observed signal-to-noise. The highly ordered porous channels seen in both n-type and p-type NIMS can be explained by preferential pore propagation in the <100> direction, which is the crystallographic orientation in both substrates.[24, 26] The "feather-like" branching found in the n-type NIMS has been observed in the literature and has been explained to result from anodizing highly doped n-type silicon in the dark.[27] Table 2.2 summarizes the pore size measured for each pSi substrate. Based on the optical and SEM characterization and the previous correlation of SEM images to MS performances, n-type Si was selected for further comparison studies.

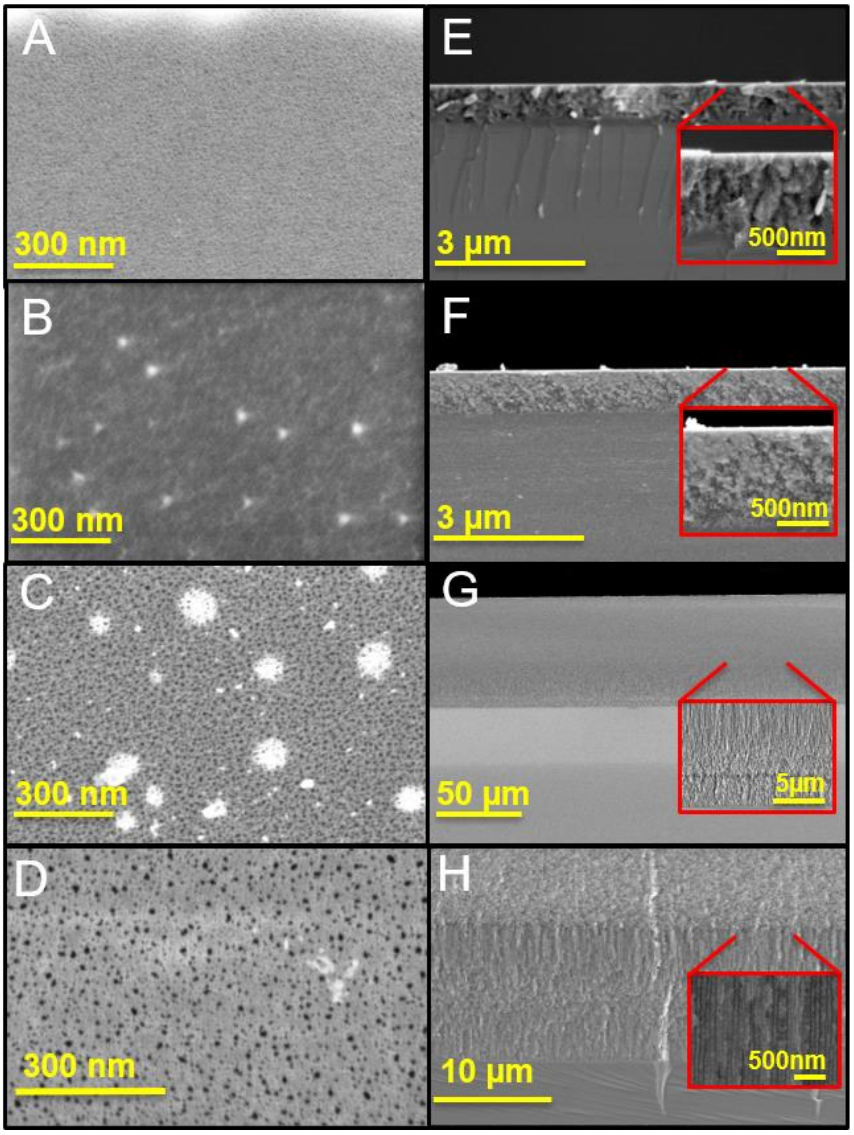

Figure 2.4: Top-down SEM images of n-type SALDI (A), p-type SALDI (B), p-type NIMS (C) and n-type NIMS (D). Cross-section images for n-type SALDI, p-type SALDI, p-type NIMS and n-type NIMS are shown in panels (E), (F), (G) and (H) respectively. Insets in panels (E) through (H) display a zoomed in view of the porous channels.

Table 2.2: Summary of pore features for SALDI and NIMS substrates.

Substrate Type	Average Pore Diameter (nm)	Average Pore Depth (μm)
n-type SALDI	9 ± 2	0.97 ± 0.06
p-type SALDI	-	1.06 ± 0.03
n-type NIMS	17 ± 6	15.7 ± 0.2
p-type NIMS	14 ± 2	45 ± 1

2.3.2 Comparison of n-type ME-SALDI, NIMS, and ME-NIMS

Three crucial parameters were used to evaluate ME-SALDI, NIMS and ME-NIMS performances in MS: signal sensitivity, reproducibility across different substrates and stability of substrates after extended storage. Signal sensitivity was the first and foremost to be studied because it directly relates to the amount of information collectable from complex samples where many important metabolic regulators are present at low concentrations. Before the sensitivity study was performed, the optimized sublimation time for ME-NIMS was carried out; ME-SALDI matrix sublimation optimization was performed previously in our lab. For this experiment, seven NIMS wafers were prepared. One wafer did not have any matrix sublimed on to it; the other six wafers had matrix sublimed with varying times from 0.5-3.0 min. The goal was to find an optimized sublimation time to utilize the advantages of both NIMS and traditional MALDI. Figure 2.5 shows the absolute ion abundance for peptides with varied sublimation times. It's interesting to notice that up to 2.5 min sublimation, the signal from the matrix is minimal compared the signal from the analytes. This is advantageous moving forward; this allows matrix to be utilized to increase ionization efficiency without the matrix suppressing signal from low molecular weight analytes of interest. The transition from traditional NIMS to ME-NIMS was determined to be at 1.0 min sublimation time. At this time point, there is an increase in analyte signal which continues to increase up to 2.0 min

sublimation time. The 2.5 min sublimation time is another transition from ME-NIMS to traditional MALDI. At this time point the signal drops but another interesting note that must be made is that the laser intensity of the instrument had to be increased when analyzing the 2.5 and 3.0 min substrates. It can be seen that at 1.5 and 2.0 min sublimation times, that the absolute ion abundance is very similar but for the 2.0 min time point, the standard error was slightly smaller. Due to this smaller standard error for the 2.0 min sublimation time, it was determined to be the optimal sublimation time and will be used for ME-NIMS sublimation times going forward, unless specifically stated.

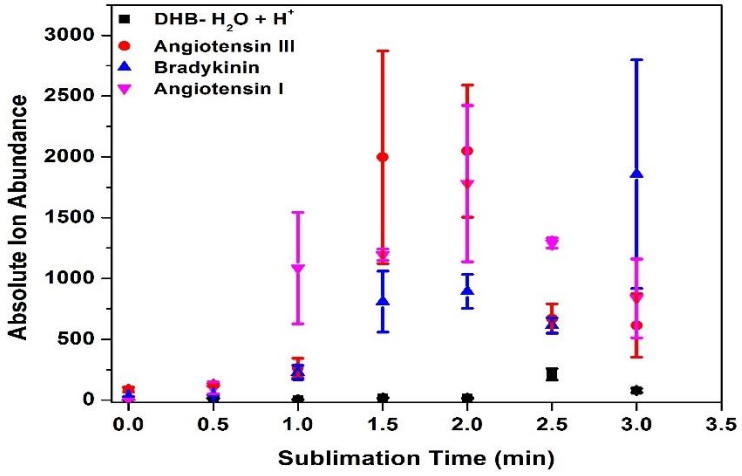

Figure 2.5: Optimized sublimation time for ME-NIMS on peptide solution. NOTE: sublimation times 2.5 and 3.0 required a higher laser intensity in order to obtain signal.

Figure 2.6 shows the absolute ion intensities and signal-to-noise ratios of the molecular ion peaks of three basic peptides. The error bars were calculated from 3 replicates. The absolute ion abundance for both ME-SALDI and ME-NIMS were greatly increased compared to NIMS, which was expected because the matrix provides a proton rich environment enhancing ionization of analytes of interest (Figure 2.6A). Meanwhile, ME-SALDI and ME-NIMS spectra showed a significant increase in background noise due to the presence of matrix

whereas NIMS exhibited cleaner spectra with an improved signal-to-noise ratio for the MH^+ detected (Figure 2.6B). Matrix peaks can be seen in both the ME-SALDI and ME-NIMS spectra, although ME-NIMS yields less signal from the matrix (Figure 2.7). The NIMS spectrum is clean in the low m/z range allowing for the analysis of small analytes of interest, but it should be noted that since the absolute ion abundance for NIMS is much lower, the analytes of interest need to be easily ionizable in order to be detected. Overall, ME-NIMS yields comparable signal-to-noise and higher absolute ion abundance to conventional NIMS. All three substrates showed significantly stronger absolute ion signals and signal-to-noise ratios than those collected from SALDI alone (not shown).

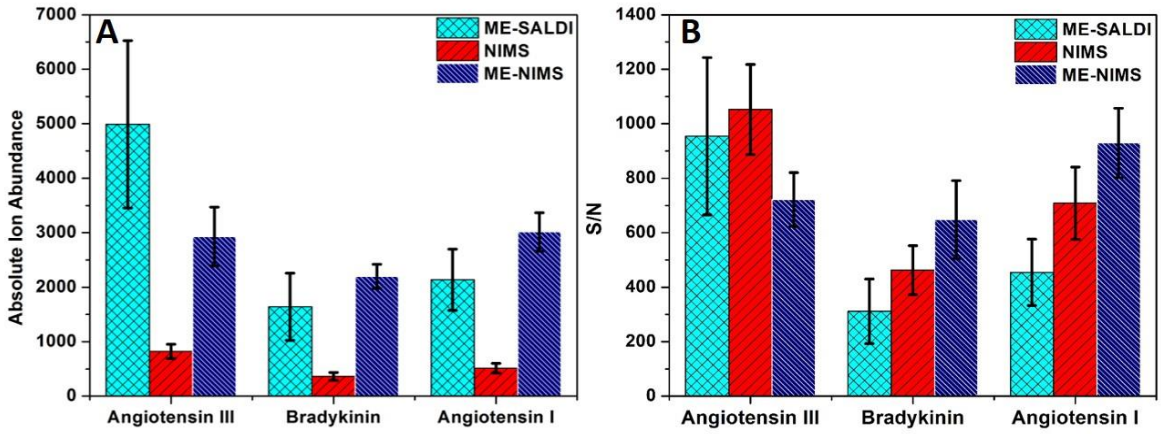

Figure 2.6: Absolute ion abundance (A) and signal-to-noise (B) comparison between ME-SALDI, NIMS and ME-NIMS.

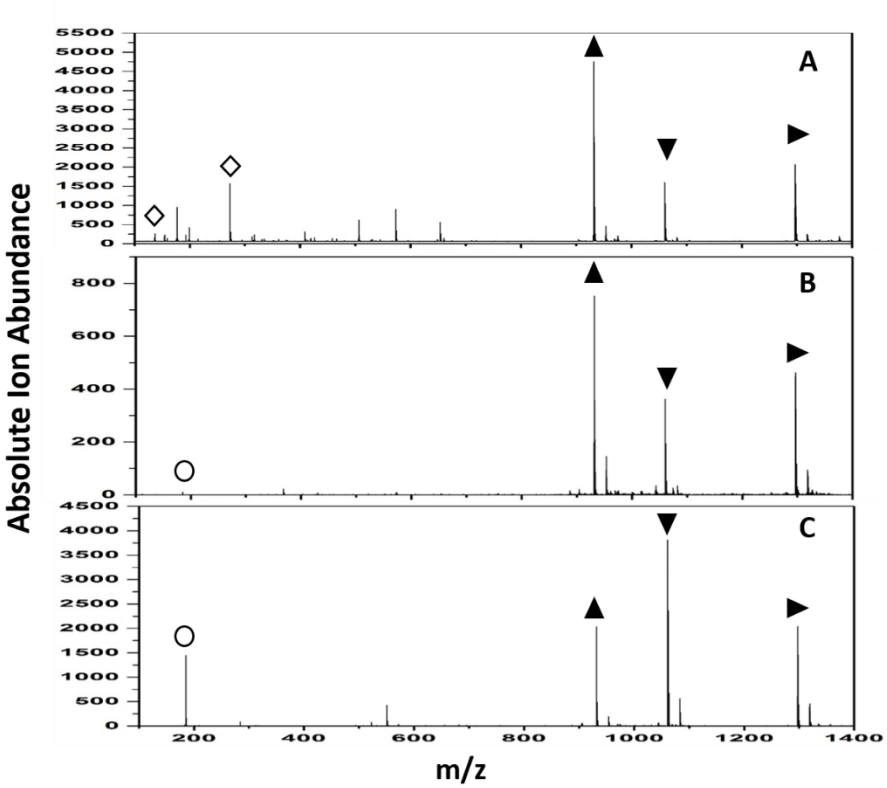

Figure 2.7: Mass spectra from peptide analysis for ME-SALDI **(A)**, NIMS **(B)**, and ME-NIMS **(C).** Concentration of all peptides were nominally $3.33x10^{-2}$ mM. Laser intensity for ME-SALDI, NIMS and ME-NIMS was 4300, 3500, and 3600, respectively. 50 total laser shots were accumulated to make each spectrum. Angiotensin III (▲), Bradykinin (▼) and Angiotensin I (►) are seen for all three techniques tested. Matrix peaks (◊) can be seen in the ME-SALDI spectrum. ME-NIMS yields signal from what is thought to be an initiator fragment (○).

Reproducibility of the substrates being used is another important factor to be considered in mass spectrometry, both within and between substrate batches. If the substrates cannot be reproducibly made, then the data collected will not be reliable and quantification cannot be consistently carried out. Five independently prepared substrates prepared on different days were examined for ME-SALDI, ME-NIMS and NIMS. For each substrate, four measurements were collected and averaged to determine the average signal-to-noise within the same batch; the inter-substrate reproducibility was carried out by measuring substrate performance across five set of substrates prepared on different days (Figure 2.8). The inter-

substrate variation of NIMS and ME-NIMS exhibited similar variations, suggesting that they are more consistent from batch-to-batch than ME-SALDI (Table 2.3). Within the same substrates, NIMS shows the smallest intra-substrate variations compared to ME-SALDI and ME-NIMS. Together, our results suggest the inter-substrate reproducibility is dictated by the nature of the substrate itself but the intra-substrate reproducibility is by the uniformity of the matrix deposition. These observations are not as expected: it has previously been shown that the performance of SALDI and ME-SALDI substrates are highly dependent on substrate fabrication conditions and large variations have been observed from batch to batch, from lab to lab. The better substrate reproducibility from different preparation in NIMS and ME-NIMS stems from the formation of high density, highly ordered, nanometer pores. The consistent average pore size and distribution under the laser beam (in the scale of tens of microns) helps in transferring the laser energy consistently from the substrate to the analytes.[28] Uneven surface oxidation prior to MS measurements could be another plausible cause for low reproducibility of conventional SALDI substrates – pSi surface oxidizes rapidly even when the substrate is immediately used after fabrication; meanwhile, for NIMS/ME-NIMS, the substrate surface is protected with a layer of highly fluorinated initiator coating that minimizes surface oxidation from exposure to air.

Table 2.3: Table of RSD% for reproducibility of ME-SALDI, NIMS and ME-NIMS substrates.

Peptide	ME-SALDI RSD%	NIMS RSD%	ME-NIMS RSD%
Angiotensin III	**41.4**	**27.5**	**28.3**
Bradykinin	**42.5**	**24.5**	**33.8**
Angiotensin I	**43.0**	**24.3**	**28.4**

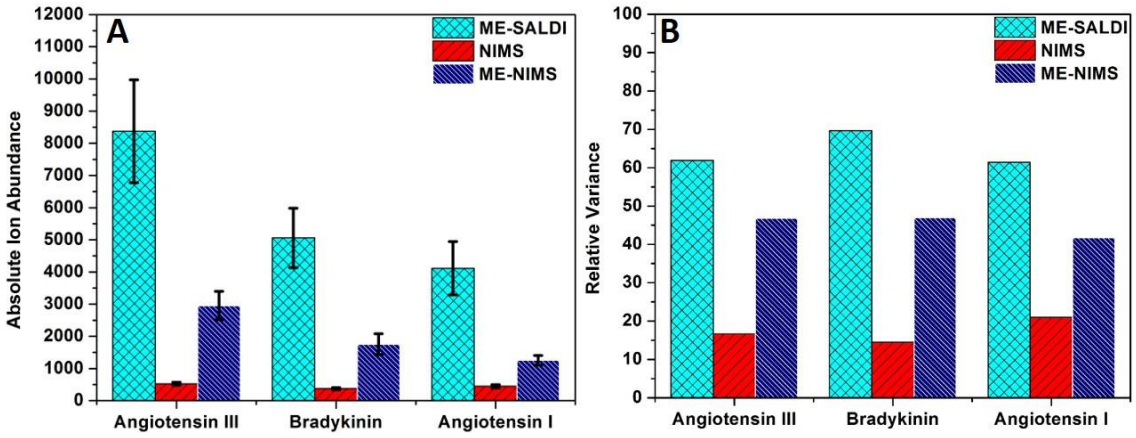

Figure 2.8: The inter-substrate reproducibility **(A)** and intra-substrate variance **(B)** of ME-SALDI, NIMS and ME-NIMS. Concentration of all peptides were nominally 3.33×10^{-2} mM. Laser intensity for ME-SALID, NIMS, and ME-NIMS was 4300, 3500, and 3700, respectively. The error bars for **(A)** were calculated by determining the standard error of five replicates. The relative variation was calculated from five different locations on the same substrate for ME-SALDI, NIMS, or ME-NIMS **(B)**.

The stability of the pSi substrate is another important aspect that is critical for reliable MSI measurements. A substrate stability study was performed over a two-week time frame (Figure 2.9). Substrates were made on different days and stored for 0, 3, 7, 10 or 14 days. All ten substrates were spotted with the peptide solution and allowed to dry before MS analysis. NIMS shows a much more consistent signal-to-noise ratio over the time frame. ME-SALDI on the other hand shows a steady decline in performance over the two-week time period. Similar to previous observations, the measurement errors are much larger from the ME-SALDI substrates compared to those of NIMS substrates. The relatively consistent MS response from NIMS in both the stability study as well as the reproducibility study are thought to be the result of reduced oxidation from the initiator-coated surface. It has been previously reported that the more hydrophobic the surface, the better the signal that can be achieved.[1] When the surface is oxidized, it becomes less hydrophobic allowing analytes in aqueous solutions to spread across

the substrate surface decreasing the localized concentration of analytes of interest. This will cause performance deterioration as well as inconsistencies within data especially when there are different degrees of oxidation between substrates and within the same substrate. ME-NIMS was not investigated here but is expected to exhibit similar shelf-life stability as NIMS since it is speculated that the NIMS initiator serves as a protecting layer for the pSi substrate from oxidation.

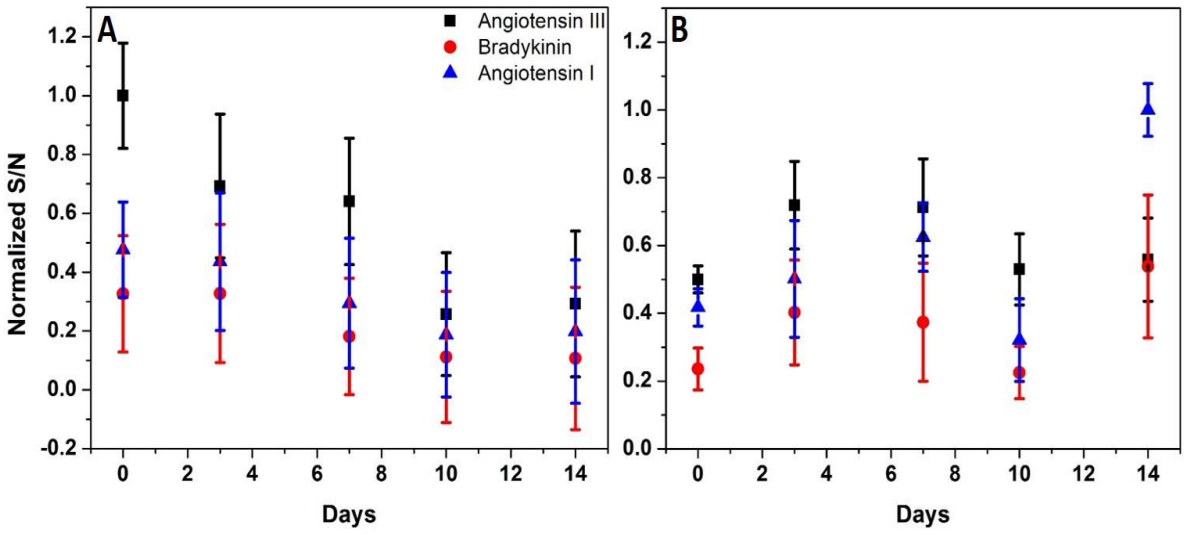

Figure 2.9: The stability of NIMS and ME-SALDI substrates over a two-week time period was investigated. ME-SALDI shows a steady decline in performance over the two-week time frame **(A)**. NIMS shows a more consistent signal-to-noise ratio over the time frame, despite the initial low ion abundance **(B)**. The intra-substrate variation for NIMS is shown to be smaller compared to ME-SALDI.

2.4 Conclusion

The fabrication of nanometer-sized features in n-type and p-type Si was carried out via electrochemical etching. N-type SALDI substrates had average pore diameters and pore depths of 9 ± 2 nm and 0.97 ± 0.06 µm, respectively. Pore diameter for p-type SALDI could not be determined due to the poor etching of the Si and low resolution of the SEM images but the

depth was measured at 1.06 ± 0.03 µm. N-type and p-type NIMS substrates exhibited average pore depths of 15.7 ± 0.2 µm and 45 ± 1 µm, and average pore diameters of 17 ± 6 nm and 14 ± 2 µm, respectively. Our prior studies showed porous substrates with the smallest pore diameter: pore depth ratio exhibit the best MS performance; hence why n-type Si was used for the comparison of ME-SALDI, NIMS and ME-NIMS. ME-NIMS, a hybrid ionization method of ME-SALDI and NIMS, was demonstrated here with improved detection sensitivity and good intra- and inter-substrate reproducibility. It is carried out by coating conventional NIMS substrates with a thin layer of matrix coating, which preserves the effective substrate properties of NIMS (i.e high density, deep pores) as well as offers a proton-rich environment in the presence of acidic matrices. The main reasoning for this improved reproducibility and stability is thought to be associated to the protection of the pSi surface by the initiator used during NIMS preparation. The initiator does not allow the surface to oxidize decreasing the variability between and within substrates and also helps with the desorption process of analytes on the surface. Our results show that ME-NIMS exhibits improved absolute ion abundance to NIMS and reasonable reproducibility in comparing to ME-SALDI and NIMS; hence offers a good alternative for small molecule profiling. Although matrix is used, ME-NIMS does show promise for continued biological research.

2.5 Reference

(1) Wei, J.; Buriak, J. M.; Siuzdak, G. Desorption-ionization mass spectrometry on porous silicon. *Nature* **1999,** *399* (6733), 243.

(2) Patti, G. J.; Woo, H. K.; Yanes, O.; Shriver, L.; Thomas, D.; Uritboonthai, W.; Apon, J. V.; Steenwyk, R.; Manchester, M.; Siuzdak, G. Detection of carbohydrates and steroids by cation-enhanced nanostructure-initiator mass spectrometry (NIMS) for biofluid analysis and tissue imaging. *Anal Chem* **2010,** *82* (1), 121.

(3) Sturm, R. M.; Greer, T.; Chen, R.; Hensen, B.; Li, L. Comparison of NIMS and MALDI platforms for neuropeptide and lipid mass spectrometric imaging in C. borealis brain tissue. *Anal Methods* **2013,** *5* (6), 1623.

(4) Liu, Q.; Xiao, Y.; Pagan-Miranda, C.; Chiu, Y. M.; He, L. Metabolite imaging using matrix-enhanced surface-assisted laser desorption/ionization mass spectrometry (ME-SALDI-MS). *J Am Soc Mass Spectrom* **2009,** *20* (1), 80.

(5) Liu, Q.; He, L. Ionic matrix for matrix-enhanced surface-assisted laser desorption ionization mass spectrometry imaging (ME-SALDI-MSI). *J Am Soc Mass Spectrom* **2009,** *20* (12), 2229.

(6) Greving, M. P.; Patti, G. J.; Siuzdak, G. Nanostructure-Initiator Mass Spectrometry Metabolite Analysis and Imaging. *Anal Chem* **2010,** *83* (1), 2.

(7) Liu, Q.; Xiao, Y.; He, L. In *Mass Spectrometry Imaging*; Rubakhin, S. S.;Sweedler, J. V., Eds.; Humana Press, 2010; Vol. 656.

(8) Liu, Q.; Brown, V. L.; He, L. Desorption/ionization on porous silicon (DIOS) for metabolite imaging. *Woodh Publ Ser Biom* **2014**, DOI:10.1533/9780857097156.2.270 10.1533/9780857097156.2.270(68), 270.

(9) Liu, Q.; He, L. Quantitative study of solvent and surface effects on analyte ionization in desorption ionization on silicon (DIOS) mass spectrometry. *J Am Soc Mass Spectrom* **2008,** *19* (1), 8.

(10) Ronci, M.; Rudd, D.; Guinan, T.; Benkendorff, K.; Voelcker, N. H. Mass spectrometry imaging on porous silicon: investigating the distribution of bioactives in marine mollusc tissues. *Anal Chem* **2012,** *84* (21), 8996.

(11) Northen, T. R.; Yanes, O.; Northen, M. T.; Marrinucci, D.; Uritboonthai, W.; Apon, J.; Golledge, S. L.; Nordstrom, A.; Siuzdak, G. Clathrate nanostructures for mass spectrometry. *Nature* **2007,** *449* (7165), 1033.

(12) Woo, H. K.; Northen, T. R.; Yanes, O.; Siuzdak, G. Nanostructure-initiator mass spectrometry: a protocol for preparing and applying NIMS surfaces for high-sensitivity mass analysis. *Nat Protoc* **2008,** *3* (8), 1341.

(13) Moening, T. N.; Brown, V. L.; He, L. Nanostructure-initiator mass spectrometry (NIMS) for molecular mapping of animal tissues. *Methods Mol Biol* **2015,** *1203*, 151.

(14) Patti, G. J.; Shriver, L. P.; Wassif, C. A.; Woo, H. K.; Uritboonthai, W.; Apon, J.; Manchester, M.; Porter, F. D.; Siuzdak, G. Nanostructure-initiator mass spectrometry (NIMS) imaging of brain cholesterol metabolites in Smith-Lemli-Opitz syndrome. *Neurosci* **2010,** *170* (3), 858.

(15) Yanes, O.; Woo, H. K.; Northen, T. R.; Oppenheimer, S. R.; Shriver, L.; Apon, J.; Estrada, M. N.; Potchoiba, M. J.; Steenwyk, R.; Manchester, M.et al. Nanostructure initiator mass spectrometry: tissue imaging and direct biofluid analysis. *Anal Chem* **2009,** *81* (8), 2969.

(16) Lee, D. Y.; Platt, V.; Bowen, B.; Louie, K.; Canaria, C. A.; McMurray, C. T.; Northen, T. Resolving brain regions using nanostructure initiator mass spectrometry imaging of phospholipids. *Integr Biol* **2012,** *4* (6), 693.

(17) O'Brien, P. J.; Lee, M.; Spilker, M. E.; Zhang, C. C.; Yan, Z.; Nichols, T. C.; Li, W.; Johnson, C. H.; Patti, G. J.; Siuzdak, G. Monitoring metabolic responses to chemotherapy in single cells and tumors using nanostructure-initiator mass spectrometry (NIMS) imaging. *Cancer Metab* **2013,** *1* (1), 4.

(18) Greving, M. P.; Patti, G. J.; Siuzdak, G. Nanostructure-initiator mass spectrometry metabolite analysis and imaging. *Anal Chem* **2011,** *83* (1), 2.

(19) Kurczy, M. E.; Northen, T. R.; Trauger, S. A.; Siuzdak, G. Nanostructure imaging mass spectrometry: the role of fluorocarbons in metabolite analysis and yoctomole level sensitivity. *Methods Mol Biol* **2015,** *1203*, 141.

(20) Louie, K. B.; Northen, T. R. Metabolic imaging using nanostructure-initiator mass spectrometry (NIMS). *Methods Mol Biol* **2014,** *1198*, 313.

(21) Wei, J.; Buriak, J. M.; Siuzdak, G. Desorption-ionization mass spectrometry on porous silicon. *Nature* **1999,** *399* (6733), 243.

(22) Woo, H.-K.; Northen, T. R.; Yanes, O.; Siuzdak, G. Nanostructure-initiator mass spectrometry: a protocol for preparing and applying NIMS surfaces for high-sensitivity mass analysis. *Nat. Protoc* **2008,** *3* (8), 1341.

(23) Robichaud, G.; Garrard, K.; Barry, J.; Muddiman, D. MSiReader: An Open-Source Interface to View and Analyze High Resolving Power MS Imaging Files on Matlab Platform. *J Am Soc Mass Spectrom* **2013,** *24* (5), 718.

(24) Sailor, M. J. In *Porous Silicon in Practice*; Wiley-VCH Verlag GmbH & Co. KGaA, 2011, DOI:10.1002/9783527641901.ch1 10.1002/9783527641901.ch1.

(25) Xiao, Y. S.; Retterer, S. T.; Thomas, D. K.; Tao, J. Y.; He, L. Impacts of Surface Morphology on Ion Desorption and Ionization in Desorption Ionization on Porous Silicon (DIOS) Mass Spectrometry. *J Phys Chem C* **2009,** *113* (8), 3076.

(26) Smith, R. L.; Collins, S. D. Porous silicon formation mechanisms. *J Appl Phys* **1992,** *71* (8), R1.

(27) Lehmann, V.; F√∂ll, H. Formation Mechanism and Properties of Electrochemically Etched Trenches in n-Type Silicon. *J Electrochem Soc* **1990,** *137* (2), 653.

(28) Gao, J.; de Raad, M.; Bowen, B. P.; Zuckermann, R. N.; Northen, T. R. Application of Black Silicon for Nanostructure-Initiator Mass Spectrometry. *Anal Chem* **2016,** *88* (3), 1625.

CHAPTER 3: DILUTE BISF17 ON POROUS SILICON

3.1 Introduction

A vital aspect in experimental science is how reproducibly the experimental data is. The more reproducible the data is obtained, the more reliable the results are and the more confident one has in the conclusion(s) reached. In the previous chapter, my preliminary study of NIMS and ME-NIMS showed measurement reproducibility between 25-43%; further improvement in the reproducibility for both techniques could be beneficial.

BisF17 is the most common initiator used for NIMS.[1-3] When BisF17 is spotted on to the pSi surface, its high viscosity limits uniform spread across the surface and sometimes even required the pSi wafer to be tilted slightly in order for the entire surface to be covered. This uneven coating in the pores and on the pSi surface was suspected as the primary culprit. To achieve a more homogenous surface coverage, the initiator was diluted with a solvent of high vapor pressure to reduce the viscosity while still allowing the initiator to cover the surface and penetrate the pores. The solvent that would be used to dilute the initiator 1) be miscible with the initiator and 2) have a high vaper pressure. The higher the vapor pressure a solvent exhibits, the quicker it evaporates. The mixing of solvent and initiator also decreased the viscosity which will allow the quick spread of initiator on the pSi surface and allow the initiator to coat the surface in a homogenous fashion. The purpose of the solvent is to aid in the spread of the initiator on the surface; not to interfere with the study of analytes of interest.

In order to try to improve the reproducibility of both NIMS and ME-NIMS, BisF17 was diluted with solvents such as chloroform, hexane and THF, respectively. It was thought that when mixing BisF17 initiator with those solvents, the solution would spread on the pSi

surface more evenly allowing for a more homogenous covered surface. With a more homogenous surface, the reproducibility should increase reducing the errors calculated. Dilute initiator in chloroform, hexane and THF, respectively, was investigated with peptide samples and compared to conventional NIMS and ME-NIMS. Tissue samples on dilute BisF17 ME-NIMS was also studied to determine if diluting the initiator would improve reproducibility. ANOVAs were calculated to show if there were significant differences across the techniques.

Once the solvents are chosen and mixed with the BisF17 initiator, the data between the dilute initiator wafers and conventional NIMS/ME-NIMS wafers were compared to determine if there are significant differences in signal achieved with each method. One way to compare more than two sample groups is to use an analysis of variance (ANOVA) test. ANOVA is used to analyze the means of more than two groups to determine if they are equal or significantly different. It is similar to performing t-tests for two samples but simplifies the comparison process by allowing more than two samples to be compared for statistical significance at once. ANOVA calculates a p-value which determines if the data between the samples are significantly different. A threshold that is widely used is a p-value of 0.05. If the p-value is greater than that, the data is not significantly different; a p-value that is equal to or less than 0.05, the sample data is significantly different.

3.2 Materials and Methods

Materials Hydrofluoric acid (HF, 49%), ethanol (95%), sulfuric acid (H_2SO_4), hydrogen peroxide (H_2O_2, 30%) and methanol (99%) were purchased from VWR (Radnor, PA). N-type Sb-doped (100) single-crystalline silicon wafers at 0.005-0.02 Ω/cm were purchased from Silicon Sense, Inc. (Nashua, NH). Bis(heptadecafluoro-1,1,2,2-tetrahydrodecyl) tetramethyldisiloxane (BisF17) was purchased from Gelest, Inc. (Morrisville, PA).

Angiotensin I, angiotensin III, bradykinin, and 2,5-dihydroxybenzoic acid (DHB) were purchased from Sigma-Aldrich (St. Louis, MO). 18 MΩ deionized (DI) H2O (Millipore, PO) was used for all experiments.

Porous Silicon (pSi) Substrate Preparation A detailed description of etching of silicon wafers and preparation of the NIMS surface has been reported.[3, 4] In a quick summary, silicon wafers were cut to approximately 1.5 cm x 1.5 cm. The cut silicon was washed in piranha solution (2:1 sulfuric acid: hydrogen peroxide) for 30 min. The wafer was rinsed with copious amounts of Milli-Q water and dried with N_2. The clean Si wafer was put in a Teflon anodic etch cell. The etching cell consists of a two-electrode system where a Pt working electrode is placed under the Si wafer and a Pt counter electrode is placed above the surface. The Teflon cell was filled with 1mL of 25% HF solution in ethanol and etched at a current of 32 mA/cm^2 for 30 min. After etching, the pSi was rinsed with ethanol and dried with N_2. The pSi wafer was placed in a 120°C oven for 5 min and allowed to cool to room temperature.

Conventional NIMS Substrate Preparation After the wafer cooled to room temperature, BisF17 initiator was applied to the pSi surface. 33µL of BisF17 initiator was pipetted on to the surface and incubated for 30 min. Any excess initiator was blown off using N_2. The NIMS chip was placed in a 120°C oven for 7-10 sec and excess initiator was blown off. This process was repeated two more times.

Dilute BisF17 NIMS Preparation For dilute BisF17 NIMS and ME-NIMS studies, 75% BisF17 was mixed with chloroform, hexane and THF respectively. 33 µL of each respective

dilute BisF17 solution was pipetted onto the pSi and allowed to soak for 30 min at room temperature (RT) to form the initiator coating. Excess dilute initiator was removed from the pSi by applying a high-flow stream of N_2, followed by a 3-5 s drying period in a 100˚C oven; this was repeated 3 times in order to sufficiently remove excess initiator solution. Dilute BisF17 NIMS substrates were stored dry in a closed petri dishes at room temperature and were used within 3 days of initial fabrication, unless otherwise specified in the text.

Dilute BisF17 and Conventional ME-NIMS Sample Preparation A thin layer of DHB matrix was deposited onto the wafer in a sublimation chamber.[5] Approximately 1 g of DHB was placed evenly over the bottom of the sublimation chamber. Using double-sided tape, a pSi substrate was attached upside down to the bottom of the condenser that was in direct contact with running water for cooling. An Edwards E2M8 vacuum pump with a vacuum meter was used to provide a controlled vacuum environment in the sublimation chamber. After maintaining the sublimation chamber for 2 min at approximately 50 torr, the apparatus was submerged into a 110˚C oil bath for 1.5 min for peptides analysis and 3 min for tissue analysis for ME-NIMS. Under these temperature and vacuum conditions, DHB immediately vaporized and re-deposited upon contact with the pSi substrate. Once matrix deposition was completed, the sublimation apparatus was removed from the oil bath and the vacuum was slowly released. Substrates coated with matrix were promptly removed from the apparatus and subsequently analyzed.

Sample Preparation for MS Measurements Stock solutions of angiotensin I, angiotensin III, and bradykinin were prepared in 50:50 acetonitrile (ACN): DI water at 12.5μM each. An

aliquot of each were then mixed at a 1:1:1 (v/v) ratio to reach a final concentration of approximately 4.2µM. For ME-NIMS, the analyte solution was applied to the wafer via drop-coating and allowed to dry before sublimation occurred. After sublimation, the samples were loaded in the MS chamber. For NIMS, the peptide solution was drop-coated onto the wafer, allowed to dry, and loaded into the MS chamber. Tissue samples were cut 5µm thick using a Leica CM1950 cyrostat. The tissue section was placed on pSi surface. For NIMS, the sample was loaded into the MS chamber; for ME-NIMS, matrix was sublimed then loaded into MS chamber.

Instrumentation An AB Sciex TOF/TOF™ 5800 System mass spectrometer (Framingham, MA) equipped with a 355 nm laser (Nd:YAG, 1000 Hz) was operated at an accelerating voltage of 20 kV in the reflector positive ion mode (MS-only) for all experiments. For sample spot analysis, the delay time was 13-15 ns to achieve optimal MS performance. A mass range of 100-1800 Da (± 0.05) and a bin size of 0.5 ns was used for all experiments. The laser intensity was 6400 to achieve optimal signal acquisition. In MS imaging mode, all mass spectra were collected in an automatic MS control mode using the AB Sciex TOF/TOF Imaging software; 50 laser pulses were averaged to yield one accumulated spectrum at each location. Mass spectra were reconstructed into 2D ion maps using the MSiReader™ software.[6]

3.3 Results and Discussion

3.3.1 Dilute BisF17 Peptide Analysis

In literature, NIMS substrates were prepared using neat BisF17 that took time to cover the surface. After the required incubation time, there was an iridescent shine representative of BisF17 being on the surface. When MS was performed on a NIMS substrate where there were

no analytes, a species could be seen at m/z 185 that corresponded with the presence of BisF17 but this species did not yield a homogenous abundance over the NIMS surface. Neat BisF17 has shown benefits in the desorption process but needed help coating the pSi surface more homogenously which was the purpose of the solvent. In this study, the effect of dilute initiator on peptides on NIMS and ME-NIMS substrates and tissue on ME-NIMS substrates was investigated and compared to neat initiator on pSi. The goal for this was to form a more homogenous initiator coating on the pSi surface in order to help increase the intra-substrate reproducibility. To do this, BisF17 was diluted to 75% with chloroform, hexane or THF, respectively. Three solvents were selected with similar vapor pressures, but different polarities and chemical structures to determine if either of those properties contributed to a change in analyte signal. Neat BisF17 is slightly viscus and took a few seconds to cover the pSi surface and sometimes even required the pSi wafer to be tilted in order to cover the whole pSi surface. When the initiator was mixed with the solvents, the solution thins out and would cover the surface immediately. For hexane and chloroform, after the excess dilute BisF17 was blown off the surface there was a visible metallic shine that also occurred when neat BisF17 was directly applied to the NIMS substrate; THF didn't visually have that metallic shine. This helped with coating the surface more homogenously. The goal of the solvent mixed with BisF17 was to aid in the coating of the surface in a quicker and more homogenous manner. These solutions were used for the initiator coating and spotted on to pSi surface as explained earlier. Once the dilute initiator NIMS surface was prepared, the peptide solution was spotted and analyzed as soon as it dried on the wafer.

Analysis of angiotensin III, bradykinin, and angiotensin I was examined on NIMS substrates prepared with 75% BisF17 in chloroform, 75% BisF17 in hexane, 75% BisF17 in

THF and neat BisF17 (i.e. conventional NIMS). It can be seen in Figure 3.1 that signal from conventional NIMS is more intense than the signal obtained from the dilute initiator for both angiotensin III and angiotensin I though comparable for bradykinin. In order to determine if the signal from the dilute initiator is significantly different than from conventional NIMS, an ANOVA was performed (Table 3.1). The p-values in Table 3.1 show that signal from angiotensin III and angiotensin I are significantly different; signal from bradykinin is not significantly different. It has been shown in past data that there is an inherent variation between NIMS signal which may partial account for some of the drop in signal seen with the dilute initiator NIMS substrates. Not only is it a possibility that the solvent plays a role in the decreased signal but the chemical structure of the peptides plays a role as well. Histidine is known to have a strong affinity for metals and although silicon is classified as a metalloid, it has many aspects to metals.[7] Angiotensin III has one histidine and angiotensin I has two histidine amino acids in its peptide chain. With less coverage of the pSi surface when the initiator is diluted, both angiotensin I and angiotensin III will display an affinity for the pSi which can lead to a decrease in the detection of these analytes.

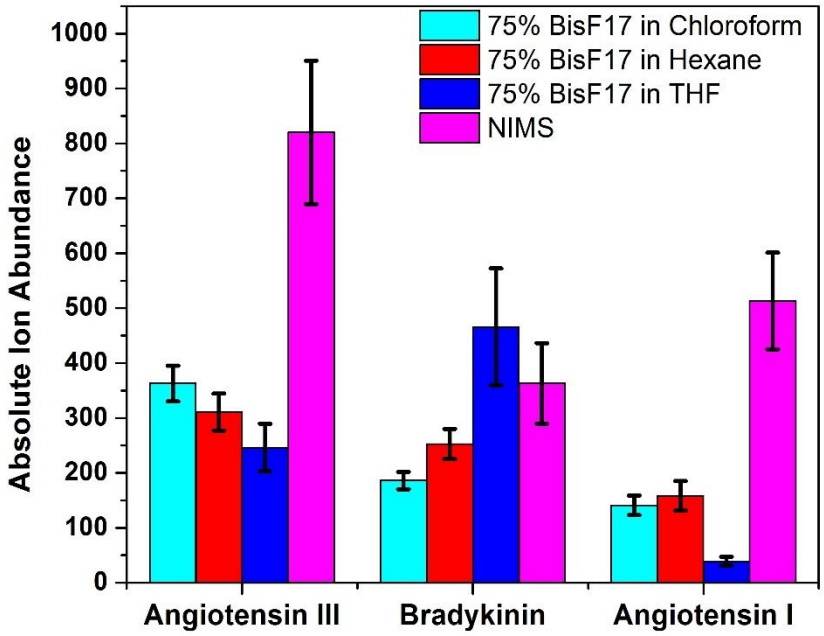

Figure 3.1: Absolute ion abundance comparison of peptides detected on a NIMS substrate prepared using 75% BisF17 diluted in chloroform, 75% BisF17 diluted in hexane, 75% BisF17 diluted in THF and neat BisF17 (conventional NIMS), respectively.

Table 3.1: ANOVA of peptides on dilute BisF17 in chloroform NIMS, dilute BisF17 in hexane NIMS, dilute BisF17 in THF NIMS and conventional NIMS.

Analyte	p-value
Angiotensin III	4.39E-04
Bradykinin	1.03e-01
Angiotensin I	3.63E-05

ME-NIMS technique was also investigated to look at the same dilute initiator solutions. It has been seen that when subliming matrix on to the NIMS wafers that the signal would increase. The same occurred when subliming onto dilute initiator wafers; signal drastically increased compared to NIMS data. For ME-NIMS, past data has shown that ME-NIMS data has varied more than NIMS data did which could account for the larger variance in signal from the dilute initiator wafers. For angiotensin III, 75% BisF17 in hexane yielded a larger signal than conventional ME-NIMS and the same occurred with 75% BisF17 in chloroform for

bradykinin (Figure 3.2). Although signal looks more comparable than NIMS, ANOVA was still performed and was determined that all three peptides had significantly different mean values (Table 3.2). ANOVA was performed between 75% BisF17 in hexane and ME-NIMS for angiotensin III and 75% BisF17 in chloroform and ME-NIMS for bradykinin data which showed no significant difference (not shown). Since 75% BisF17 in THF returned significant difference in both NIMS and ME-NIMS, it will not be tested in further experiments.

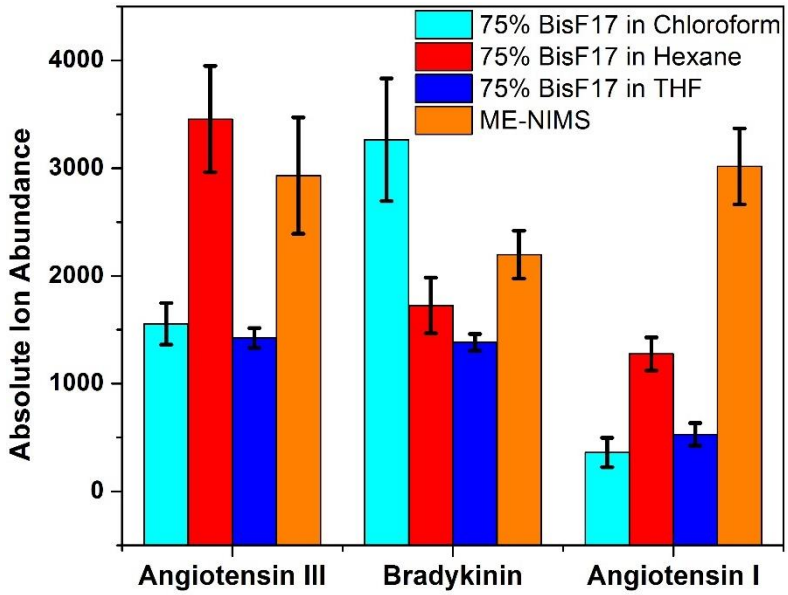

Figure 3.2: Absolute ion abundance comparison of peptides detected on a ME-NIMS substrate prepared using 75% BisF17 diluted in chloroform, 75% BisF17 diluted in hexane, 75% BisF17 diluted in THF and neat BisF17 (conventional ME-NIMS), respectively.

Table 3.2: ANOVA of peptides on dilute BisF17 in chloroform ME-NIMS, dilute BisF17 in hexane ME-NIMS, dilute BisF17 in THF ME-NIMS and ME-NIMS.

Analyte	p-value
Angiotensin III	8.05E-03
Bradykinin	1.42E-02
Angiotensin I	1.91E-06

3.3.2 Dilute BisF17 Tissue Analysis

With ME-NIMS showing increased signal over NIMS as well as 75% BisF17 in chloroform and 75% BisF17 in hexane not showing significant difference compared to

conventional ME-NIMS, those two solvent solutions were used to investigate further to look at tissue samples utilizing MSI. It was expected that the signal from the dilute initiator would be lower than that of conventional ME-NIMS but still be comparable. For ME-NIMS analysis of angiotensin III and bradykinin, both dilute initiator in chloroform and hexane showed no significant difference in data. This was thought to continue for tissue analysis. The lipids investigated all had a smaller molecular weight than the peptides studied. If molecular weight played a factor in ion abundance than the peptides should have more comparable abundance to conventional ME-NIMS. In Figure 3.3, it can be seen that signal from the dilute initiator ME-NIMS wafers was drastically lower than conventional ME-NIMS MSI. It was expected that the signal would drop from peptide analysis to tissue analysis but the signal specifically for dilute initiator dropped much more than anticipated. This was proven by performing an ANOVA on the five lipids typically seen in mouse brain tissue samples.

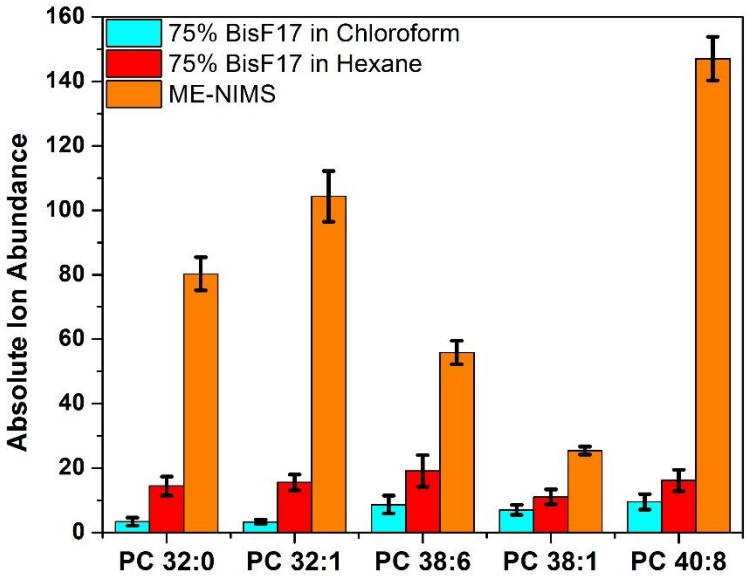

Figure 3.3: Absolute ion abundance comparison of lipids detected on a ME-NIMS substrate prepared using 75% BisF17 diluted in chloroform, 75% BisF17 diluted in hexane, and neat BisF17 (conventional ME-NIMS), respectively.

Table 3.3: ANOVA of lipids from tissue samples on dilute BisF17 in chloroform ME-NIMS, dilute BisF17 in hexane ME-NIMS, and ME-NIMS.

Analyte	p-value
PC 32:0	2.22E-13
PC 34:1	3.48E-13
PC 38:6	5.26E-08
PC 38:1	7.09E-07
PC 40:8	6.74E-17

A few reasons could account for the significant decrease in signal when using dilute initiator on pSi wafers. It has been thought that when the laser irradiates the NIMS/ME-NIMS surface that the initiator expands and vaporizes, aiding in the desorption of analytes of interest.[1] With the decrease in the amount initiator that was put on the pSi wafer, the amount that got vaporized is also decreased. This could account for a decline in performance across both NIMS and ME-NIMS techniques. Another factor that could add to this decrease is the solvent that was mixed with the BisF17 initiator. When the initiator solution was incubated on the pSi surface, solvent and initiator went into the pores of the wafer. Although the solvent is thought to evaporate, the initiator as well as the solvent were likely trapped in the pores together. When the surface was irradiated, both initiator and solvent would vaporize together. Since the solvent is vaporized as well, it hinders the amount of initiator that can be vaporized out of the pores which correlates to the amount of analyte of interest desorbed from the surface. It has been hypothesized that the solvent may help release impurities from the NIMS surface. The vaporization of initiator, solvent and impurities would contribute to the background noise of the spectrum. The presence of the solvent at such a high quantity on the surface would be a major factor in the substantial decrease in signal. The use of dilute initiator will not be utilized moving forward with the NIMS and ME-NIMS techniques.

3.4 Conclusion

The NIMS performance comparison of substrates prepared in 75% BisF17 in chloroform, hexane and THF, and neat BisF17 (conventional NIMS), respectively, showed a significant difference in signal intensities for angiotensin I and angiotensin III whereas bradykinin showed no significant difference between the 4 methods investigated. A similar outcome was obtained for ME-NIMS. Testing NIMS substrates prepared with diluted BisF17 in tissue ME-NIMS imaging showed significantly lower ion intensities for all five lipids commonly seen with tissue analysis. It was clear that although diluting the initiator allowed the initiator to cover the surface faster and more uniformly, there were issues causing severe deterioration of NIMS performance in MS analysis. I suspect that the dilution the initiator resulted to fewer initiator molecules on the surface and in the pores, which reduced the spalling force to aid the desorption of analytes.

3.4 References

(1) Northen, T. R.; Yanes, O.; Northen, M. T.; Marrinucci, D.; Uritboonthai, W.; Apon, J.; Golledge, S. L.; Nordstrom, A.; Siuzdak, G. Clathrate nanostructures for mass spectrometry. *Nature* **2007,** *449* (7165), 1033.

(2) Kurczy, M. E.; Northen, T. R.; Trauger, S. A.; Siuzdak, G. Nanostructure imaging mass spectrometry: the role of fluorocarbons in metabolite analysis and yoctomole level sensitivity. *Methods Mol Biol* **2015,** *1203*, 141.

(3) Woo, H. K.; Northen, T. R.; Yanes, O.; Siuzdak, G. Nanostructure-initiator mass spectrometry: a protocol for preparing and applying NIMS surfaces for high-sensitivity mass analysis. *Nature Protoc* **2008,** *3* (8), 1341.

(4) Wei, J.; Buriak, J. M.; Siuzdak, G. Desorption-ionization mass spectrometry on porous silicon. *Nature* **1999,** *399* (6733), 243.

(5) Liu, Q.; Xiao, Y.; He, L. In *Mass Spectrometry Imaging*; Rubakhin, S. S.;Sweedler, J. V., Eds.; Humana Press, 2010; Vol. 656.

(6) Robichaud, G.; Garrard, K. P.; Barry, J. A.; Muddiman, D. C. MSiReader: an open-source interface to view and analyze high resolving power MS imaging files on Matlab platform. *J Am Soc Mass Spectrom* **2013,** *24* (5), 718.

(7) Magdeldin, S.; Mose, A. In *Affinity Chromatography*; Magdeldin, D. S., Ed., 2012, DOI:10.5772/39087 10.5772/39087.

CHAPTER 4: SPATIAL RESOLUTION AND BIOLOGICAL MASS SPECTROMETRY IMAGING

4.1 Introduction

Imaging techniques are important, especially in the medical field where proteins, metabolites, drugs, etc. are studied to understand their interactions and roles within the body. It allows doctors and researchers to detect problem areas such as tumors or to detect biomarkers for specific diseases. Most of the current techniques used for medical and research imaging are relying on optical, magnetic, or radioactive probes to illustrate the physical location of targeted species, such as in Positron Emission Tomography (PET), Whole Body Autoradiography (WBA), and Magnetic Resonance Imaging (MRI). A few issues arise with these techniques such as typically only one molecule of interest can be investigated per experiment, the molecule of interest requires a tag/label, this tag/label may cause the molecule of interest to act differently, and the tag/label may not be preserved through metabolism. One was to circumvent these problems is to use mass spectrometry imaging (MSI). MSI does not require a tag or label on the molecule of interest and multiple molecules of interest can be investigated at a time.[1-8]

In MSI, the ionization beam will raster across the sample being imaged from left to right, top to bottom. At each point where the laser irradiates the surface, a MS spectrum is collected. The spectra are accumulated and processed using MSI software to make an image. Figure 4.1 shows a schematic of the MSI process. Once an image is processed, any m/z value within the mass range analyzed can be chosen to see the distribution of that analyte throughout the image. The images generated are important in showing the identity, location as well as quantity of molecules throughout the sample. An important factor when performing MSI on

tissue samples is achieving the highest spatial resolution as possible. This will help determine how drug compounds are distributed, as well as how biological molecules compose the sample.

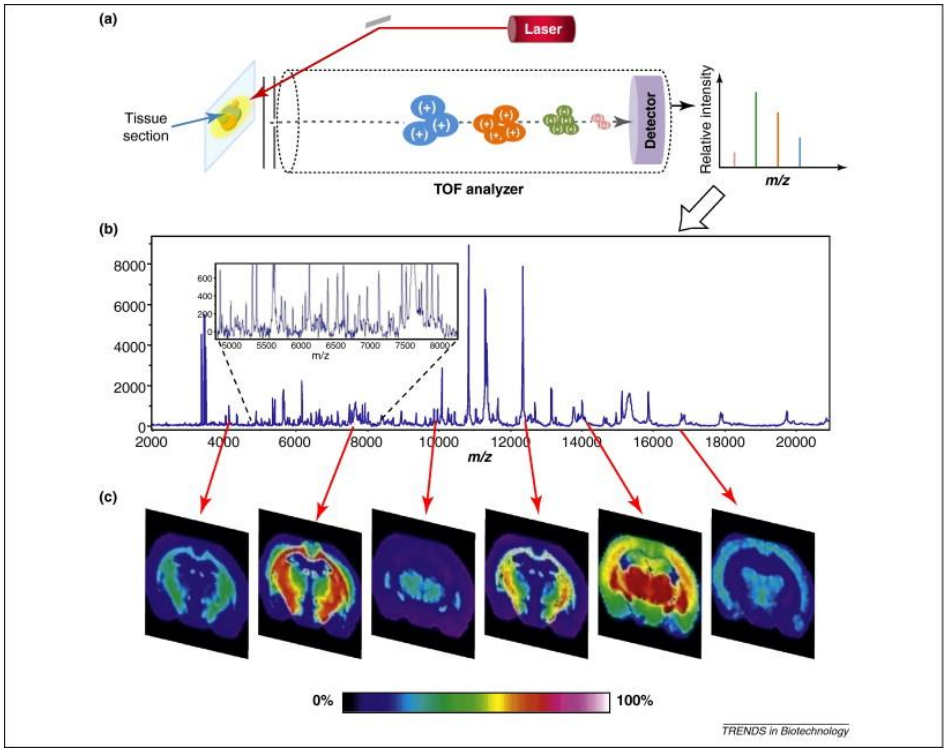

Figure 4.1: A schematic of MSI process.[9] **(a)** A sample is placed on top of a conductive surface and a laser is fired at the sample. At each point where the laser fires at the surface, a mass spectrum is collected. **(b)** A representative mass spectrum is collected from the sample where the inlet shows the complexity of the collected spectrum. **(c)** By averaging the spectra across the entire sample, m/z images are generated. This shows the location and abundance of different molecules throughout the sample being investigated.

Figure 4.2 shows a schematic of how the laser diameter and step size will effect under- and oversampling. Undersampling occurs when the laser step size is larger than the diameter of the laser causing gaps between the laser spots that leave analytes on the surface. When larger step sizes are used, the image that is generated is typically blurry. As the laser step size decreases, the gap between laser spots diminishes and the spots will begin to overlap causing oversampling. By overlapping the laser spots, every section in the sample area is irradiated by the laser allowing for a more detail generated image. With a higher quality image, the

distribution of molecules throughout the sample is better seen and can give valuable information about the sample. For example, when a tissue sample is imaged with a small laser step size, a more detailed map of the distribution of biological molecules is obtained which can help in disease detection and with pharmacology studies. There are trade-offs to high spatial resolution; one being the length of time it takes to perform the imaging experiment. As the laser step size decreases in MSI experiments, the time it takes to image the same size experiment exponentially increases. This time has to be thought about when preparing to perform MSI; if high resolution is a necessity than longer experiment times will be required. If shorter analysis times are required, than the spatial resolution will be lower.

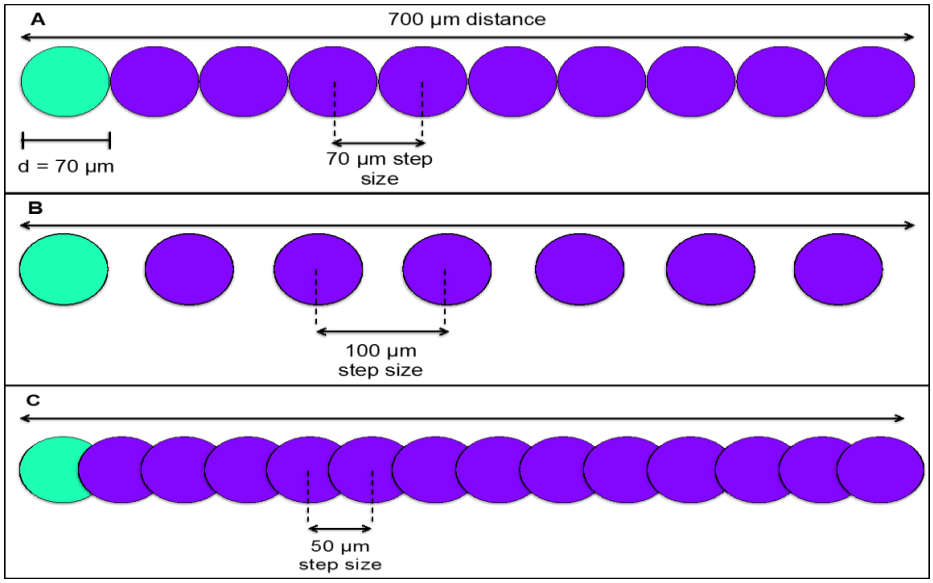

Figure 4.2: Schematic of laser shots during MSI showing standard **(A)**, under- **(B)** and oversampling **(C)** of the sample area. With a 70µm diameter laser spot size and a 70µm laser step size, it can be seen that theoretically the laser spot edges will just touch each other with no gap or overlap. When the laser step size increases to 100µm, there is now a gap between the laser spots causing the sample area to be undersampled. Once the laser step size is lower than the diameter of the laser, the laser spots will begin to overlap each other causing oversampling to occur.

The higher the spatial resolution, the more information can be obtained from the images but that also greatly increases the complexity of the spectra since more analytes will be

desorbed from the surface. Spatial resolution is determined primarily by the step size of the translational stage, not necessarily by the individual laser spot size. When the spatial resolution is high, the laser begins to overlap and over-sample the area being imaged which allows analytes that are at low quantity to be exposed and desorbed, allowing them to be investigated along with the analytes at higher quantities. With the MALDI instrument used for this study, the unmodified instrument laser diameter is 70µm. In order to obtain the highest possible spatial resolution, oversampling of the sample area was performed.

Spatial resolution is an important aspect of MSI when analyzing samples, especially biological samples. MSI can be used to monitor protein and lipid abundances, drug distribution throughout tissue samples as well as to determine biomarkers for disease. In order to accurately monitor those processes, a high spatial resolution is needed. Ideally, cellular level resolution would be desired to study drug distribution within tissue samples as well as to study cellular function in areas of diseased and unhealthy cells. It has been shown that down to a few hundred nanometers spatial resolution has been seen using SIMS but this technique is not feasible in studying large proteins.[6, 10-15] SIMS uses a primary (i.e. Ga^+, Cs^+) or cluster (i.e. Au, Bi, Ar) ion beam to desorb and produce secondary ions.[11, 14, 16-18] Since these high energy primary and cluster ion beams are used, SIMS has a mass range up to approximately 1500 Da and typically cause extensive fragmentation. Desorption electrospray ionization (DESI) and nanospray DESI (nano-DESI) are ambient ionization techniques capable of analyzing proteins and imaging tissue samples. DESI has recently been improved to 35 µm spatial resolution and nano-DESI has an achievable spatial resolution of 12 µm.[19-23] A downfall to these ambient techniques is sensitivity. Since there is no sample preparation required, molecules of interest tend to be lost under the signal of more abundant molecules. Techniques like MALDI, SALDI

and NIMS are able to analyze proteins better than SIMS and since there is sample preparation there can be enrichment of molecules of interest. The highest spatial resolutions achievable for these techniques are 10μm for MALDI and SALDI and 5 μm for NIMS.[6, 10, 12, 15, 24-26] Although these high spatial resolutions have been achieved, they can vary depending on the instrument used as well as if there were any modifications to the instrument; i.e. changes to laser diameter.

Continuing my previous study on ME-NIMS, spatial resolution was investigated comparing conventional MALDI, NIMS, and ME-NIMS methods. The achievable laser spot size and the step size is determined by the commercial instrument (the irradiation laser and translational stage are in the sample chamber) used in the study; no customized modification was carried out to further reduce the laser beam size or stage moving steps. For conventional MALDI and ME-NIMS, DHB was sublimed on to a flat Si or pSi wafer, respectively, over a TEM grid to form a pattern on the surface which was then imaged. Rhodamine 6G dye was transferred in a grid pattern onto the NIMS surface by stamping and was imaged in the same manner as MALDI and ME-NIMS MSI. For all experiments, the laser step size was decreased to as small as possible until no signal was able to be seen. After achievable resolution was determined, MSI of biological samples was performed for NIMS and ME-NIMS to show optimization of tissue on pSi.

4.2 Materials and Methods

Materials Hydrofluoric acid (HF, 49%), ethanol (95%), sulfuric acid (H_2SO_4) and hydrogen peroxide (H_2O_2, 30%) were purchased from VWR (Radnor, PA). N-type Sb-doped (100) single-crystalline silicon wafers at 0.005-0.02 Ω/cm were purchased from Silicon Sense, Inc. (Nashua, NH). Bis(heptadecafluoro-1,1,2,2-tetrahydrodecyl)tetramethyldisiloxane (BisF17)

was purchased from Gelest, Inc. (Morrisville, PA). Angiotensin I, angiotensin III, bradykinin, and 2,5-dihydroxybenzoic acid (DHB) were purchased from Sigma-Aldrich (St. Louis, MO). 18 MΩ deionized (DI) H2O (Millipore, PO) was used for all experiments. Sylgard® 184 silicone elastomer base and Sylgard® 184 silicone elastomer curing agent was purchased from Dow Corning (Midland, MI).

Porous Silicon (pSi) Substrate Preparation A detailed description of etching of silicon wafers and preparation of the NIMS surface has been reported.[27] In a quick summary, silicon wafers were cut to approximately 1.5 cm x 1.5 cm. The cut silicon was washed in piranha solution (2:1 sulfuric acid: hydrogen peroxide) for 30 min. The wafer was rinsed with copious amounts of Milli-Q water and dried with N_2. The clean Si wafer was put in a Teflon anodic etch cell. The etching cell consists of a two-electrode system where a Pt working electrode is placed under the Si wafer and a Pt counter electrode is placed above the surface. The Teflon cell was filled with 1mL of 25% HF solution in ethanol and etched at a current of 32 mA/cm^2 for 30 min. After etching, the pSi was rinsed with ethanol and dried with N_2. The pSi wafer was placed in a 120°C oven for 5 min and allowed to cool to room temperature before the application of BisF17 initiator. 33µL of BisF17 initiator was pipetted on to the surface and incubated for 30 min. Any excess initiator was blown off using N_2. The NIMS chip was placed in a 120°C oven for 7-10 sec and excess initiator was blown off. This process was repeated two more times.

MALDI and ME-NIMS Sample Preparation For conventional MALDI and ME-NIMS resolution studies, a 50-mesh TEM grid was taped to a Si wafer. A thin layer of DHB matrix

was deposited onto the wafer in a sublimation chamber. Approximately 1 g of DHB was placed evenly over the bottom of the sublimation chamber. Using double-sided tape, a substrate (flat Si for MALDI and pSi for ME-NIMS) was attached upside down to the bottom of the condenser that was in direct contact with running water for cooling. An Edwards E2M8 vacuum pump with a vacuum meter was used to provide a controlled vacuum environment in the sublimation chamber. After maintaining the sublimation chamber for 2 min at approximately 50 torr, the apparatus was submerged into a 110˚C oil bath for 3 min for MALDI and 3 min for ME-NIMS. Under these temperature and vacuum conditions, DHB immediately vaporized and re-deposited upon contact with the pSi substrate. Once matrix deposition was completed, the sublimation apparatus was removed from the oil bath and the vacuum was slowly released. Substrates coated with matrix were promptly removed from the apparatus. the tape on the TEM grid was slowly and carefully removed along with the TEM grid. This left a grid pattern on the Si wafer which was subsequently imaged.

NIMS Sample Preparation NIMS substrates were etched using the conditions described above. In order to reduce any surface damage, a polydimethylsiloxane (PDMS) stamp with a 50-mesh TEM grid pattern was made. The PDMS stamp was made by mixing Sylgard® 184 silicone elastomer base and Sylgard® 184 silicone elastomer curing agent in a w/w 3:1 ratio. It was then mixed and carefully poured over TEM grids then placed in an 80°C oven for 4 hr. Rhodamine 6G dye solution in 25% methanol was dropped on the surface and completely covered the grid patteren. After removing excess solution, a NIMS substrate was placed on top of the PDMS stamp (Figure 4.3). The pattern was transferred from the stamp to the NIMS substrate and subsequently imaged.

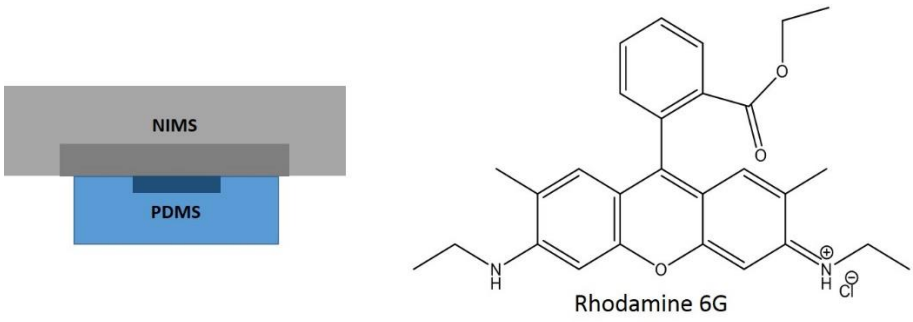

Figure 4.3: Schematic of PDMS stamp with NIMS substrate on top and chemical structure of rhodamine 6G.

Instrumentation An AB Sciex TOF/TOF™ 5800 System mass spectrometer (Framingham, MA) equipped with a 355 nm laser (Nd:YAG, 1000 Hz) was operated at an accelerating voltage of 20 kV in the reflector positive ion mode (MS-only) for all experiments. For sample spot analysis, the delay time was 13-15 ns to achieve optimal MS performance. A mass range of 100-500 Da (± 0.05) for resolution experiments and 100-1800 Da (± 0.05) for tissue analysis and a bin size of 0.5 ns was used for all experiments. The laser intensity was varied between 4700 and 6300 to achieve optimal signal acquisition. In MS imaging mode, all mass spectra were collected in an automatic MS control mode using the AB Sciex TOF/TOF Imaging software; 5-500 laser pulses, as specified in the text, were averaged to yield one accumulated spectrum at each location. Laser step size is specified for resolution studies and 150 µm for MSI of tissue. Mass spectra were reconstructed into 2D ion maps using the MSiReader™ software.

4.3 Results and Discussion

4.3.1 Technique Resolution

In this study, the achievable resolution for conventional MALDI, NIMS and ME-NIMS was investigated by performing imaging experiments while varying the laser step size. In order to determine the resolution for conventional MALDI, a TEM grid was used to make a pattern on the surface of a flat Si wafer; for ME-NIMS a TEM grid was used on a pSi surface. DHB matrix was sublimed onto either the flat Si for MALDI or pSi wafer for ME-NIMS over the TEM grid; the grid was then carefully removed leaving a grid pattern on the surface. For NIMS, a polymer stamp was made with the same TEM pattern. A dye, Rhodamine 6G, in 25% ethanol was pipetted into the stamp pattern then transferred to the NIMS pSi wafer. The dye allowed direct visualization of location of the grid on the substrate during experiment set-up; however, it was noted that different analytes were used for MALDI and ME-NIMS compared to conventional NIMS. This difference in analyte results will be discussed later. Experiments started at 200 μm laser step size and was decreased gradually to 40 μm. Because MS signals are collected by accumulating multiple laser shots, optimization of total laser pulses per spot is the first task to be carried out to achieve the best single-to-noise.

The laser was fired at the exact same position on the surface of either the flat Si wafer for MALDI or the pSi wafer for NIMS and the spectra were collected. For conventional MALDI, it is seen that after the initial laser irradiations with 5 pulses per irradation, all the analyte is completely ablated from the surface (Figure 4.4). It should be noted that for MALDI, 500 pulses per irradiation was attempted but the signal was drastically lower (not shown in Figure 4.4). Interestingly this is not the case for NIMS. Although the signal does drop significantly after the initial irradiation, the laser can irradiate the exact same position multiply

times and signal is still detected. This data suggests that analyte is going into the pores of the substrate and after the initial laser shot, additional analyte is still able to desorb out of the pores. It also appears that a consistent amount of analyte is being desorbed with each fire of the laser after the initial irradiation. It should be noted that ME-NIMS was not tested but with the same type of pSi wafer being utilized, similar results compared to NIMS would be expected.

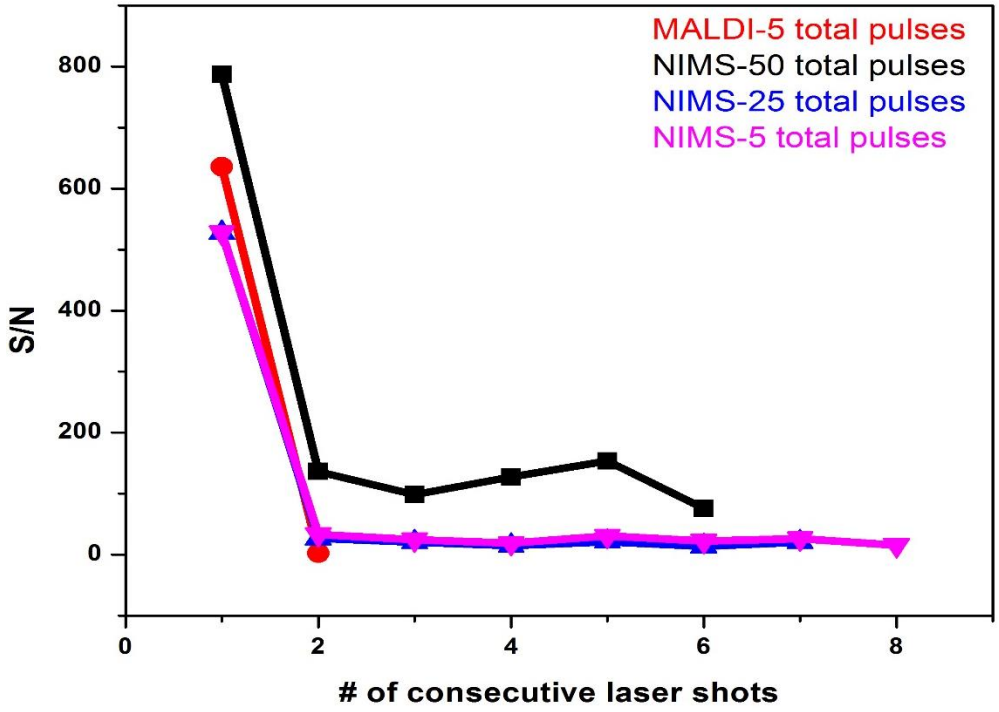

Figure 4.4: Graph showing the signal-to-noise ratio versus number of consecutive laser shots.

Figure 4.5 shows the images from averaging 5 total laser pulses per spectrum for MALDI imaging. It can be seen that the abundance of the DHB drastically decreases as the step size becomes smaller. This was expected as all the analyte on the surface is being completely ablated. When the laser hits the flat Si surface, all of the analyte under the laser is desorbed from the surface so when the laser steps over there is less analyte under the laser. This is what causes the drop in signal as the step size is decreased for conventional MALDI. For conventional MALDI, 40µm step size was the lowest achievable step size that yielded MS

signal; a smaller step size was tried but yielded no signal from DHB. It can be seen that the boundary of the boxes of the TEM grid is hard to distinguish when the laser step size is large. With the 100 µm laser step size and larger, the laser spot would always include the DHB surface area, even when the beam steps over the width of the bar between the boxes since that width is 83 µm. This is also a potential issue with the 70 µm laser step size because it may step over part of that bar width causing the jagged appearance in Figure 4.5B. As the step size decreased, the laser couldn't step over the width of the TEM bars which would help enhance the clarity of the TEM boxes. Note that the imaging reconstructing software occasionally may case slight misalignment that led to the zigzag appearance of the straight lines.

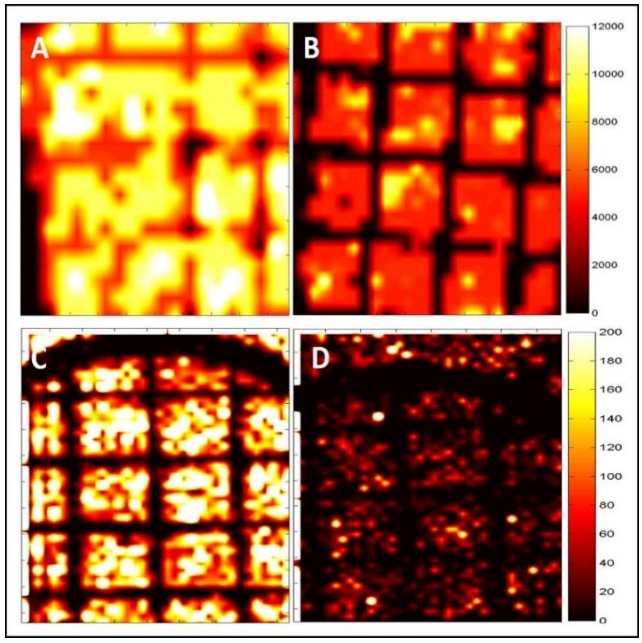

Figure 4.5: Images of conventional MALDI MSI of DHB at different laser step sizes: **(A)** 100 µm, **(B)** 70 µm, **(C)** 50 µm, and **(D)** 40 µm.

When performing NIMS resolution studies, it was determined that 50 total laser pulses averaged per spectrum gave the best results and this was used for all NIMS imaging experiments. The reason that 50 total laser pulses was decided upon as optimal is based on

Figure 4.4 showing 50 laser pulses achieved enhanced signal. It was shown for conventional MALDI that 500 total pulses were too many to be accumulated especially at smaller laser step sizes where little to no signal was detected when using 500 total laser pulses at a step size less than 70 µm (Figure 4.6). What is thought to be happening when 500 total pulses are being accumulated is that most of the analyte is desorbed in the first few pulses and for the remaining pulses, the signal is essentially zero. So when all 500 pulses were averaged for MALDI, the signal is much lower than what would be observed if fewer pulses were used. Because no signal was detected with 500 laser pulses with smaller than 70 µm step sizes, fewer total pulses were used; 5 total pulses for conventional MALDI. Since the number of laser pulses per irradiation doesn't play as vital of a role as it does for MALDI and as shown above a consistent amount of signal is detected after the first irradiation for NIMS, 50 total pulses for NIMS and ME-NIMS was used.

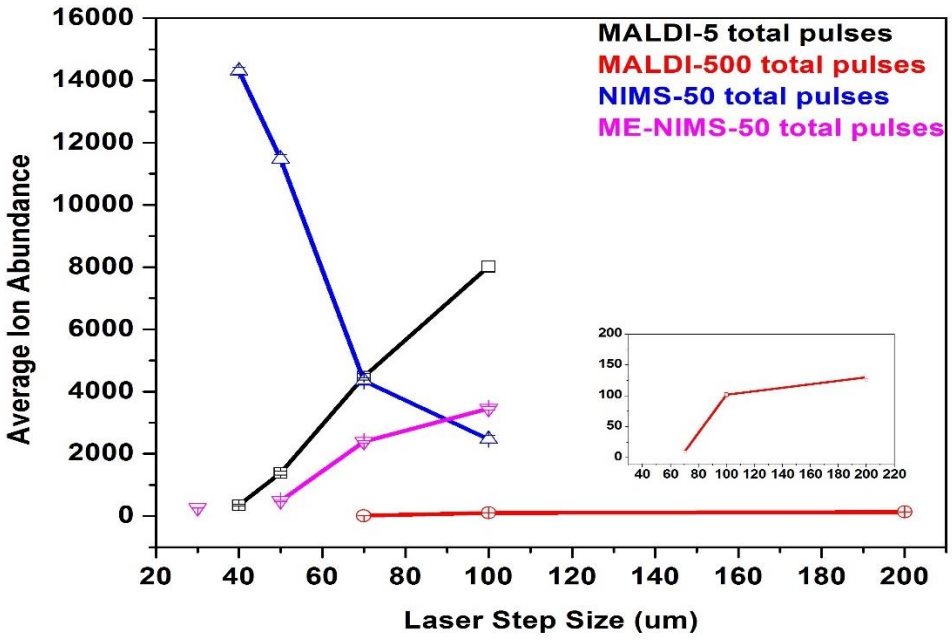

Figure 4.6: Graph showing the effect on average ion abundance versus laser step size.

It was difficult to transfer the entire pattern to the NIMS surface, fluorescent images of Rhodamine 6G were taken and overlapped with the MSI image to verify the pattern that was seen when a MSI image was generated (images not shown). When performing the NIMS resolution studies, interesting results were collected. First it is interesting to see how the dye transferred from the PDMS stamp to the NIMS surface. In some of the images, the dye is in the bars from the TEM grid and sometimes the dye is on the boxes. It's thought that the pressure of which the NIMS substrate is placed on the PDMS stamp will cause this difference. When the substrate is lightly placed on the PDMS stamp, the dye tended to stay in the bars of the grid, in which case the dye that transferred would look similar to Figure 4.7A. If the substrate was placed on the stamp with slightly more pressure, the dye appeared to come out of the bars from the grid and would be trapped between the boxes from the grid and the NIMS substrate making a pattern similar to Figure 4.7B. As seen in Figure 4.7, the abundance of the rhodamine dye became more intense as the laser step size decreased. This is the opposite result that was seen when performing this spatial resolution study on conventional MALDI (Figure 4.6); it needs to be stated again that the analytes used from MALDI and NIMS resolution studies were different. This increase in ion abundance for NIMS was surprising and prompted the question as to how this was occurring; this will be discussed shortly.

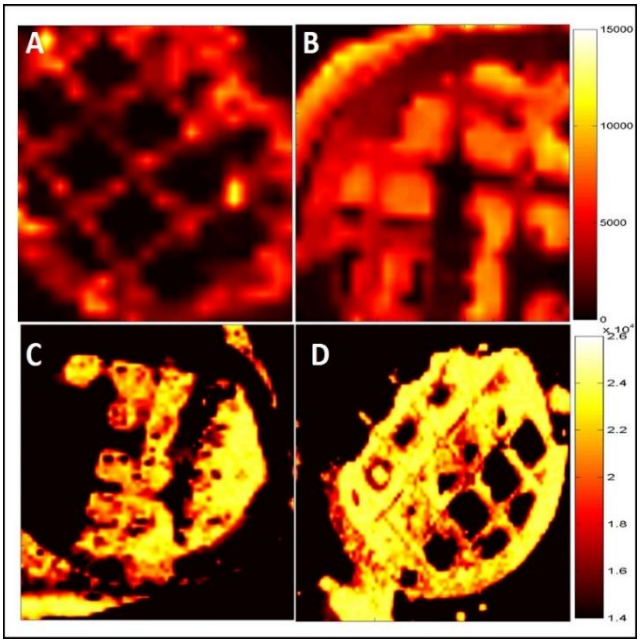

Figure 4.7: Images of NIMS MSI of rhodamine 6G dye at different laser step sizes: **(A)** 100 µm, **(B)** 70 µm, **(C)** 50 µm, and **(D)** 40 µm.

ME-NIMS was studied in order to push the limits of spatial resolution. Same as NIMS, it was also performed with 50 total laser pulses. Similar to MALDI resolution studies, ME-NIMS studies were performed by taping a TEM grid to the pSi wafer. The DHB matrix was then sublimed in the same manner on to the pSi wafer which was then subsequently imaged at varying laser step sizes. As expected since a majority of the analytes were desorbed after the first laser irradiation, it can be seen (Figure 4.8) that the DHB ion abundance decreases as the distance between laser step size becomes smaller. For ME-NIMS, the resolution was able to be pushed down to 30µm laser step size. Lower step sizes were attempted but without instrument modifications, this was the lowest achievable with these techniques. A lack of bar width and zigzag from the TEM grid can be seen for the 100 µm and 70 µm laser steps. It's not as noticeable since the imaging was performed on the entire TEM grid instead of a small

section. The reasoning for this phenomenon is the same as explained for MALDI imaging. This shows the benefit of the ME-NIMS technique for MSI capabilities.

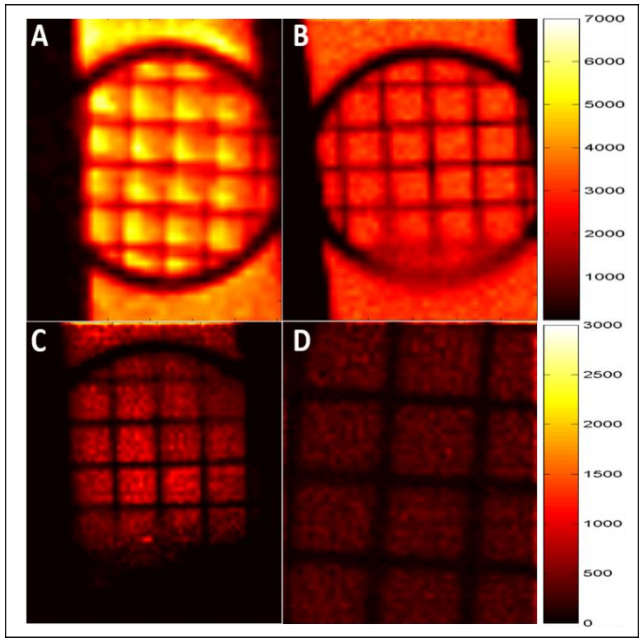

Figure 4.8: Images of ME-NIMS MSI of DHB at different laser step sizes: **(A)** 100µm, **(B)** 70µm, **(C)** 50µm, and **(D)** 30µm.

There were a couple reasons as to why the results turned out as they did. The main reason for the increase in ion abundance for NIMS is that a different analyte was used for that technique compared to MALDI and ME-NIMS. The thought as it why the signal increased for NIMS is possibly that since the Rhodamine 6G dye is a liquid and that the pores are so small, there is a capillary force that pulls the liquid into the pores. As the laser moves across the surface, there is still dye in the pores even after the first irradiation, having an additive effect increasing the signal with this specific analyte. With MALDI and ME-NIMS, a solid was sublimed to the Si surface. For MALDI, there were no pores for the matrix to go into but for ME-NIMS, there are pores for the solid matrix to enter. There isn't that capillary force to fill

the pores with matrix but rather the matrix will enter the pores as a gas but upon cooling changes back to a solid not allowing the matrix to penetrate the pores as deeply.

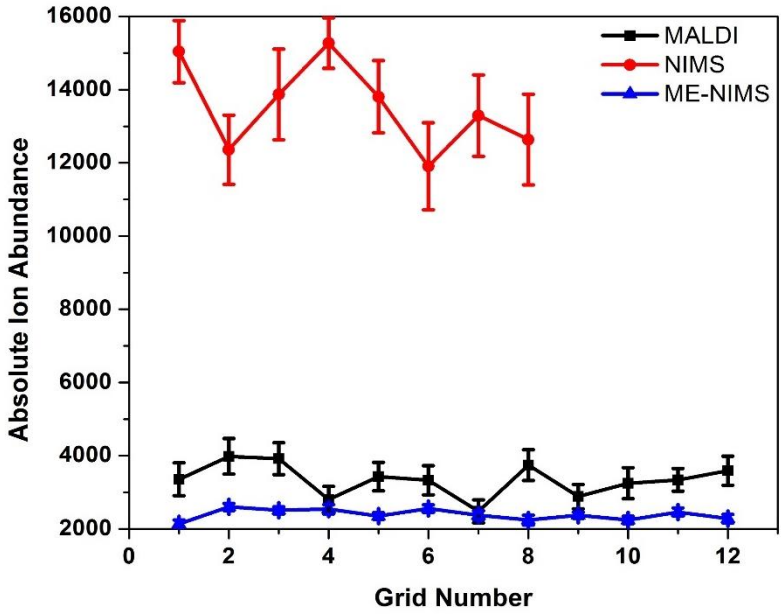

Figure 4.9: Absolute ion abundance vs grid number of MALDI, NIMS, and ME-NIMS MSI resolution studies. It must be noted that the ion abundance for NIMS is much higher than signal from MALDI and ME-NIMS due to a different analyte being used during these experiments.

As for the signal comparison for MALDI and ME-NIMS, since they utilized the same analyte, undersampling and oversampling plays a role. For MALDI, when the laser hits the Si surface, due to the high thermal conductivity of the highly doped surface, the heat rapidly dissipates across the surface effecting a larger area than just the size of the laser diameter. So if the laser step size is 100µm for a 70µm laser diameter, there is more analyte being desorbed than what is just under the laser, causing a small amount of analyte to remain on the surface; a much smaller amount then what would be anticipated to remain in a 30 µm gap between laser shots. When the laser step size is equal to the diameter of the laser, there is essentially no area on the flat Si that is not effected; either the analyte is directly desorbed from under the laser spot or it is desorbed from when the thermal energy from the laser is spread over the surface.

On NIMS and ME-NIMS substrates however, surface defects induced by etching lead to dangling bonds that trap excited electrons locally. As a result, heat is mostly contained locally with little dissipation across the large surface area. When the pSi surface was irradiated by a laser, there is some thermal radiation across the surface but the area effected is drastically reduced compared to the area effected by conventional MALDI. This lack of surface radiation is most likely caused because of the porous surface; instead of radiating the surface, the thermal energy will affect the pores which won't allow the energy to spread over the surface as much. This can be seen when looking at the ion abundance of the grids from the top to the bottom of the image (Figure 4.9). It can be seen that though there is a slight fluctuation of signal over the TEM grid pattern as a whole, there is no significant change from the top of the image to the bottom with respect to the ion abundance. This represents that even though there is a thermal radiation over the surface due to the laser, it is a consistent dissipation from the beginning to the end of the MSI image. For NIMS, when the laser step size is larger than the diameter of the laser, there will be areas of the sample area that will not be desorbed at all; even when the laser step size is equal to the laser diameter, this can also be true (Figure 4.2B) (i.e. undersampling). Once the laser step size is less than the diameter of the laser beam, the laser spots begin to overlap causing some areas of the sample to actually be sampled more than once (i.e. oversampling); some areas of the sample can be hit by the laser as many as four times. A purposed idea to what is happening is that the first shot from the laser ablates/desorbs the analyte that is on the surface under the laser spot. When the laser moves over, it will desorb analyte that is on the surface under the laser spot as well as analyte that is adsorbed in the pores where the surface analyte had already been desorbed. This process continues until the entire surface area is imaged. This reasoning helps explain how the signal for NIMS spatial resolution

increases whereas MALDI and ME-NIMS signal decreases. The NIMS signal during imaging is an additive process since analyte is desorbing from the surface as well as out of the pores.

4.3.2 Biological Mass Spectrometry Imaging (MSI)

Although the above data shows the lowest achievable resolution for each technique, a larger resolution was used initially for parameter optimization and to determine which technique would be beneficial for future studies. The parameter that needed optimized was the sublimation time for the analysis of tissue samples for imaging. The goal was to sublime enough matrix to aid in desorption/ionization of analytes of interest but not too much where the matrix will over power the spectrum and actually hinder the signal of those analytes of interest. DHB matrix was sublimed on to the pSi NIMS surface at 0, 1, 2 and 3 mins to determine what yielded the highest signal (Figure 4.10). The data from 5 lipids were compared to MALDI data with a 3 min sublimation time. It can be seen that with 1 and 2 min sublimation times the signal from these lipids actually decrease which was not expected. It was thought that with the addition of matrix, the signal would increase steadily reaching a maximum signal until the matrix layer was too thick in which the signal would subsequently decrease. It was thought that possible not enough matrix was on the surface to aid in desorption/ionization but enough was on the tissue surface to hinder and block the analytes from being desorbed. At 3 min sublimation time, enough matrix was on the tissue surface to promote desorption/ionization allowing the signal to increase. Although the error bars were larger, the signal was higher than both conventional MALDI and NIMS. The 3 min sublimation time was determined to optimal and was used for all further MSI experiments that utilized ME-NIMS. To show the improved detection of tissue samples utilizing ME-NIMS, a side-to-side

comparison was performed. The improved ionization efficiency is illustrated in Figure 4.11 where lipids as well as the PC lipid headgroup were imaged. The reconstructed lipid 2D spatial distribution maps correlate well to the outline of the tissue samples with ME-NIMS producing much more intense overall ion abundance. We suspect the improved performance of ME-NIMS comes from the use of the pSi wafer to improve desorption efficiency at lower laser flux that produced lower background noise than in MALDI and the use of a thin layer of acidic matrix to provide a proton rich environment to improve ionization efficiency of analytes of interest more than in conventional NIMS.

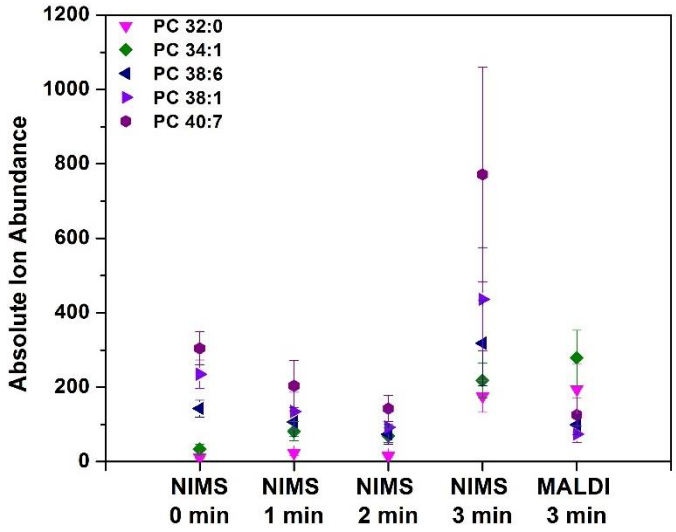

Figure 4.10: DHB sublimation times on tissue samples. Laser intensity for all wafers was 6300. Tissue slices were 5 µm thick. The error bars were calculated from 3 replicates.

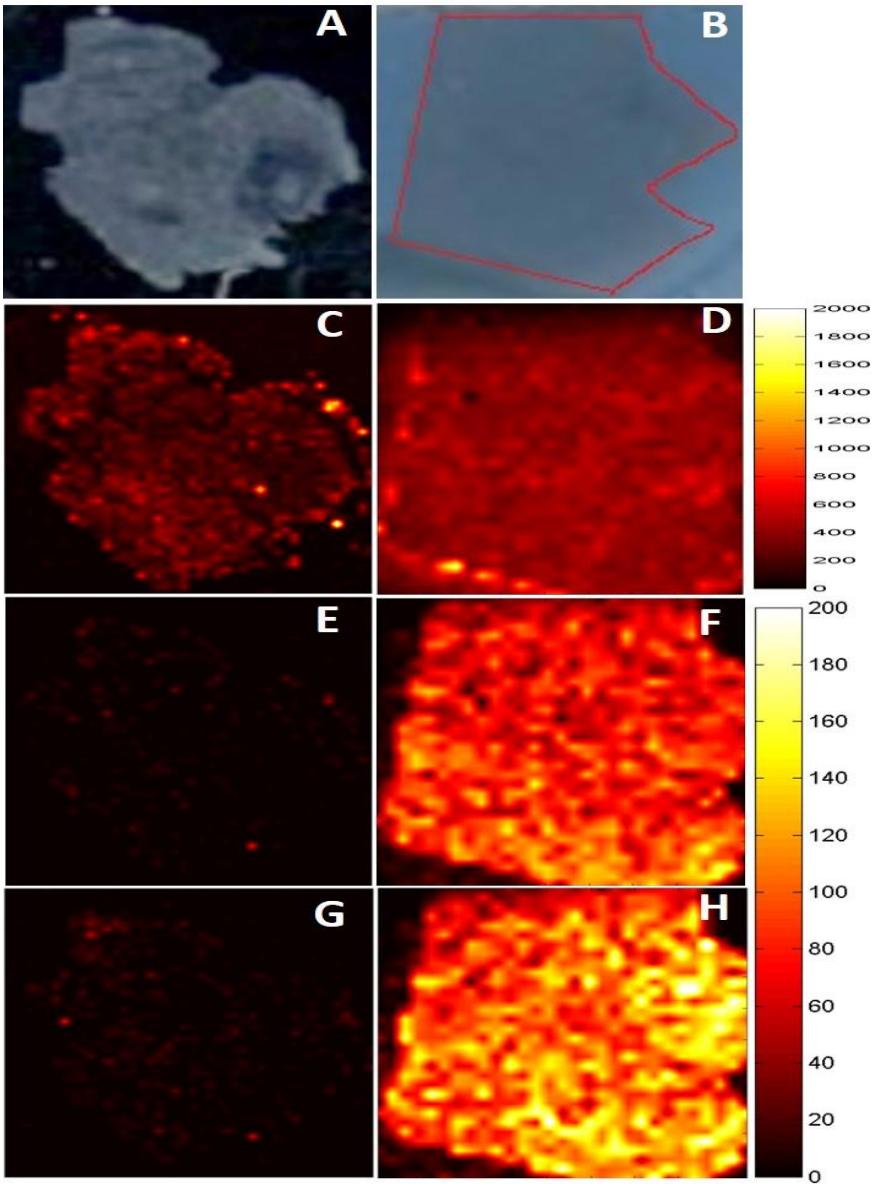

Figure 4.11: NIMS (left column) and ME-NIMS (right column) MSI. NIMS optical image of tissue **(A)**. ME-NIMS optical image of tissue (outlined in red) **(B)**. m/z 184 (PC headgroup) **(C)** and **(D)**. m/z 773 (PC 32:0) **(E)** and **(F)**. m/z 799 (PC 34:1) **(G)** and **(H).** MSI images were generated using MSiReader.

4.4 Conclusion

It has been shown that the spatial resolution for MALDI, NIMS and ME-NIMS was being pushed to the limits of the instrument being used without making any modifications to

the laser. For MALDI, the lowest laser step size feasible was 40µm before all of the analyte was completely ablated from the surface. For NIMS, 40µm was also achievable but produced a much higher ion abundance and although smaller laser step sizes were investigated this was the lowest achievable resolution. ME-NIMS was able to achieve the smallest laser step size at 30µm. ME-NIMS acted much like MALDI in that the abundance of the DHB signal decreased as the step size became smaller.

It was seen that at lower laser step sizes for NIMS MSI that the ion abundance actually increased and a couple ideas were purposed as to why this had occurred. The main and most likely reason for this increase in signal was due to the fact that a different analyte was used from NIMS compared to MALDI and ME-NIMS. Also it is thought that the ion abundance is an additive process since analytes are adsorbing into the pores as well as onto the surface of the pSi. Even after multiple laser shots at the exact same location on the NIMS surface, analyte signal is still seen, backing up this idea of the analyte desorbing out of the pores and adding to the ion abundance of the analyte that is desorbing off of just the surface.

The sublimation time for ME-NIMS was also optimized for the further use in MSI experiments. It's thought that enough matrix needed to be sublimed onto the pSi surface in order to aid in the desorption and ionization of the analytes of interest but if too much matrix was added it would over power the spectrum not allowing analytes to be seen at low concentrations. It was determined that this optimal sublimation time for tissue samples for ME-NIMS was 3 min. This time will be used for all further MSI experiments when ME-NIMS is utilized. In a side-to-side comparison for NIMS and ME-NIMS MSI of tissue, ME-NIMS results showed a higher ion abundance of the lipids and the PC lipid headgroup being looked

at. With this increased abundance, it shows the benefits that ME-NIMS provides for biological MSI.

4.5 References

(1) Addie, R. D.; Balluff, B.; Bovee, J. V.; Morreau, H.; McDonnell, L. A. Current State and Future Challenges of Mass Spectrometry Imaging for Clinical Research. *Anal Chem* **2015,** *87* (13), 6426.

(2) Calligaris, D.; Norton, I.; Feldman, D. R.; Ide, J. L.; Dunn, I. F.; Eberlin, L. S.; Cooks, R. G.; Jolesz, F. A.; Golby, A. J.; Santagata, S.et al. Mass spectrometry imaging as a tool for surgical decision-making. *J Mass Spectrom : JMS* **2013,** *48* (11), 1178.

(3) Liu, X.; Ide, J. L.; Norton, I.; Marchionni, M. A.; Ebling, M. C.; Wang, L. Y.; Davis, E.; Sauvageot, C. M.; Kesari, S.; Kellersberger, K. A.et al. Molecular imaging of drug transit through the blood-brain barrier with MALDI mass spectrometry imaging. *Sci Rep* **2013,** *3*, 2859.

(4) McDonnell, L. A.; Heeren, R. M. Imaging mass spectrometry. *Mass Spectrom Rev* **2007,** *26* (4), 606.

(5) Eriksson, C.; Masaki, N.; Yao, I.; Hayasaka, T.; Setou, M. MALDI Imaging Mass Spectrometry-A Mini Review of Methods and Recent Developments. *Mass Spectrom (Tokyo)* **2013,** *2* (Spec Iss), S0022.

(6) Greer, T.; Sturm, R.; Li, L. Mass spectrometry imaging for drugs and metabolites. *J Proteomics* **2011,** *74* (12), 2617.

(7) Seeley, E. H.; Caprioli, R. M. *Imaging Mass Spectrometry of Intact Biomolecules in Tissue Sections*, 2013. 393

(8) Lietz, C. B.; Gemperline, E.; Li, L. Qualitative and quantitative mass spectrometry imaging of drugs and metabolites. *Adv Drug Delivery Rev* **2013,** *65* (8), 1074.

(9) Seeley, E. H.; Caprioli, R. M. MALDI imaging mass spectrometry of human tissue: method challenges and clinical perspectives. *Trends Biotechnol* **2011,** *29* (3), 136.

(10) Rubakhin, S. S.; Jurchen, J. C.; Monroe, E. B.; Sweedler, J. V. Imaging mass spectrometry: fundamentals and applications to drug discovery. *Drug Discov Today* **2005,** *10* (12), 823.

(11) Ninomiya, S.; Ichiki, K.; Yamada, H.; Nakata, Y.; Seki, T.; Aoki, T.; Matsuo, J. Precise and fast secondary ion mass spectrometry depth profiling of polymer materials with large Ar cluster ion beams. *Rapid CommunMass Spectrom : RCM* **2009,** *23* (11), 1601.

(12) Wirtz, T.; Philipp, P.; Audinot, J. N.; Dowsett, D.; Eswara, S. High-resolution high-sensitivity elemental imaging by secondary ion mass spectrometry: from traditional 2D and 3D imaging to correlative microscopy. *Nanotechnol* **2015,** *26* (43), 434001.

(13) Murray, K. K.; Seneviratne, C. A.; Ghorai, S. High resolution laser mass spectrometry bioimaging. *Methods* **2016,** *104*, 118.

(14) Bich, C.; Touboul, D.; Brunelle, A. Cluster TOF-SIMS imaging as a tool for micrometric histology of lipids in tissue. *Mass Spectrom Rev* **2014,** *33* (6), 442.

(15) Ogrinc Potocnik, N.; Porta, T.; Becker, M.; Heeren, R. M.; Ellis, S. R. Use of advantageous, volatile matrices enabled by next-generation high-speed matrix-assisted laser desorption/ionization time-of-flight imaging employing a scanning laser beam. *Rapid Commun Mass Spectrom : RCM* **2015,** *29* (23), 2195.

(16) Amstalden van Hove, E. R.; Smith, D. F.; Heeren, R. M. A concise review of mass spectrometry imaging. *J Chromatogr A* **2010,** *1217* (25), 3946.

(17) Greving, M. P.; Patti, G. J.; Siuzdak, G. Nanostructure-initiator mass spectrometry metabolite analysis and imaging. *Anal Chem* **2011,** *83* (1), 2.

(18) Ding, Y.; Zhou, Y.; Yao, J.; Szymanski, C.; Fredrickson, J.; Shi, L.; Cao, B.; Zhu, Z.; Yu, X. Y. In Situ Molecular Imaging of the Biofilm and Its Matrix. *Anal Chem* **2016,** *88* (22), 11244.

(19) Campbell, D. I.; Ferreira, C. R.; Eberlin, L. S.; Cooks, R. G. Improved spatial resolution in the imaging of biological tissue using desorption electrospray ionization. *Anal Bioanal Chem* **2012,** *404* (2), 389.

(20) Fernandes, A. M.; Vendramini, P. H.; Galaverna, R.; Schwab, N. V.; Alberici, L. C.; Augusti, R.; Castilho, R. F.; Eberlin, M. N. Direct Visualization of Neurotransmitters in Rat Brain Slices by Desorption Electrospray Ionization Mass Spectrometry Imaging (DESI - MS). *J Am Soc Mass Spectrom* **2016,** *27* (12), 1944.

(21) Kertesz, V.; Van Berkel, G. J. Improved imaging resolution in desorption electrospray ionization mass spectrometry. *Rapid Commun Mass Spectrom: RCM* **2008,** *22* (17), 2639.

(22) Hartmanova, L.; Lorencova, I.; Volny, M.; Frycak, P.; Havlicek, V.; Chmelickova, H.; Ingr, T.; Lemr, K. Lateral resolution of desorption nanoelectrospray: a nanospray tip without nebulizing gas as a source of primary charged droplets. *The Analyst* **2016,** *141* (7), 2150.

(23) Laskin, J.; Heath, B. S.; Roach, P. J.; Cazares, L.; Semmes, O. J. Tissue imaging using nanospray desorption electrospray ionization mass spectrometry. *Anal Chem* **2012,** *84* (1), 141.

(24) Monroe, E. B.; Annangudi, S. P.; Hatcher, N. G.; Gutstein, H. B.; Rubakhin, S. S.; Sweedler, J. V. SIMS and MALDI MS imaging of the spinal cord. *Proteomics* **2008,** *8* (18), 3746.

(25) Liu, Q.; Guo, Z.; He, L. Mass spectrometry imaging of small molecules using desorption/ionization on silicon. *Anal Chem* **2007,** *79* (10), 3535.

(26) O'Brien, P. J.; Lee, M.; Spilker, M. E.; Zhang, C. C.; Yan, Z.; Nichols, T. C.; Li, W.; Johnson, C. H.; Patti, G. J.; Siuzdak, G. Monitoring metabolic responses to chemotherapy in single cells and tumors using nanostructure-initiator mass spectrometry (NIMS) imaging. *Cancer Metab* **2013,** *1* (1), 4.

(27) Woo, H. K.; Northen, T. R.; Yanes, O.; Siuzdak, G. Nanostructure-initiator mass spectrometry: a protocol for preparing and applying NIMS surfaces for high-sensitivity mass analysis. *Nature Protoc* **2008,** *3* (8), 1341.

CHAPTER 5: ANALYSIS OF DRUG COMPOUNDS

5.1 Introduction

Analysis and identification of molecules of interest is always imperative especially when studying drug compounds and how they behave in biological samples. There are techniques such as high pressure liquid chromatography (HPLC) and nuclear magnetic resonance (NMR) that are used for biological analysis and identification of proteins, lipids and other biological analytes.[1-7] For HPLC analysis of complex biological samples, a digestion method typically is employed in order to isolate and extract specific analytes of interest to simplify the sample. HPLC is often seen coupled with mass spectrometry in order to aid in the analysis and identification of analytes of interest. This does allow for separation to occur with HPLC and mass spectrometry to perform molecular analysis. NMR also uses extraction methods during preparation to extract metabolites of interest from tissue samples. Depending on the molecular complexity, NMR spectra can be difficult to use when identifying molecules of interest as well. Also these techniques alone cannot analyze biological samples in their native state where other techniques such as fluorenscence and flow cytometry can; this won't allow studies to be done on how biological molecules of interest behave in the presence of drug compounds.[8, 9] MALDI can perform the analysis of biological fluids and tissue by directly applying the samples to a MALDI plate which gives MALDI on advantage of a faster and easier approach.

One method in identifying analytes, especially in complex samples, is to perform tandem mass spectrometry (MS/MS). MS/MS fragments the molecule of interest in a unique pattern differing that specific molecule from molecules with similar molecular weights. There

are many ways to invoke the fragmentation of molecules of interest such as post-source decay (PSD), collision-induced dissociation (CID), and electron transfer dissociation (ETD); just to name a few. PSD is primarily used with MALDI where it uses the energy from the laser irradiation and collision between molecules of interest to induce fragmentation.[10-14] Since no other source is introduced to aid in fragmentation, PSD typically causes the weakest bonds in the molecule of interest to break which generally produces minimal fragments compared to other MS/MS methods.

Identification of molecules of interest is just as important as determining the limit of detection (LOD), the lowest quantity of a substance that can be distinguished from matrix.[10] MALDI MS does not require the extraction of proteins, lipids or other biological analytes of interest. They can be directly analyzed using MALDI or other such MS techniques such as NIMS and ME-NIMS. This allows for easier analysis of biological samples and drug compounds. In particular, developing an efficient and fast method to monitor drug compounds administered at low concentrations is crucial to study its metabolic pathways and to minimize toxicity effects the drug may cause to the patient. The capability to quantify trace amounts of drug and its metabolites with information of spatial distribution makes MSI a desirable technique for the studies.

In this chapter, pentamidine (PTA) was investigated using both NIMS and ME-NIMS. PTA is a drug compound used in the treatment of human African trypanosomiasis (HAT) which a parasitic brain disease that is fatal if left untreated.[15-17] The LOD for PTA was looked at in the absence of tissue for NIMS and ME-NIMS and presence of tissue samples for ME-NIMS. This showed the dynamic range for each of these techniques when looking at PTA. MS/MS of PTA was also investigated using NIMS in the absence and presence of tissue. ME-

NIMS was not explored with MS/MS although it would be expected that the ion abundance would increase upon the use of matrix which would provide a proton rich environment.

5.2 Materials and Methods

Materials Hydrofluoric acid (HF, 49%), ethanol (95%), sulfuric acid (H_2SO_4), hydrogen peroxide (H_2O_2, 30%) and methanol (99%) were purchased from VWR (Radnor, PA). N-type Sb-doped (100) single-crystalline silicon wafers at 0.005-0.02 Ω/cm were purchased from Silicon Sense, Inc. (Nashua, NH). Bis(heptadecafluoro-1,1,2,2-tetrahydrodecyl) tetramethyldisiloxane (BisF17) was purchased from Gelest, Inc. (Morrisville, PA). Angiotensin I, angiotensin III, bradykinin, 2,5-dihydroxybenzoic acid (DHB) and pentamidine (PTA) were purchased from Sigma-Aldrich (St. Louis, MO). 18 MΩ deionized (DI) H2O (Millipore, PO) was used for all experiments.

Porous Silicon (pSi) Substrate Preparation A detailed description of etching of silicon wafers and preparation of the NIMS surface has been reported.[18, 19] In a quick summary, silicon wafers were cut to approximately 1.5 cm x 1.5 cm. The cut silicon was washed in piranha solution (2:1 sulfuric acid: hydrogen peroxide) for 30 min. The wafer was rinsed with copious amounts of Milli-Q water and dried with N_2. The clean Si wafer was put in a Teflon anodic etch cell The etching cell consists of a two-electrode system where a Pt working electrode is placed under the Si wafer and a Pt counter electrode is placed above the surface. The Teflon cell was filled with 1mL of 25% HF solution in ethanol and etched at a current of 32 mA/cm^2 for 30 min. After etching, the pSi was rinsed with ethanol and dried with N_2. The pSi wafer was placed in a 120°C oven for 5 min and allowed to cool to room temperature. After the wafer cooled to room temperature, BisF17 initiator was applied to the pSi surface. 33µL of BisF17

initiator was pipetted on to the surface and incubated for 30 min. Any excess initiator was blown off using N_2. The NIMS chip was placed in a 120°C oven for 7-10 sec and excess initiator was blown off. This process was repeated two more times.

ME-NIMS Sample Preparation A thin layer of DHB matrix was deposited onto the wafer in a sublimation chamber.[20] Approximately 1 g of DHB was placed evenly over the bottom of the sublimation chamber. Using double-sided tape, a pSi substrate was attached upside down to the bottom of the condenser that was in direct contact with running water for cooling. An Edwards E2M8 vacuum pump with a vacuum meter was used to provide a controlled vacuum environment in the sublimation chamber. After maintaining the sublimation chamber for 2 min at approximately 50 torr, the apparatus was submerged into a 110˚C oil bath for 1.5 min for peptides analysis and 3 min for tissue analysis for ME-NIMS. Under these temperature and vacuum conditions, DHB immediately vaporized and re-deposited upon contact with the pSi substrate. Once matrix deposition was completed, the sublimation apparatus was removed from the oil bath and the vacuum was slowly released. Substrates coated with matrix were promptly removed from the apparatus and subsequently analyzed.

Sample Preparation for MS Measurements Stock solutions of angiotensin I, angiotensin III, and bradykinin were prepared in 50:50 acetonitrile (ACN): DI water at 12.5µM each. An aliquot of each were then mixed at a 1:1:1 (v/v) ratio to reach a final concentration of approximately 4.2µM. A stock solution of pentamidine (PTA) was prepared in 60:40 methanol: DI water at 1.23mM. The stock solution was used to make further dilutions of PTA at concentrations from 0.005µM up to 90µM. For ME-NIMS, the analyte solution was applied to

the wafer via drop-coating and allowed to dry before sublimation occurred. After sublimation, the samples were loaded in the MS chamber. For NIMS, the peptide solution was drop-coated onto the wafer, allowed to dry, and loaded into the MS chamber. Tissue samples were cut 5µm thick using a Leica CM1950 cyrostat. The tissue section was placed on pSi surface. For NIMS, the sample was loaded into the MS chamber; for ME-NIMS, matrix was sublimed then loaded into MS chamber.

Instrumentation An AB Sciex TOF/TOF™ 5800 System mass spectrometer (Framingham, MA) equipped with a 355 nm laser (Nd:YAG, 1000 Hz) was operated at an accelerating voltage of 20 kV in the reflector positive ion mode (MS-only) for all experiments. For sample spot analysis, the delay time was 13-15 ns to achieve optimal MS performance. A mass range of 100-1800 Da (± 0.05) and a bin size of 0.5 ns was used for all experiments. The laser intensity was 6400 to achieve optimal signal acquisition. In MS imaging mode, all mass spectra were collected in an automatic MS control mode using the AB Sciex TOF/TOF Imaging software; 50 laser pulses were averaged to yield one accumulated spectrum at each location. Mass spectra were reconstructed into 2D ion maps using the MSiReader™ software.[21]

5.3 Results and Discussion

5.3.1 Tandem Mass Spectrometry of Pentamidine

Under few scenarios, drugs can be directly analyzed from the NIMS/ME-NIMS surface, most of the time the drugs being investigated will be within the tissue since they are injected intravenously or intraperitoneal so it is important to be able to detect the drug compound on tissue samples.[15, 22] To determine if PTA could be seen on tissue samples, it was spotted onto mouse brain tissue slices and upon drying matrix was sublimed and subsequently

imaged. In Figure 5.1, the PTA spot can be seen along with the PC headgroup and PC lipids typically detected in mouse brain tissue. In Figure 5.1 A, C and D, there is a distinct ring which corresponds directly to where the PTA was spotted onto the tissue. This may have been caused from the solvent in the PTA solution. Methanol is often used in lipid extraction solutions so the methanol on the outside of the drop could have had an interaction with the lipids in the form of disrupting electrostatic forces between lipids.[23] It does seem that the lipids under the PTA spot may have suppressed signal which could be from the high concentration of PTA that was spotted.

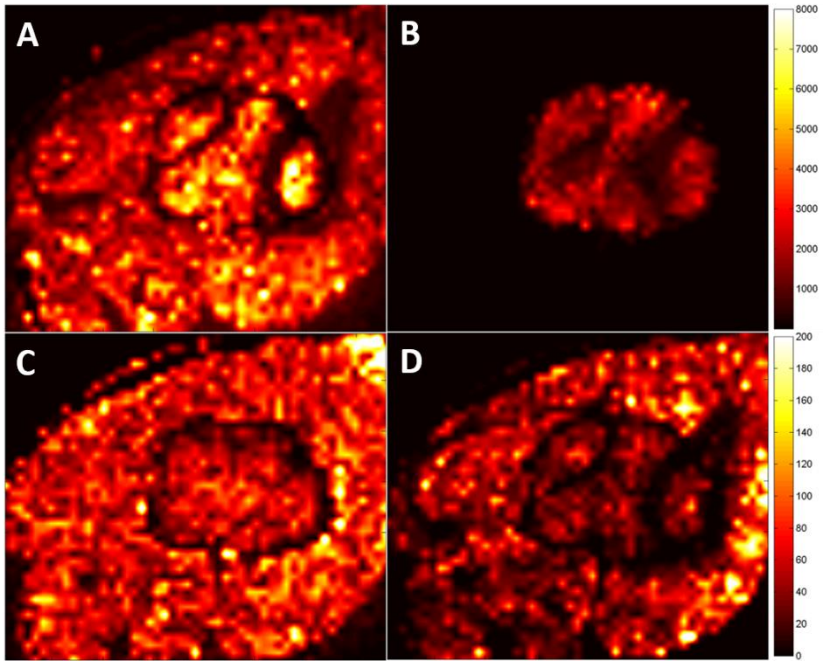

Figure 5.1: PTA spotted on a tissue slice: PC headgroup (A), PTA (B), PC 34:1 (C), and PC 40:8. Laser intensity was 6300. Laser step size was 150 µm.

Tandem MS (MS/MS) allows selective detection of species of similar parent m/z values in a complex sample that cannot be easily separated by upstream chromatographic methods.[13, 24-28] There are many molecules that have very similar molecular weights but their molecular

structure is very different. For example, PTA has a molecular weight of 340.42, which could also be $C_{14}H_{20}N_4O_4S$, a biotin and aspartate moiety. When MS/MS is applied to these molecules, a unique fragmentation pattern is obtained for the different molecules. This is an important method in confirming the detection of a molecule of interest when it is present in a complex sample which may have molecules that have similar molecular weights as the molecule being investigated. PTA was explored in order to determine its unique fragmentation pattern. When examining PTA on tissue samples, there is more background noise around m/z 340 which is why MS/MS was employed to verify that signal was from PTA and do show that the daughter ion was not needed for quantification. First MS/MS was performed by spotting PTA onto a NIMS wafer. Post source decay (PSD) was used for MS/MS of PTA. PSD utilizes the energy from the laser irradiation to fragment the molecule of interest.[10, 12-14, 29] PSD typically fragments at weaker bonds which in turn yields fewer fragmentations since the laser energy is used for both desorption of the analyte from the surface and fragmentation. For PTA, one main fragment was detected at m/z 324.4 (Figure 5.2A). This was determined to be a loss of $-NH_2$ (Figure 5.2D). Since the $-NH_2$ bond is the weakest bond on PTA and with two sites where $-NH_2$ could fragment off, the signal is intense. Next MS/MS of PTA was performed on a more complex sample. PTA was spotted onto a tissue sample and analyzed by NIMS. By knowing the fragmentation pattern of PTA alone on NIMS, PTA MS/MS fragmentation on a tissue sample should exhibit similar patterns. It can be seen in Figure 5.2B that again only one main fragment was detected at m/z 324.4 showing a similar spectrum to that of just PTA on a NIMS wafer. ME-NIMS MS/MS was not performed on PTA but it would be expected to exhibit higher ion intensities based on past data comparing NIMS and ME-NIMS results. Being able to identify the fragmentation pattern of PTA within tissue samples is beneficial when there

are other molecules of similar molecular weight but with a different structure. It acts as a molecular fingerprint allowing for easier identification of the molecule of interest being investigated.

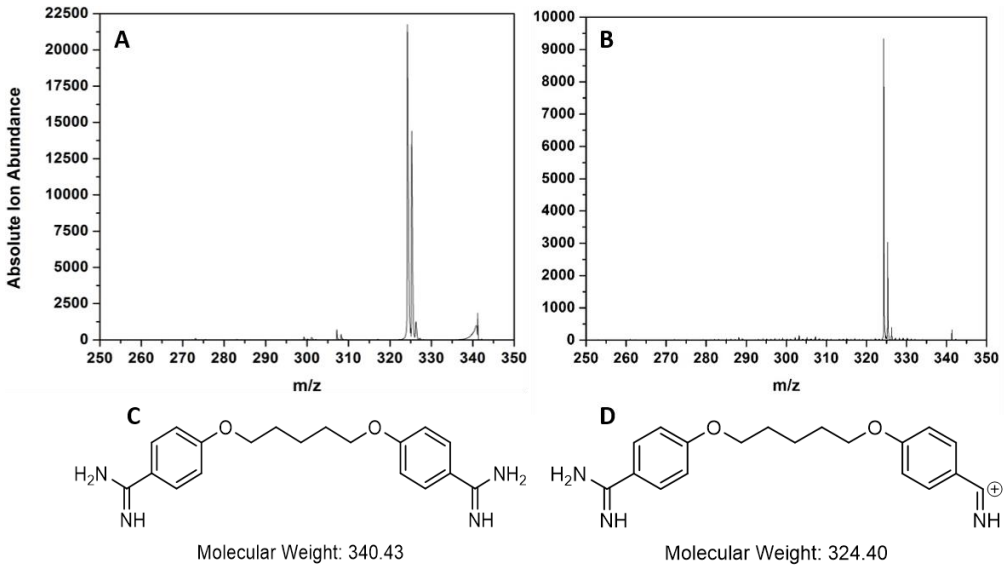

Figure 5.2: MS/MS of PTA in the absence of tissue **(A)** and presence of tissue **(B)**. The structure of PTA **(C)** and the main fragment from PTA **(D)**.

5.3.2 Pentamidine Limit of Detection (LOD)

An important part of drug analysis is to determine the limit of detection (LOD) with the technique that is being used to analyze the drug. In this study, the LOD of PTA was investigated utilizing both NIMS and ME-NIMS. PTA is an important drug for treatment of Human African Trypanosomiasis (HAT).[15, 16] First the analysis of PTA directly on NIMS and ME-NIMS wafers were examined. Six PTA solutions with a range of concentrations from 0.005 µM to1 µM were spotted directly on a NIMS wafer and imaged. For ME-NIMS, those six concentrations were also spotted and allowed to dry before the sublimation of DHB matrix onto the wafer. Once the matrix was sublimed MSI was performed and subsequently analyzed. The ion intensities measured for each concentration were extracted from each pixel in the MSI

images and averaged across the whole spot before being plotted against its concentration (Figure 5.3). It is clear to see that ME-NIMS shows better sensitivity – corroborating the notion that the presence of proton-rich chemical environment consistently facilitates PTA detection across different concentrations. At the lowest concentration tested (0.005 µM) in ME-NIMS, the ion signal is noticeably above the baseline noise; whereas for NIMS, 0.005 µM could not be seen. The signal is also more intense in ME-NIMS than what is seen from the 0.05 µM spot detected in NIMS, suggesting at least one order of magnitude improvement in detection sensitivity. NIMS has a range from 0.05 µM to 1 µM where ME-NIMS can detect down to 0.005 µM up to 1 µM. This shows that the detection limit and the detectable dynamic range is larger for ME-NIMS compared to NIMS.

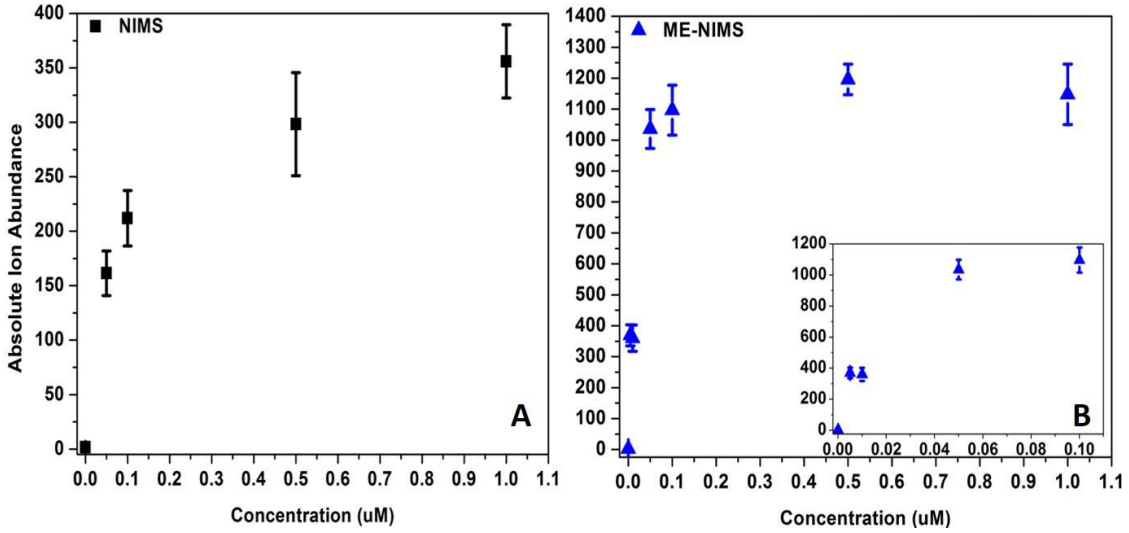

Figure 5.3: NIMS **(A)** and ME-NIMS LOD curve **(B)**. Inset **(B)** shows a zoom in of the concentration range 0-0.1 µM for ME-NIMS. Laser intensity for NIMS and ME-NIMS were 4400 and 4600, respectively. For both NIMS and ME-NIMS, data was extracted from three wafers per technique.

Since ME-NIMS was determined to be a more sensitive technique detecting PTA concentration down to 0.005 µM for PTA LOD on the wafer surface, only ME-NIMS was investigated for PTA spotted onto tissue samples. PTA was spotted at six different

concentrations ranging from 5 µM up to 90 µM onto tissue. Due to the spreading of the drug solution, tissue samples had to be cut into smaller pieces then placed onto the wafer. Once on the wafer each smaller piece was spotted with a different concentration of PTA solution in order to minimize the spreading of solution. Upon the solution drying on the tissue samples, matrix was sublimed on the wafer and immediately imaged. In the study of LOD of PTA on tissue, the imaging step size was 100µm. After all the data was collected, intensity profiles were extracted for m/z 341.4 for each concentration point. The average abundance across pixals was plotted as a function of PTA concentration to determine PTA LOD on tissue samples (Figure 5.4). It can be seen that ME-NIMS again yields a wide dynamic range. It is clear that there is a lack of response at the lower concentrations (5 and 10 µM) due to the presence of thick tissue. The trend for the PTA LOD is a steady increase with increasing concentration of PTA. Although the LOD for PTA on tissue is higher than the LOD directly from the NIMS wafer, it is still beneficial to determine. The concentration of PTA that is administered is different depending on the route of administration. Typical administration routes are intravenous, oral and intraperitoneal with corresponding PTA concentrations approximately 10 µM, 130 µM and 85 µM, respectively. With this data, PTA can be analyzed two different ways: analysis of bodily fluid or analysis of tissue. The analysis type would depend on how the drug and at what concentration was administered.

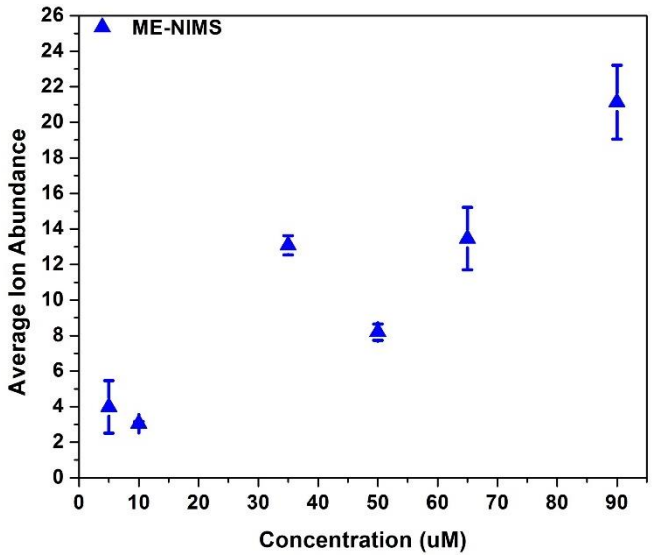

Figure 5.4: ME-NIMS LOD of PTA on tissue samples. Laser intensity was 6400. Data was extracted from two wafers.

5.4 Conclusion

Analysis and identification of drug compounds is an important factor with biological research. One method to identify the analyte of interest is to perform MS/MS which fragments the molecule allowing for identification of the analyte of interest. MS/MS analysis of PTA in the absence and presence of tissue was carried out. PTA yielded one major fragment during MS/MS which was determined to be the loss of $-NH_2$. Even with PTA spotted on tissue, which generally has an increase in background noise, the MS/MS spectrum was clean, having very little background noise and again yielding one main fragment. With a large dynamic range and clean MS/MS spectrum, these experiments show advantageous results for biological research using ME-NIMS. One analysis that is significant is to determine the dynamic range of particular drug compounds of interest. In this study, the dynamic range for PTA in the absence and presence of tissue utilizing NIMS and ME-NIMS was investigated. First PTA was looked at with the absence of tissue for both NIMS and ME-NIMS. This showed that the dynamic

range using the ME-NIMS technique was 10 fold higher than with NIMS. NIMS showed a LOD from 0.05 µM up to 1.0 µM where ME-NIMS detected PTA down to 0.005 µM. With ME-NIMS yielding an order of magnitude better detection than NIMS, LOD of PTA on tissue samples was explored using the ME-NIMS technique. Six different concentrations of PTA were spotted onto mouse brain tissue ranging from 5 µM up to 90 µM. All six concentration points were detected on tissue and plotted resembling an exponential curve. Although the concentrations of PTA on the tissue samples were higher than the concentrations directly analyzed from the pSi surface, its advantageous to see the dynamic range detected for direct analysis and analysis from tissue. Sometimes, especially in more complex samples, there are other molecules with a similar molecular weight to the analyte that is being investigated. PTA can be detected in both blood and tissue samples, allowing for a wide range of concentrations to be detected depending on which analysis method is employed.

5.5 References

(1) Matthews, S. J. NMR of proteins and nucleic acids. *Nuc Magn Reson* **2007,** *36*, 262.

(2) Ali, I.; Aboul-Enein, H. Y.; Gupta, V. K.; Singh, P.; Negi, U. Analyses of Chloramphenicol in Biological Samples by HPLC. *Anal Lett* **2009,** *42* (10), 1368.

(3) Row, K. H.; Lee, S. K.; Polyakova, Y. Degradation analysis of human hemoglobin by high-performance liquid chromatography. *J Ind Eng Chem* **2004,** *10* (3), 478.

(4) Li, F.; Yang, X. W. Determination of dehydrodiisoeugenol in rat tissues using HPLC method. *Biomed Chromatogr* **2008,** *22* (11), 1206.

(5) Sturaro, A.; De Marchi, M.; Masi, A.; Cassandro, M. Quantification of whey proteins by reversed phase-HPLC and effectiveness of mid-infrared spectroscopy for their rapid prediction in sweet whey. *J Dairy Sci* **2016,** *99* (1), 68.

(6) Nierenberg, D. W.; Nann, S. L. A method for determining concentrations of retinol, tocopherol, and five carotenoids in human plasma and tissue samples. *Am J Clin Nutr* **1992,** *56* (2), 417.

(7) Beckonert, O.; Keun, H. C.; Ebbels, T. M.; Bundy, J.; Holmes, E.; Lindon, J. C.; Nicholson, J. K. Metabolic profiling, metabolomic and metabonomic procedures for NMR spectroscopy of urine, plasma, serum and tissue extracts. *Nat Protoc* **2007,** *2* (11), 2692.

(8) Eftink, M. R. Fluorescence techniques for studying protein structure. *Methods Biochem Anal* **1991,** *35*, 127.

(9) Gronthos, S.; Franklin, D. M.; Leddy, H. A.; Robey, P. G.; Storms, R. W.; Gimble, J. M. Surface protein characterization of human adipose tissue-derived stromal cells. *J Cell Physiol* **2001,** *189* (1), 54.

(10) Spengler, B.; Kirsch, D.; Kaufmann, R. Fundamental-Aspects of Postsource Decay in Matrix-Assisted Laser Desorption Mass-Spectrometry .1. Residual-Gas Effects. *J Phys Chem-Us* **1992,** *96* (24), 9678.

(11) Sleno, L.; Volmer, D. A. Ion activation methods for tandem mass spectrometry. *J Mass Spectrom : JMS* **2004,** *39* (10), 1091.

(12) Spengler, B.; Kirsch, D.; Kaufmann, R. Metastable Decay of Peptides and Proteins in Matrix-Assisted Laser-Desorption Mass-Spectrometry. *Rapid Commun Mass Spectrom* **1991,** *5* (4), 198.

(13) Spengler, B. Post-source decay analysis in matrix-assisted laser desorption/ionization mass spectrometry of biomolecules. *J Mass Spectrom* **1997,** *32* (10), 1019.

(14) Kaufmann, R.; Chaurand, P.; Kirsch, D.; Spengler, B. Post-source Decay and Delayed Extraction in Matrix-assisted Laser Desorption/Ionization-Reflectron Time-of-Flight Mass Spectrometry. Are There Trade-offs? *Rapid Commun Mass Spectrom* **1996**.

(15) Brun, R.; Don, R.; Jacobs, R. T.; Wang, M. Z.; Barrett, M. P. Development of novel drugs for human African trypanosomiasis. *Future Microbiol* **2011,** *6* (6), 677.

(16) Simarro, P. P.; Jannin, J.; Cattand, P. Eliminating human African trypanosomiasis: where do we stand and what comes next? *PLoS medicine* **2008,** *5* (2), e55.

(17) Brun, R.; Blum, J.; Chappuis, F.; Burri, C. Human African trypanosomiasis. *Lancet* **2010,** *375* (9709), 148.

(18) Wei, J.; Buriak, J. M.; Siuzdak, G. Desorption-ionization mass spectrometry on porous silicon. *Nature* **1999,** *399* (6733), 243.

(19) Woo, H. K.; Northen, T. R.; Yanes, O.; Siuzdak, G. Nanostructure-initiator mass spectrometry: a protocol for preparing and applying NIMS surfaces for high-sensitivity mass analysis. *Nat Protoc* **2008,** *3* (8), 1341.

(20) Liu, Q.; Xiao, Y.; He, L. In *Mass Spectrometry Imaging*; Rubakhin, S. S.;Sweedler, J. V., Eds.; Humana Press, 2010; Vol. 656.

(21) Robichaud, G.; Garrard, K. P.; Barry, J. A.; Muddiman, D. C. MSiReader: an open-source interface to view and analyze high resolving power MS imaging files on Matlab platform. *J Am Soc Mass Spectrom* **2013,** *24* (5), 718.

(22) Wenzler, T.; Yang, S.; Braissant, O.; Boykin, D. W.; Brun, R.; Wang, M. Z. Pharmacokinetics, Trypanosoma brucei gambiense efficacy, and time of drug action of DB829, a preclinical candidate for treatment of second-stage human African trypanosomiasis. *Antimicrob Agents Chemother* **2013,** *57* (11), 5330.

(23) Reis, A.; Rudnitskaya, A.; Blackburn, G. J.; Mohd Fauzi, N.; Pitt, A. R.; Spickett, C. M. A comparison of five lipid extraction solvent systems for lipidomic studies of human LDL. *J Lipid Res* **2013,** *54* (7), 1812.

(24) Al-Saad, K. A.; Siems, W. F.; Hill, H. H.; Zabrouskov, V.; Knowles, N. R. Structural analysis of phosphatidylcholines by post-source decay matrix-assisted laser desorption/ionization time-of-flight mass spectrometry. *J Am Soc Mass Spectrom* **2003,** *14* (4), 373.

(25) Dongre, A. R.; Eng, J. K.; Yates, J. R., 3rd. Emerging tandem-mass-spectrometry techniques for the rapid identification of proteins. *Trends Biotechnol* **1997,** *15* (10), 418.

(26) Johnson, A. R.; Carlson, E. E. Collision-Induced Dissociation Mass Spectrometry: A Powerful Tool for Natural Product Structure Elucidation. *Anal Chem* **2015,** *87* (21), 10668.

(27) Li, B.; An, H. J.; Hedrick, J. L.; Lebrilla, C. B. Collision-induced dissociation tandem mass spectrometry for structural elucidation of glycans. *Methods in Mol Biol* **2009,** *534*, 133.

(28) Mitchell Wells, J.; McLuckey, S. A. Collision-Induced Dissociation (CID) of Peptides and Proteins. *Biol Mass Spectrom* **2005,** *402*, 148.

(29) Purcell, A. W.; Gorman, J. J. The use of post-source decay in matrix-assisted laser desorption/ionisation mass spectrometry to delineate T cell determinants. *J Immunol Methods* **2001,** *249* (1-2), 17.